
**Microporous metal imidazoles:
Synthesis and characterization of
nano- and microcrystals as well as
membranes and investigation of the
mechanisms of crystallization**

Von der Naturwissenschaftlichen Fakultät der Gottfried Wilhelm Leibniz
Universität Hannover zur Erlangung des Grades:

Doktor der Naturwissenschaften

Dr. rer. nat.

genehmigte Dissertation von

Dipl.-Chem. Janosch Cravillon

geboren am 07.11.1982, in Hildesheim

2011

Referent: Prof. Dr. Peter Behrens

Korreferent: Prof. Dr. Jürgen Caro

Tag der Promotion: 08.12.2011

Erklärung zu dieser Dissertation

Hiermit erkläre ich, die vorliegende Dissertation selbständig verfasst und keine anderen als die angegebenen Quellen und Hilfsmittel benutzt sowie evtl. zur Hilfeleistung herangezogene Institutionen vollständig angegeben zu haben.

Diese Dissertation wurde nicht schon als Diplomarbeit oder Dissertation an einer in- oder ausländischen Hochschule eingereicht.

Hannover, den 29. Dezember 2011

Janosch Cravillon

Abstract

This dissertation deals in seven publications with size- and shape-controlled syntheses of the microporous metal-organic framework (MOF) ZIF-8 (zeolitic imidazolate framework 8) as well as with investigations of the nucleation and growth processes using various in-situ and ex-situ experiments. The knowledge obtained was adopted to synthesize gas separating supported ZIF-8 membranes.

It could be shown that the size of ZIF-8 crystals can be controlled between 10 and 1000 nm by using an excess of the bridging bidentate ligand 2-methylimidazole and various monodentate ligands (modulators). The function of the monodentate ligands in the size-controlled syntheses can be understood as a modulation of complex formation and deprotonation equilibria in the reaction solutions.

The fast nucleation and early growth of ZIF-8 nanocrystals was monitored by time-resolved in-situ synchrotron small-angle and wide-angle X-ray scattering (SAXS/WAXS) with a time resolution of one second. Very small particles (clusters) with a diameter of about 2 nm formed instantaneously upon mixing the component solutions of metal salt and bridging ligand. The formation of ZIF-8 particles started after 15 seconds. The particles grew rapidly to a size of about 25 nm. In addition, the synthesis of much larger ZIF-8 crystals (up to 200 μm in size) by a formate-modulated solvothermal reaction was possible. This reaction was monitored by in-situ energy-dispersive X-ray diffraction (EDXRD) measurements. Analyses of crystallization curves gave insights into the kinetics and mechanism of crystal growth. It could be shown that formate acts as a base to deprotonate the bridging ligand. In contrast, in room-temperature syntheses formate acts as a competitive ligand in complex formation equilibria, as could be shown by in-situ static light scattering experiments.

Another achievement was the synthesis of supported ZIF-8 membranes by using in-situ crystallization as well as the method of seeding and secondary growth. The latter method allowed the synthesis of oriented ZIF-8 membranes. All membranes exhibited excellent selectivities for the separation of H_2 from other gas molecules.

Moreover, polymer-ZIF-8 nanofibers could be produced by electrospinning which have possible applications in gas adsorption. The micropores of the embedded ZIF-8 nanocrystals were easily accessible for gas.

Keywords: metal-organic frameworks, MOFs, zeolitic imidazolate frameworks, ZIFs, nanomaterials, modulated synthesis, nucleation, crystal growth, in-situ scattering methods

Kurzzusammenfassung

Diese Dissertation befasst sich in sieben Publikationen mit gezielten größen- und formkontrollierenden Synthesen der metall-organischen Gerüstverbindung (MOF) ZIF-8 (zeolitic imidazolate framework 8) und Untersuchungen der Nukleations- und Wachstumsprozesse mittels verschiedener in-situ und ex-situ Methoden. Das erlangte Verständnis wurde eingesetzt, um gastrennende ZIF-8-Membranen zu synthetisieren.

Es zeigte sich, dass die Größe der ZIF-8 Kristallite zwischen 10 und 1000 nm eingestellt werden kann, indem ein Überschuss des zweizähligen Brückenliganden 2-Methylimidazol und verschiedene einzählige Liganden (Modulatoren) verwendet werden. Die Funktion dieser Modulatoren in den Synthesen kann als Modulation der Komplexbildungs- und Deprotonierungsgleichgewichte der Reaktionslösungen verstanden werden.

Die schnelle Nukleation und das frühe Wachstum von ZIF-8-Nanokristallen konnte mittels in-situ Kleinwinkel- und Weitwinkel-Röntgenstreuung (SAXS/WAXS) mit einer Zeitauflösung von einer Sekunde beobachtet werden. Sehr kleine Partikel (Cluster) mit einem Durchmesser von 2 nm bildeten sich augenblicklich nach dem Mischen der beiden Eduktlösungen. ZIF-8-Partikel entstanden nach 15 Sekunden und wuchsen schnell auf eine Größe von 25 nm. Auch größere ZIF-8-Kristalle (bis zu 200 μm) konnten durch Formiat-modulierte solvothermale Reaktionen erhalten werden, welche mittels in-situ energie-dispersiver Röntgenbeugung verfolgt wurden. Analysen der Kristallisationskurven ermöglichten Einblicke in Kinetik und Mechanismen des Kristallwachstums. Außerdem wurde gezeigt, dass Formiat als Base fungiert, um 2-Methylimidazol zu deprotonieren. Im Gegenteil hierzu wirkt Formiat in Raumtemperatursynthesen modulierend auf die Komplexbildungsgleichgewichte, was durch in-situ-Untersuchungen mittels statischer Lichtstreuung gezeigt werden konnte.

Ein weiterer Erfolg war die Synthese von geträgerten ZIF-8-Membranen. Diese wurden sowohl durch in-situ-Kristallisation, als auch durch Anheftung von Keimkristallen an die Trägeroberfläche und anschließendes Wachstum hergestellt. Die letztere Methode erlaubte die Synthese von orientierten ZIF-8-Membranen. Alle Membranen zeigten exzellente Selektivitäten für die Trennung von H_2 von anderen Gasmolekülen.

Ferner konnten Polymer-ZIF-8-Fasern durch Elektrosponnen hergestellt werden, welche mögliche Anwendungen in der Gasadsorption haben, da die Mikroporen der eingebetteten ZIF-8 Nanokristalle gute Zugänglichkeit für Gase zeigten.

Schlagwörter: metall-organische Gerüststrukturen, MOFs, zeolitische Imidazolat-Gerüststrukturen, ZIFs, Nanomaterialien, modulierte Synthese, Keimbildung, Kristallwachstum, in-situ-Streumethoden

Danksagung

Diese Arbeit wäre ohne die Hilfe von vielen Menschen nicht im Entferntesten möglich gewesen.

Zu Beginn möchte ich mich natürlich bei Prof. Dr. Peter Behrens für die Aufnahme in seinen Arbeitskreis und die Möglichkeit, meine Dissertation bei ihm anfertigen zu dürfen, bedanken.

Auch Herrn Prof. Dr. Jürgen Caro gilt Dank auszusprechen für die Übernahme des Koreferates, die vielen wissenschaftlichen Diskussionen und die Unterstützung während meiner Arbeit.

Bei einem Menschen will ich mich ganz besonders bedanken: Herrn Dr. Michael Wiebcke, der mich mit all seinen Möglichkeiten (und das manchmal bis an die Grenzen) unermüdlich unterstützt hat. Das Arbeitsklima war stets ein freundliches, kollegiales, wodurch viele interessante fachliche und auch weniger fachliche Diskussionen entstanden sind, an die ich mich immer gerne zurückerinnern werde.

Des Weiteren möchte ich Christian A. Schröder heraus heben, der ein halbes Jahr nachdem ich bei Dr. Wiebcke meine Arbeit begann, die Arbeitsgruppe erweiterte. Viele Tage und Nächte verbrachten wir zusammen vor Messungetümen, an diversen Synchrotron-Laboratorien oder an statischen Lichtstreuanlagen. Er war immer für mich da, wenn ich ihn gebraucht hab. Die Unterstützung die er für meine Dissertation geleistet hat, ist kaum aufzuwiegen.

Bedanken möchte ich mich auch beim gesamten Arbeitskreis Behrens für die bisher wohl tollste Zeit im meinem Leben. Die fachlichen und privaten Diskussionen führten über ein kollegiales Verhältnis weit hinaus, so dass ich weniger in einem Arbeitskreis als in einem Freundeskreis gearbeitet habe. Die langen Film- oder feucht-fröhlichen Musik-Diskussions-Abende werde ich wohl nicht so bald vergessen.

Natürlich möchte ich mich auch für die wissenschaftliche Hilfe bedanken. Sei es bei Roman Nayuk und Todor Hikov für die großartige Unterstützung bei den SLS- und Synchrotron-Messungen oder bei Georg Platz für seinen unermüdlichen Kampf gegen Windmühlen während der Sorptionsmessungen, aber auch bei Andreas Schaate, Birgit Beißer und Christian Schröder für die vielen TG/DTA-Messungen.

Auch Dr. Rainer Ostermann und dem Arbeitskreis von Prof. Dr. Bernd Smarsly ist für die produktiven Kooperationen und wissenschaftlichen Diskussionen Dank auszusprechen.

Auch Florian Waltz, Imke Bremer, Sebastian Liliental, Anne Christel und Marc Kieke bin ich zu Dank verpflichtet, die immer ein paar Minuten für eine Raucherpause übrig hatten.

Bei meinen Eltern will ich mich für die große Unterstützung im Studium, sei es durch Finanzspritzen oder ein leckeres Mittagessen, bedanken. Ohne sie wäre ich gar nicht bis ins Chemie Studium gekommen.

Auch bei Caroline Behrens will ich mich bedanken, für die Unterstützung die sie mir in der Doktorarbeit aber auch während meiner Krankheit hat zukommen lassen. Gerade zu dieser Zeit war sie für mich das Rettungsboot auf stürmischer See.

Preface

The results which are presented in this dissertation were achieved in the last three years during my work as scientific assistant in the Institute of Inorganic Chemistry of the Gottfried Wilhelm Leibniz University of Hannover in the group of Prof. Dr. Peter Behrens. The work was supported by the Deutsche Forschungsgemeinschaft (DFG) within the frame of the Priority Program 1362 (*Porous Metal-Organic Frameworks*) as a joint project of four groups entitled “*Transport in microporous MOFs: From molecular diffusion to membrane permeation*” (grant number Wi1156/2-1) and was supervised by Dr. Michael Wiebcke.

The dissertation consists of seven scientific publications. For four publications I am the first author, whereas for the other three publications I am a coauthor. In the following I will describe my contributions to the publications. I have to thank the authors and coauthors for the great cooperation and the fruitful discussions and support during the manuscript preparations, especially Dr. Michael Wiebcke.

The two articles in chapter 3 of this thesis deal with the synthesis of ZIF-8 nano- and microcrystals at room-temperature and the control over crystal size and morphology. I am the first author of both articles. Preparation and characterization of the materials was performed by myself. Parts of the interpretation of the in-situ static light scattering (SLS) data were performed by Roman Nayuk and Prof. Dr. Klaus Huber from the Chemistry Department of the University of Paderborn. The development of the synthesis protocol of ZIF-8 nanocrystals without size control had already been part of my diploma thesis “*Synthese und Charakterisierung von Nanokristallen ionischer Verbindungen*”.[#]

The two articles in chapter 4 present in-situ synchrotron X-ray diffraction studies, which provided significant insights into the nucleation and growth of ZIF-8 nanocrystals at room-temperature and ZIF-8 macrocrystals under solvothermal conditions. The X-ray scattering experiments and data reduction reported in the article *Fast Nucleation and Growth of ZIF-8 Nanocrystals Monitored by Time-Resolved In Situ Small-Angle and Wide-Angle X-Ray Scattering* were performed by myself, Christian A. Schröder, Roman Nayuk and Dr. Michael Wiebcke at beamline

[#] J. Cravillon, *Synthese und Charakterisierung von Nanokristallen ionischer Verbindungen*, diploma thesis, Leibniz University Hannover, **2009**.

ID02 at the ERSF (European Synchrotron Radiation Facility) in Grenoble, France. The evaluation of the SAXS data was performed by Dr. Michael Wiebcke, Prof. Dr. Klaus Huber and Roman Nayuk, while the data evaluation of the WAXS data was performed by myself and Christian A. Schröder. The X-ray diffraction experiments for the second article *Formate modulated solvothermal synthesis of ZIF-8 investigated using time-resolved in situ X-ray diffraction and ex situ electron microscopy* were performed at the HASYLAB (Hamburger Synchrotron Laboratorium) at DESY (Deutsches Elektronen Synchrotron) in Hamburg, Germany. All the experiments and data evaluation were performed by myself.

During the long synchrotron experiments Christian A. Schröder and Dr. Andre Rothkirch (HASYLAB) were a great help and always open for fruitful discussions. The ex-situ syntheses and powder X-ray diffraction (XRD) as well as scanning electron microscopy (SEM) investigations were also performed by myself.

In chapter 5 results of ZIF-8 membrane syntheses are presented in two articles. The experimental work was performed by Dr. Helge Bux (group of Prof. Dr. Jürgen Caro, Leibniz University Hannover), my cooperation partner in the DFG priority program. My contributions to the publications *Zeolitic Imidazolate Framework Membrane with Molecular Sieving Properties by Microwave-Assisted Solvothermal Synthesis* and *Oriented Zeolitic Imidazolate Framework-8 Membrane with Sharp H_2/C_3H_8 Molecular Sieve Separation* were intense discussions during the development of the membrane synthesis procedures. Crystal morphology evaluation and the synthesis of ZIF-8 nanocrystals for the seeding procedures were performed by myself.

The publication in chapter 6 entitled *Metal-organic framework nanofibers via electrospinning* is the result of a cooperation with Dr. Rainer Ostermann from the Justus-Liebig-University of Giessen, from the group of Prof. Dr. Bernd Smarsly. My contribution to this cooperation was the synthesis and characterization of the ZIF-8 nanocrystals by XRD and SEM.

Table of Contents

1. Introduction	1
1.1 Metal-Organic Frameworks (MOFs)	1
1.2 Zeolitic Imidazolate Frameworks (ZIFs)	3
1.3 Potential Applications	6
1.3.1 Separation.....	6
1.3.2 Storage.....	7
1.3.3 Composites	8
1.3.4 Catalysis	8
1.3.5 Sensors	9
1.3.6 Biomaterials	9
1.4 Size- and Morphology Controlled Syntheses of MOFs	10
1.4.1 Common Synthesis.....	10
1.4.2 Methods of Size and Shape Control in MOF Synthesis.....	11
1.4.3 Controlled Synthesis Using Coordination Modulation	12
1.5 Investigations on the Mechanisms of MOF Nucleation and Growth.....	14
1.6 Supported Polycrystalline MOF Membrane Synthesis	16
1.6.1 In-Situ Crystallization	16
1.6.2 Seeding and Secondary Growth	17
1.6.3 Further Methods	18
2. Bibliography.....	21
3. Controlling Size and Shape of ZIF-8 Crystals	27
3.1 Summary	27
3.2 Rapid Room-Temperature Synthesis and Characterization of Nanocrystals of a Prototypical Zeolitic Imidazolate Framework.....	29

3.3 Controlling Zeolitic Imidazolate Framework Nano- and Microcrystal Formation: Insight into Crystal Growth by Time-Resolved In Situ Static Light Scattering.....	33
4. Monitoring ZIF-8 Syntheses by Time-Resolved In-Situ Synchrotron X-ray Scattering Experiments	47
4.1 Summary	47
4.2 Fast Nucleation and Growth of ZIF-8 Nanocrystals Monitored by Time-Resolved In Situ Small-Angle and Wide-Angle X-Ray Scattering	49
4.3 Formate Modulated Solvothermal Synthesis of ZIF-8 Investigated Using Time-Resolved In-Situ X-ray Diffraction and Scanning Electron Microscopy.....	55
5. Syntheses of Supported ZIF-8 Membranes.....	63
5.1 Summary	63
5.2 Zeolitic Imidazolate Framework Membrane with Molecular Sieving Properties by Microwave-Assisted Solvothermal Synthesis.....	64
5.3 Oriented Zeolitic Imidazolate Framework-8 Membrane with Sharp H ₂ /C ₃ H ₈ Molecular Sieve Separation.....	67
6. Syntheses of ZIF-8 Composite Nanofibers Using Electrospinning.....	77
6.1 Summary	77
6.2 Metal-Organic Framework Nanofibers <i>via</i> Electrospinning.....	78
7. Curriculum Vitae.....	83
8. List of Publications	85

1. Introduction

This thesis deals with size- and shape-controlled syntheses as well as with in-situ and ex-situ scattering and microscopy experiments on the mechanisms of formation and with possible applications of a prototypical metal-organic framework (MOF) material called zeolitic imidazolate framework 8 (ZIF-8). First, in this chapter, a brief description of the structures, properties and main potential applications of MOFs and ZIFs is given. Further methods of size- and shape-controlled synthesis, in-situ investigations of the mechanisms of crystallization and membranes synthesis are briefly introduced.

1.1 Metal-Organic Frameworks (MOFs)

MOFs are a novel class of crystalline porous materials.^[1-4] Approximately 10% of all MOF materials exhibit a permanent porosity.^[5] These materials are also called “porous coordination polymers”.

They are coordination compounds, in which a discrete metal ion or cluster (so-called connector) is coordinated by multidentate (at minimum bidentate) ligands (so-called linkers) to form a three-dimensional coordination polymer (see Figure 1). The clusters are also called (SBUs for secondary building units).

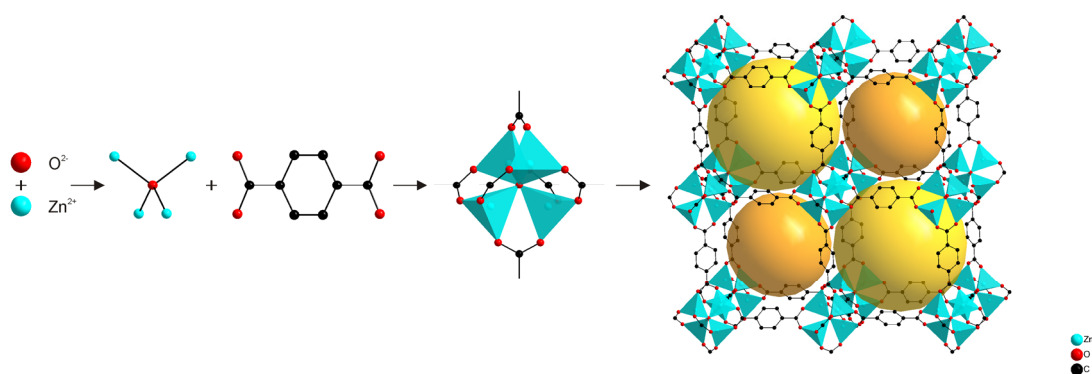


Figure 1: Structure of MOF-5 (Metal Organic Framework 5). A central μ_4 -oxygen is tetrahedrally surrounded by four zinc cations which in turn are pairwise bridged by the carboxylate groups of six terephthalate anions forming the SBU (secondary building unit). The 3D framework structure is formally generated by connecting these SBUs via the benzene rings of the terephthalate anions (linker). The final framework generates a 3D pore system consisting of two alternating cavities with diameters of 15.2 Å and 11.0 Å respectively.^[6]

A promising class of MOFs are carboxylate-based MOFs, which often contain metal oxygen clusters like MOF-5 ($Zn_4O(BDC)_3$, H_2BDC = terephthalic acid), UiO-66 ($Zr_6O_4(OH)_4BDC_6$), MIL-53 ($Al(OH)BDC$) or HKUST-1 ($Cu_3(BTC)_2$), BTC = benzene-1,3,5-tricarboxylate). Another class are the pillar-layer MOFs, constructed

by paddle-wheel SBUs made of copper or zinc ions, which are connected via dicarboxylates like terephthalate into 2D layers that in turn are pillared by diamines like 4,4'-bipyridine to generate 3D frameworks. A younger distinct class of MOFs are the zeolitic imidazolate frameworks. They consist of discrete divalent metal cations like Zn^{2+} or Co^{2+} , that are linked via substituted imidazolate anions and typically possess zeolite-related topologies.

The pore networks in MOFs are wide-ranged and tunable compared to purely inorganic porous compounds like zeolites or mesoporous silica. The organic-inorganic MOF hybrid materials offer much more variability in pore diameter and functionality than these materials due to the nearly infinite pool of different organic linkers and inorganic connectors. For example, the pore walls can be made hydrophobic or hydrophilic. Open metal sites for catalytic reactions or functionalized linkers for post-synthetic modifications can be introduced. Also the pore sizes can be tuned without changing framework topology by using linkers of different length (isorecticular MOFs, IRMOFs).^[6] MOFs can exhibit large intra-crystalline surface areas of up to 6240 m²/g calculated with the Brunauer-Emmett-Teller equation and 10400 m²/g calculated using the Langmuir model. These are significantly larger than those of classical adsorbents like zeolites or activated carbon.^[7]

The choice of the metal ion (connector) in MOFs is hardly restricted. Often used connectors are Fe^{2+}/Fe^{3+} , Co^{2+} , Ni^{2+} or Zn^{2+} , but also Mg^{2+} , Al^{3+} , Ti^{4+} , Zr^{4+} or Pd^{2+} are suitable.^[05] Some popular MOFs are already commercially available like MIL-53 (Basolite® A100), HKUST-1 (Basolite® C300) and ZIF-8 (Basolite® Z1200). Another special feature of some MOFs, differentiating them from zeolites or activated carbons, is their ability to “breathe”, which means that the framework expands or shrinks considerably upon guest uptake or release (so-called breathing effect). Some MOFs exhibit a gate-opening effect, which means that the pore system only becomes accessible at a critical pressure threshold.^[8]

1.2 Zeolitic Imidazolate Frameworks (ZIFs)

As mentioned before, ZIFs are a younger and distinct class of MOFs. Due to the similarity of the metal-imidazolate-metal (M-Im-M) and silicon-oxygen-silicon (Si-O-Si) angles of approximately 145° in ZIFs and zeolites, respectively (see Figure 2), the tetrahedral frameworks exhibit analogous topologies (see Figure 3).^[2, 9]

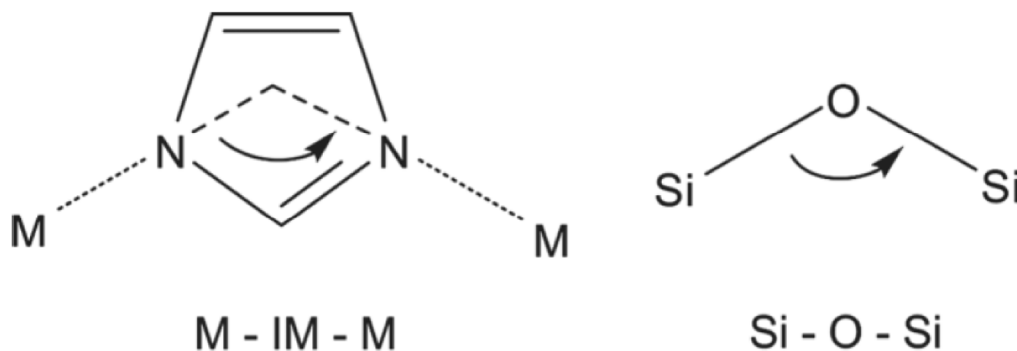


Figure 2: Illustration of the angles at the linkers in ZIFs and zeolites.^[10]

An important advantage of ZIFs over zeolites is the larger cages, due to the longer imidazolate linkers compared to the bridging oxygen atoms in zeolites. This can be seen by comparing the metal-to-metal distances. In ZIFs, zinc centers typically exhibit a distance of ca. 6 Å, as compared to the distance of only ca. 3.2 Å between neighboring silicon atoms in zeolites. In spite of this, the pore openings in ZIFs are comparable in size to those of zeolites. This is caused by the bulkiness of the imidazole linkers. Therefore, the adsorption of guest molecules into ZIF cages is similarly size- and shape-specific as in zeolites, but the larger ZIF cages allow molecules to pass each other and hence blocking effects are avoided, which may limit the diffusion in zeolites. As other MOFs, ZIFs show some framework flexibility, which is caused by twisting of the linker molecules. This was very recently demonstrated for the prototypical ZIF-8.^[11] Due to this flexibility, molecules larger than the crystallographically estimated pore diameters can pass the pore openings and a sharp cut off for gas separation is usually not observed. This was proven for a number of ZIF membranes by Caro and coworkers (see also chapter 5)^[12-17] and bulk ZIF materials^[18].

The choice of the imidazolate derivative has an influence on the framework topology and allows the control of the pore diameters as well as the chemical nature of the pore walls (hydrophilic or hydrophobic character). All C_2 -substituted imidazolates typically generate a sodalite topology if zinc is the metal center as is the

case for ZIF-8 (linker = 2-methylimidazolate) or ZIF-90 (linker = 2-carbaldehydeimidazolate).

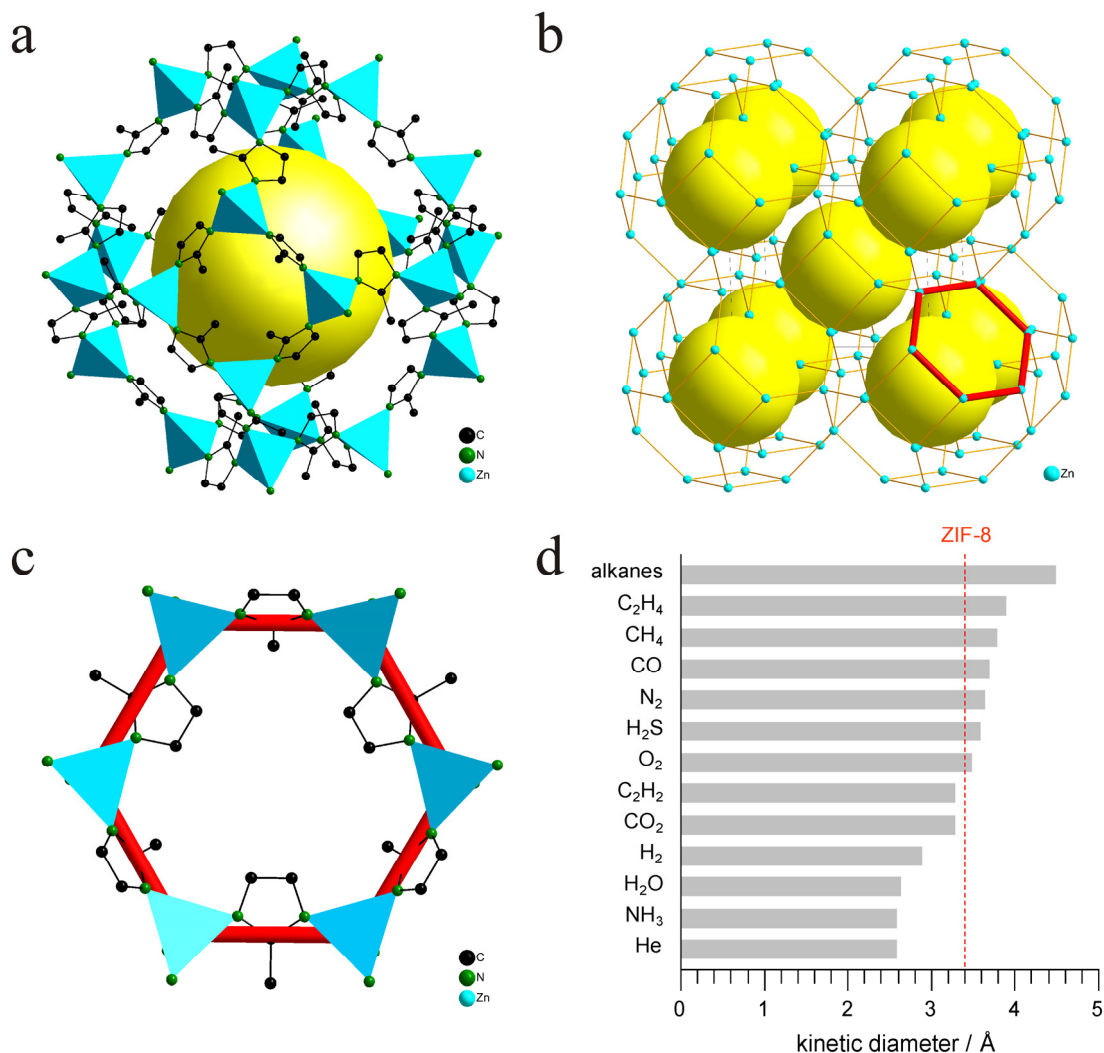


Figure 3: a) Truncated octahedral cage (β -cage) of the ZIF-8 framework structure. The zinc cations are tetrahedrally coordinated by the linker 2-methylimidazolate; b) sodalite (SOD) topology of ZIF-8; c) illustration of a pore opening corresponding to a six-membered ring of ZnN₄ tetrahedra and linker molecules; d) comparison of the crystallographically estimated pore diameter with the kinetic diameters of a number of small gas molecules.

Also the solvent may affect the framework structure. For example, in the case of benzimidazolate, the synthesis in DMF (N,N-dimethylformamide) yields ZIF-7, while in DEF (N,N-diethylformamide) ZIF-11 is obtained.^[10] While zinc compounds with unsubstituted imidazolates exhibit a large number of polymorphous forms,^[19-22] the polymorphism of substituted zinc imidazolates is significantly restricted due to the stereochemical requirements of the bulky substituents. This results in an increased thermal and chemical stability. A number of ZIFs shows long term stability against boiling solvents such as methanol and benzene or even water and aqueous sodium hydroxide solutions.^[10] The thermal stability can reach 400 °C in air and even higher temperatures under inert gas atmosphere. Such properties are rarely

found for other MOFs. For example, most carboxylate-based MOFs are not stable against water. Because of this combination of properties, ZIFs seem to be promising candidates for application as gas-separating membranes.

In this work, ZIF-8 plays the central role. This material combines all properties mentioned above. The three-dimensional pore network consists of large cages with a free diameter of 11.6 Å and small openings with a free diameter of 3.4 Å (see Figure 3).

1.3 Potential Applications

Potential applications for MOFs are gas storage and separation, catalysis, sensor systems and biomaterials, similarly to other porous materials like zeolites or mesoporous silica.

1.3.1 Separation

The gas separation properties of MOFs are affected by two mechanisms: (i) Separation caused by different diffusivities, which is in turn caused by different sizes and shapes and (ii) separation caused by adsorbate-surface interactions. Separation caused by different diffusivities (i) is based on Fick's first law, which includes the coefficient of diffusion, the flux density and the gradient of concentration. An extreme case is the sterical size exclusion also known as molecular sieving effect, which is size- and shape-selective, as defined by the geometry of the specific pore windows of the networks. Larger molecules are discriminated and their coefficient of diffusion is extremely low. The adsorbate-surface interactions (ii) are caused by multipolar and van der Waals interactions, depending on the surface properties of the pore walls. Gas species with stronger interactions with the framework stay longer in the pore system while non-interacting molecules can pass the system easily until an equilibrium is established. In most cases, both mechanisms control the permeance, which is defined as the pressure-normalized flux.

Besides adsorptive separation techniques, gas-separating membranes, which are already established for zeolites, are an important application. MOF membranes can be divided into two classes: (i) Supported polycrystalline membranes and (ii) organic polymer-MOF composite membranes (mixed matrix membranes).

In the last few years, the number of publications dealing with polycrystalline MOF membranes increased strongly.^[23] Only a few publications deal with carboxylate MOFs like HKUST-1^[24-26], MIL-53^[27] or MOF-5^[28-29]. However, the strongest development happened in the field of ZIFs (see also chapter 5),^[12-17, 30-33] which is due to their high thermal and chemical stability as well as their high potential in adsorption and separation of the greenhouse gas CO₂^[02]. First ZIF-69 membranes, for example, showed high separation selectivity of CO over CO₂.^[30] Also H₂ separation from larger gas molecules like CH₄, CO₂, O₂ or N₂ is possible with high selectivities with some ZIF membranes of appropriate pore diameter. Good candidates are ZIF-7^[12-13], ZIF-8 (see also chapter 5)^[30-33], ZIF-22^[14] and ZIF-90^[15-16]. Also post-synthetic modification of such membranes is possible, which leads to a

variability of the inner surface chemistry and the pore diameter. In the case of ZIF-90, aldehyde groups were transformed by a condensation reaction with amines into imine groups which enhanced the separation factor for H₂/CO₂ from 7.3 up to ~65.^[16] By using an appropriate MOF (ZIF-8) with matching pore windows and adsorption kinetics it was even possible to separate ethane and ethene^[17] or propane and propene^[31]. With this membrane also larger hydrocarbons can be separated quite easily from smaller gases like H₂ with high selectivities (see section 5.3).

Mixed matrix membranes were also achieved with MOF particles. Such membranes consist of MOF particles (mostly nanoparticles) embedded in a polymer matrix. Usually used polymers are for example matrimex®, poly(vinyl acetate) or polysiloxanes. Different MOF systems were used to fabricate such membranes as MOF-5,^[34] HKUST-1,^[35-36] ZIF-8^[37-38], ZIF-90^[39] or MIL-53^[40]. An advantage of these membranes over polycrystalline membranes is the flexibility of the polymer matrix whereby the strain resistance is increased.

Besides membrane separation other applications are possible. In recent publications it was shown that MIL-101^[41], ZIF-8^[42] or MIL-53^[43] can be used as a stationary phase in columns for gas chromatography. It was demonstrated that capillaries coated with ZIF-8 nanocrystals show excellent capabilities in sieving linear alkanes from branched alkanes as well as different linear alkanes from each other. This is caused by the narrow pore windows as well as the different van der Waals interactions of the linear alkanes with the hydrophobic inner surface of ZIF-8.^[42]

1.3.2 Storage

Gas storage is a main point of interest in MOF research. Due to their properties mentioned above, MOFs seem to be perfect candidates for application in the storage of mobile energy sources like CH₄ or H₂ but also greenhouse gases like CO₂. A number of publications deal with H₂ storage in different MOFs^[44-45], but up to now no MOF achieves enough storage capacity for application. For CO₂ capture, ZIFs seem to be particularly suited materials. The group of Yaghi showed that ZIFs like ZIF-68, -69, -78 and -79 have remarkable adsorption selectivities and capacities for CO₂.^[46-48]

1.3.3 Composites

Besides mixed matrix membranes other MOF composite materials were synthesized. A crucial improvement of microporous composite materials is the better handling than bulk material as well as the possibility to synthesize hierarchical structures for better adsorption and desorption of gasses and liquids.

The first investigations on MOF composites dealt with HKUST-1^[49] and SIM-1 (Substituted Imidazolate Material 1)^[50-51] beads, which are an attractive viable alternative to bulk MOF materials for heterogeneous catalysis. HKUST-1 could also be synthesized on polymer materials.^[52-54] Beside this system nanofibers could be synthesized via electrospinning of HKUST-1^[54] and ZIF-8 (see chapter 6). The accessibility of the pore networks of the MOFs in such composites can be varied by using different amounts of polymer and bulk MOF phase. Also the usage of MOF nanoparticles for such systems is important to reach a higher surface and thereby a faster adsorption of the guests in the MOF. By the successful syntheses of ZIF-8 nanofibers and other nanoparticulate MOF materials a broad range of MOF-composites should be accessible (see chapter 6).

1.3.4 Catalysis

Another important application is heterogeneous catalysis.^[55-56] In this field, ZIF-8 plays also an important role. Bats et al. have shown by cluster density functional theory calculations, that low-coordinated zinc cations (two- or three-coordinated) at the ZIF-8 surfaces are potential Lewis acids, while negatively charged N atoms of the imidazolate linkers are potential Lewis bases.^[57] Reported examples for such catalytic activities of ZIF-8 are Knoevenagel^[58] condensations and transesterifications^[59]. The usage of metal clusters encapsulated in MOFs is also an important option for catalysis. Some groups have shown that it is possible to deposit metal clusters like gold or platinum into the cages of MOF-5, ZIF-8 and ZIF-90 via chemical vapor deposition of organometallic precursors and subsequent reduction with H₂.^[60-63] Au@ZIF-8 shows a high catalytic activity in the oxidation of benzyl alcohol in methanol and benzene as well as in the oxidation of carbon monoxide^[61-62], while Pt@ZIF-8 shows good photocatalytic properties in the degradation of phenol when it is encapsulated in TiO₂ nanotubes.^[63]

Very recently, the group of Fischer showed the selective dehydrocoupling of BH₃·NMe₂H to yield BH₂·NMe₂ and H₂. This reaction works at room temperature in ZIF-8 cages and has a possible application in hydrogen storage based on

aminoboranes.^[64] Mild reaction conditions can be applied because of the heterogeneous catalytic properties of ZIF-8 by combining strong cage effects with polar and Lewis acid / base properties.

1.3.5 Sensors

Because of the variability of metal-organic frameworks, some MOFs can act as sensors. Some MOF sensors have been described which work with luminescent MOFs containing lanthanide cations^[65], but recent publications have shown the prospects of ZIF-8 to act as sensor material, too. Thin films of ZIF-8 of different thickness can be used as a Fabry-Pérot device to sense different vapors and gases.^[66] Furthermore, the ZIF-8 luminescence intensity shows a high sensitivity to copper and cadmium ions as well as to small molecules like acetone.^[67] Also thin films of ZIF-8 nanocrystals showed good selective adsorption of organic vapors over water in several cycles.^[68] All these publications indicate that ZIF-8 is an interesting candidate for sensor applications.

1.3.6 Biomaterials

MOFs offer many prospects in biomedical applications. They can act for example as drug delivery systems or as bioactive MOF.^[69] A recent publication has shown first results with ZIFs as drug encapsulator. An indium-containing zeolite-like metal-organic framework was used to synthesize composite materials for drug release tests using procainamide as model system. Unfortunately, this system exhibits a burst release effect.^[70]

1.4 Size- and Morphology Controlled Syntheses of MOFs

1.4.1 Common Synthesis

The synthesis of MOFs and ZIFs is usually carried out solvothermally in DMF or DEF. Many of the reactants, namely metal salts and linker molecules, have a high or at least sufficient solubility in these formamides. In addition, these high boiling solvents seem to have a structure-directing character and also appear to exert an influence on the crystallinity. An example is the synthesis of ZIF-7 and ZIF-11. Both materials are built up from benzimidazolate and zinc ions, but have different framework topologies and different cage sizes. Whereas the usage of DMF yields the sodalite system ZIF-7, in DEF ZIF-11 with a ROH topology is produced.^[10] In some cases, the high boiling temperatures and the comparatively large size of the molecules of DEF and DMF may cause problems. During the post-synthetic activation process of MOFs, which implies the removal of the solvent and other species from the pore system by heating and / or reduced pressure, the high stress exerted in the crystals sometimes may result in the collapse of the framework structure. Alcohols can also be used to synthesize some MOF systems. With these solvents, the activation is less problematic due to the high volatility of these solvents and their usually smaller kinetic diameters. However, when using alcohols, in many cases the syntheses do not lead to highly crystalline materials.

Over the last years new methods have been developed to synthesize MOFs (or to enhance the crystallinity and / or syntheses procedures). An example is ionothermal synthesis, which employs ionic liquids as solvents *and* simultaneously structure-directing agents and which can be applied successfully to a number of MOF systems. A problem of using ionic liquids in the synthesis of MOFs is the low thermal stability of the hybrid materials. Calcination is often not possible, because removal of the ionic guests leads to a collapse of the network structure due to the strong charge coupling between the cationic guests and the anionic framework.^[71] Another example of a well-known method which was used to synthesize MOFs is mechanochemistry. Recently, Beldon et al. published a rapid room-temperature method to synthesize ZIFs mechanochemically using an ion- and liquid-assisted grinding procedure with ZnO as the zinc source.^[72]

Nevertheless, the solvothermal synthesis in DMF or other formamides is still the most common way for the preparation of MOFs. An important point of DMF and DEF is the degradation taking place at higher temperatures in the presence of a small

amount of water, leading to formate and a dialkylamine in a zinc-catalyzed reaction.^[73] These species can influence the crystallization mechanism and the crystallinity as described in section 1.4.3.

1.4.2 Methods of Size and Shape Control in MOF Synthesis

For many applications mentioned above the control over the size and shape of MOF crystals is a crucial point of interest. During the last years, different synthesis procedures were developed to reach this goal. This was first achieved by Huang et al. who directly mixed the component solutions of zinc salt and organic linker at room temperature to obtain MOF-5 nanocrystals.^[74] The morphology of the nanocrystals could be varied by using surfactants (e.g. Brij 30) or a template (ordered alumina membrane with cylindrical channels). Another method is the use of microwave-assisted solvothermal synthesis. In comparison to the solvothermal synthesis by conventional heating, the microwave heating is faster and therefore the homogeneous nucleation rate is enhanced. By this method it was possible to obtain nanoparticles of IRMOF-1 and IRMOF-3 as reported by Ni et al.^[75] and of MIL-101 as reported by Jhung et al.^[76] The nucleation rate can also be enhanced by using ultrasonic treatment. This was shown for a MOF system consisting of zinc ions and benzene-1,3,5-tricarboxylate as well as for HKUST-1 by Qiu et al.^[77] They could show that the crystals increase in size with longer ultrasonic irradiation. As in microwave syntheses, the formation of so-called hot spots (high energy at a local point) is known to occur under ultrasonic treatment, too. This may be the reason for the high homogeneous nucleation rate in these cases. Another well-known approach to MOF nanocrystals is the use of reverse microemulsions. Different types of MOFs (mostly lanthanide-containing coordination polymers) were synthesized by this method by Rieter et al.^[78-79] and Daiguebonne et al.^[80] A further method is described in section 3.2. It utilizes an excess of the bridging ligand to procedure ZIF-8 nanocrystals. An excess of the bridging benzimidazolate ligand was also used for the synthesis of ZIF-7 nanocrystals by Li and coworkers.^[12-13, 81] They also pointed out that the counter ion, in this case chloride instead of the typical nitrate, has a significant influence on the final shape of the ZIF-7 nanocrystals, which crystallize in a hexagonal crystal system. If zinc chloride was used, the nanoparticles grew to nanorods, which indicated a preferential interaction of the chloride anions with the {110} and {101} faces. In contrast, with zinc nitrate isotropic nanocrystals were obtained.^[81] This

underlines the role of counter-anions in the reaction solution to control the size and shape of porous coordination polymers.

Recently, a novel synthetic method for controlling size, morphology and crystallinity of MOFs has been developed. This so-called coordination modulation method was applied so far for some MOF systems and is described in the following section.

1.4.3 Controlled Synthesis Using Coordination Modulation

Kitagawa and coworkers have introduced the idea of coordination modulation in 2009 which offers the opportunity to gain control over the particle size and morphology by using monodentate ligands (modulators) which act as competitive ligand to the bridging ligands. These ligands can act as capping groups to restrict the growth of specific crystal faces and / or to influence the number of prenucleation units made of the corresponding metal ion and linker molecules so that the nucleation rate is reduced.^[82] A similar method was also used earlier by Fischer et al. during their in-situ investigations on MOF-5 growth. Monodentate capping ligands were added with a delay after the start of the reactions to inhibit further growth of the nanocrystals.^[83]

The coordination modulation approach was extensively investigated for the size-controlled synthesis of HKUST-1 in combination with microwave heating. It was shown that nanocrystals at high dilution can be obtained by using monocarboxylic acids as modulators, whereas at higher concentrations of the starting materials and modulator microcrystals were formed.^[84]

This approach was recently adopted by different groups. The group of Behrens has shown that the addition of benzoic acid as modulator in the synthesis of zirconium-containing MOFs (e.g. UiO-66 and UiO-67)^[85] increases the reproducibility of synthesis protocols and the crystallinity of the product. In some cases, control of size and aggregation was possible. Coordination modulation also allowed the synthesis of new zirconium MOFs with long linear dicarboxylate linkers, called PIZOFs (porous interpenetrated zirconium organic frameworks).^[86] Also a $\text{Eu}_{1-x}\text{Tb}_x$ -containing metal-organic framework for the production of luminescent films could be synthesized in a nanocrystalline form by using this approach.^[87] The group of Oh has shown that not only a size- but also a shape-control is possible with modulators.^[88]

Unfortunately all the mentioned systems are carboxylate-based MOFs. To proof this synthesis concept for other MOFs, the adoptability to MOFs containing N-heterocyclic linkers was necessary. This is successfully shown for ZIF-8 as described in section 3.3 and 4.3. These sections also present an extension of the concept by considering deprotonation modulation in addition to coordination modulation.

Based on the described functions of modulators in MOF formation it becomes furthermore understandable why DMF and DEF are such favorable solvents in MOF syntheses. Besides of the good solubility of the reactants and the possibility to act as modulator itself, DMF and DEF decompose at higher temperatures by reaction with a small amount of water to form formic acid and diamines. These species can markedly influence the formation processes by acting in coordination *and* deprotonation.

1.5 Investigations on the Mechanisms of MOF Nucleation and Growth

To gain an understanding of the crystallization processes of MOFs, in-situ and ex-situ investigations should be performed. Such studies could in turn also enable better control over crystal size and shape.

Up to now, only a few investigations of the mechanisms of growth processes of MOFs are reported and the mechanisms of nucleation are almost unexplored.^[89-90] For example, electron spray ionization mass spectrometry (ESI-MS) during the formation of a magnesium-containing MOF^[91] as well as extended X-ray absorption fine structure spectroscopy (EXAFS) during the formation of MIL-89^[92] have been used to detect prenucleation species made of multi-nuclear metal complexes (SBUs) of the final MOFs.

To gain insights into the nucleation process, scattering experiments are promising methods. For example, time-resolved in-situ dynamic light scattering was used to observe the evolution of nanoparticles of MOF-5, HKUST-1 and ZIF-8 from solution with high time resolution. For MOF-5, a burst nucleation occurs in supersaturated solutions after an initiation phase. After this, a slow particle growth follows.^[83] In contrast to that, homogeneous nucleation and particle growth occurs in parallel during the synthesis of HKUST-1, where continuous comparatively slow nucleation occurs together with fast particle growth for an extended period of time.^[93] In the case of ZIF-8 nanocrystals, a rapid growth of the primary particles to a size of ca. 50 nm occurs, while simultaneously a continuous nucleation takes place. These results are presented in sections 3.2 and 3.3. Besides light scattering, X-ray scattering experiments seem to be auspicious methods to follow the nucleation process of such systems in the small nanometer region. This was done by the group of Kapteijn, who used small-angle and wide-angle X-ray scattering experiments (SAXS/WAXS) to monitor the formation of NH₂-MIL-53 and NH₂-MIL-101, which can be synthesized from the same precursors. The initially formed NH₂-MOF-235 nanoparticles dissolved to form NH₂-MIL-101 which in turn subsequently dissolved at higher temperatures to generate NH₂-MIL-53, the thermodynamically stable phase. Unfortunately, the first detectable particles in solution had already a size of about 60 nm, which means that the first step of nuclei formation could not be monitored in this work.^[94-95] SAXS/WAXS was also used to gain insights into the formation of ZIF-8 nanocrystals. The results of these experiments are discussed in section 4.2.

In the last two years, another method, time-resolved in-situ energy dispersive X-ray diffraction (EDXRD), has increasingly been adopted to gain insights into the growth kinetics and mechanisms of MOFs, such as HKUST-1^[96], MOF-14^[97], CAU-1^[98] (Christian-Albrechts-Universität-1) and ZIF-8. Applying the Avrami-Erofe'ev model^[99-100], which describes the nucleation and growth of crystallization processes, in combination with the Sharp-Hancock method^[101], which is based on a linearization of the Avrami-Erofe'ev equation to extract kinetic parameters, it was possible to evaluate crystallization curves and obtain information about the rate-limiting reaction step. It was found to be the nucleation step in the case of HKUST-1 synthesis, and a phase-boundary reaction during crystal growth in the case of the synthesis with conventional heating for CAU-1. Also a decoupling of the kinetics of nucleation and crystal growth is possible by applying the Gualtieri model.^[102] In the case of HKUST-1 and MOF-14 the Gualtieri model suggested that nucleation is the rate-limiting reaction step. This observation was also recently made for the formation of ZIF-8 nanocrystals by Venna et al. They applied ex-situ XRD diffraction and the Avrami-Erofe'ev method.^[103] By using time-resolved in-situ EDXRD measurements, a formate-modulated solvothermal synthesis of ZIF-8 was also monitored, which is discussed in section 4.3.

In-situ AFM investigations lead also to new insights into crystal growth. The group of Attfield has shown with this approach that HKUST-1 grows by a layer-by-layer mechanism of a constituent 1.5 nm crystal spacing step. In addition it was shown that defects form in the course of crystal growth.^[104-105] The same system was analyzed by Szelagowska-Kunstman et al. with ex-situ AFM.^[106]

1.6 Supported Polycrystalline MOF Membrane Synthesis

As mentioned before, gas-separating membranes are interesting applications for porous MOFs. So far, only a few systems have been prepared as supported polycrystalline membranes: HKUST-1^[24-26], MOF-5^[28-29], MIL-53,^[27] ZIF-8 (see chapter 5)^[17, 31-33], ZIF-7^[11-12], ZIF-90^[15-16], ZIF-22,^[14] ZIF-69^[30] and SIM-1^[107]. As can be seen, ZIF systems are in the center of attention due to their high thermal and chemical stability as well as variability of the pore systems. Important characteristics of such polycrystalline membranes are dense, defect-free and well intergrown crystal layer. Also the thickness of the layer and the orientation of the crystals in respect to the support surface play a significant role. The thinner the membranes are, the better is the permeate flux. In the case of non-cubic MOF crystals, the orientation of the channels has to be perpendicular to the support surface in order to permit the gas flow. As is the case for zeolite membranes, polycrystalline MOF membranes can be synthesized in two different ways: (i) In-situ crystallization and (ii) seeding and subsequent secondary growth. For both methods, asymmetric porous ceramic discs, for example of TiO₂ or α -Al₂O₃, were most commonly used as support.

1.6.1 In-Situ Crystallization

In the in-situ crystallization process the MOF layer is directly prepared on the surface of a porous ceramic support in a one-step synthesis. This approach has worked for many MOF systems such as MOF-5^[28], ZIF-8^[17] (see also section 5.2) and SIM-1^[107].

During such syntheses, heterogeneous nucleation on the support surface has to take place. After nuclei formation a growth process follows. The thickness of this layer is directly related to the number and density of nuclei generated at the support surface, because a larger number of nuclei can intergrow more easily. To increase the density of nuclei species, the affinity of the precursors to the surface of the support has to be high. This affinity is affected by a number of factors such as charge and functional groups on the surfaces of the support as well as the precursors and particles. Also competitive homogeneous nucleation in the solution, which depends on the supersaturation and the time for the homogeneous formation of nuclei, plays a role. By measuring the zeta-potential as function of the pH value for the MOF systems as well as for the support materials, a prediction of the most suitable support is possible on the basis of opposite charges. This was used for the in-situ synthesis of a ZIF-8 membrane. ZIF-8 nanoparticles exhibit a strongly positive zeta potential in

methanol. To support the growth of this system on the surface, a ceramic was chosen which exhibits a negative surface charge, as described in section 5.2.

It is also possible to modify the surface of the ceramics by introducing functional groups via surface reactions or by using charged organic polymers to reverse the charge on the surface. In the case of a ZIF-22 membrane the surface of the TiO₂ support was modified with APTES (3-aminopropyltriethoxysilane) to obtain surface amino groups. This modification offers two opportunities. On the one hand, the surface charge can be changed by variation of the pH value and on the other hand, there are free amino groups on the surface which can interact with the metal centers at the ZIF-surface via coordination bonds. It is also possible that the high surface-amine concentration helps to generate a high concentration of nuclei at the surface by deprotonation of the bridging purine ligands (local supersaturation of deprotonated linker) which in turn accelerates the surface crystallization. With these advantages of APTES modification, the synthesis of ZIF-22 membranes on TiO₂ supports was possible while in the case of non-modified TiO₂ supports dense layers could not be obtained.^[14] The same modification was used to synthesize ZIF-90 membranes on porous α -Al₂O₃ supports.^[15] Another possibility to enhance surface nucleation was introduced by Jeong et al. for the in-situ growth of ZIF-8 and ZIF-7 membranes. They dropped methanolic ligand solutions directly on an α -Al₂O₃ support preheated to 200 °C. By this procedure, Al-N coordination bonds between non-saturated aluminium ions on the support surface and the ligand molecules (2-methylimidazole and benzimidazole) could be established.^[33]

1.6.2 Seeding and Secondary Growth

The advantage of this method is the decoupling of nuclei formation and crystal growth. Nanocrystals of the MOF systems are presynthesized and then attached to the support surface. Good adhesion between support and MOF crystals can be established taking the above mentioned effects into account. For the ZIF-7 system, the polymer PEI (polyethylenimine) was chosen, which adheres to the ceramic surface via the formation of hydrogen bonds. The nanoparticles could now interact with the polymer via coordination bonds between the free amino groups and the zinc centers on the surfaces of the ZIF-7 nanocrystals.^[12-13] It was also possible to synthesize the ZIF-7 seed crystals already in the presence of this polymer, which acts as a base to accelerate nuclei formation. Hence, the method could be reduced to a

one-step procedure without prior separation and purification of ZIF-7 seed crystals. After the seeding step, a secondary growth process had to be carried out.^[81]

By the secondary growth method, control over the size and also over the orientation of the crystals in the membranes is easier to achieve than by using in-situ crystallization. Through the high concentration of the nuclei at the support surface, a dense well-intergrown layer can be obtained with a much smaller layer thickness, as shown in the case of ZIF-7 membranes.^[12-13] This has of course a positive influence on the permeate flux.

An explanation for the formation of oriented membranes starting from a layer of randomly oriented seeds is given by the evolutionary selection growth model of van der Drift.^[108] This model predicts that those faces of the seed crystals that have the highest vertical growth perpendicular to the support surface grow fastest and finally dominate the orientation of the membrane. Oriented crystals are particularly important for the preparation of MOF membranes of non-cubic MOFs as ZIF-69, which has a one-dimensional system of parallel, non-interconnecting channels running along the hexagonal *c* axis. A *c*-oriented supported ZIF-69 membrane was recently obtained by Lai and coworkers.^[30] This synthesis procedure was also adopted to produce an oriented ZIF-8 membrane which is discussed in section 5.3. But also non-oriented membranes of HKUST-1^[26] and MOF-5^[29] were fabricated by using secondary growths.

1.6.3 Further Methods

Syntheses procedures different from those described before were evaluated for the systems HKUST-1 and ZIF-8. Nan et al. has shown in a recent publication that HKUST-1 seeds can be synthesized directly on a porous α -Al₂O₃ support by dipping it step by step into the two reactant solutions.^[26] Also the synthesis of a HKUST-1 layer on a copper grid was realized in a water/ethanol solvent.^[25] In this case two copper sources were used, the nitrate salt as well as the copper grid itself. This membrane reached high separation factors for H₂ over N₂, CO₂ and CH₄. Unfortunately such metal grids are not as rigid as ceramics are. This can impair the stability of a polycrystalline layer which is quite brittle.

Venna et al. have reported that a gas separating ZIF-8 membrane can be prepared by hydrothermal reaction of an α -Al₂O₃ support in a dispersion of ZIF-8 nanocrystals.^[32] Unfortunately, the obtained membrane does not seem to be gas tight due to mesopores between the crystal grains. These layers also exhibited impurities

as can be seen on the reported XRD patterns. Another method was presented by Yao et al. They used a polymer substrate (nylon) and successfully prepared thin ZIF-8 layers on both sides of the substrate using a counter-diffusion method, in which the substrate separated the two solutions containing the zinc salt and the bridging linker.^[109]

As already mentioned, post-synthetic modifications of MOFs are possible. Recently Huang et al. have presented a post-synthetic modification of a ZIF-90 membrane to alter its hydrophobicity and thereby the separation factor for H₂/gas mixtures.^[16] This ZIF contains 2-carbaldehydeimidazolate as bridging ligand which allows a covalent functionalization via an imine condensation reaction with ethanolamine. The separation factor for H₂/CO₂ was increased by this method from 7.3 to 62.5, which is an impressive result and clearly demonstrates the opportunities and potentials of MOF membrane modification.^[16]

2. Bibliography

- [1] G. Férey, *Chem. Soc. Rev.* **2008**, 37, 191.
- [2] A. Phan, C. J. Doonan, F. J. Uribe-Romo, C. B. Knobler, M. O’Keeffe and O. M. Yaghi, *Acc. Chem. Res.* **2010**, 43, 58.
- [3] S. Kitagawa, R. Kitaura and S. Noro, *Angew. Chem., Int. Ed.* **2004**, 43, 2334.
- [4] Special Issue *Chem. Soc. Rev.* **2009**, 38.
- [5] S. Kaskel, *Chem. Ing. Tech.* **2010**, 82, 1.
- [6] M. Eddaoudi, J. Kim, N. Rosi, D. Vodak, J. Wachter, M. O’Keeffe and O. M. Yaghi, *Science* **2002**, 295, 469.
- [7] H. Furukawa, N. Ko, Y. B. Go, N. Aratani, S. B. Choi, E. Choi, A. Ö. Yazaydin, R. Q. Snurr, M. O’Keeffe, J. Kim and O. M. Yaghi, *Science* **2010**, 329, 424.
- [8] G. Férey and C. Serre, *Chem. Soc. Rev.* **2009**, 38, 1380.
- [9] X.-C. Huang, Y.-Y. Lin, J.-P. Zhang and X.-M. Chen, *Angew. Chem., Int. Ed.* **2006**, 45, 1557.
- [10] K. S. Park, Z. Ni, A. P. Côté, J. Y. Choi, R. Huang, F. J. Uribe-Romo, H. K. Chae, M. O’Keeffe and O. M. Yaghi, *Proc. Nat. Acad. Sci. USA* **2006**, 103, 10186.
- [11] D. Fairen-Jimenez, S. A. Moggach, M. T. Wharmby, P. A. Wright, S. Parson and T. Düren, *J. Am. Chem. Soc.* **2011**, 133, 8900.
- [12] Y.-S. Li, F.-Y. Liang, H. Bux, A. Feldhoff, W.-S. Yang and J. Caro, *Angew. Chem., Int. Ed.* **2010**, 49, 548.
- [13] Y. Li, F. Liang, H. Bux, W. Yang and J. Caro, *J. Membr. Sci.* **2010**, 354, 48.
- [14] A. Huang, H. Bux, F. Steinbach and J. Caro, *Angew. Chem., Int. Ed.* **2010**, 49, 4958.
- [15] A. Huang, W. Dou and J. Caro, *J. Am. Chem. Soc.* **2010**, 132, 15562.
- [16] A. Huang and J. Caro, *Angew. Chem., Int. Ed.* **2011**, 50, 4979.
- [17] H. Bux, C. Chmelik, R. Krishna and J. Caro, *J. Membr. Sci.* **2011**, 369, 284.
- [18] C. Gücüyener, J. van den Bergh, J. Gascon and F. Kapteijn, *J. Am. Chem. Soc.* **2010**, 132, 17704.
- [19] I. A. Baburin and S. Leoni, *CrystEngComm* **2010**, 12, 2809.
-

- [20] I. A. Baburin, S. Leoni and G. Seifert, *J. Phys. Chem. B* **2008**, *112*, 9437.
- [21] Y.-Q. Tian, C.-X. Cai, X.-M. Ren, C.-Y. Duan, Y. Xu, S. Gao and X.-Z. You, *Chem. Eur. J.* **2003**, *9*, 5673.
- [22] Y.-Q. Tian, Y.-M. Zhao, Z.-X. Chen, G.-N. Zhang, L.-H. Weng and D.-Y. Zhao, *Chem. Eur. J.* **2007**, *13*, 4146.
- [23] J. Gascon and F. Kapteijn, *Angew. Chem., Int. Ed.* **2010**, *49*, 1530.
- [24] J. Nan, X. Dong, W. Wang, W. Jin and N. Xu, *Langmuir* **2011**, *27*, 4309.
- [25] H. Guo, G. Zhu, I. J. Hewitt and S. Qiu, *J. Am. Chem. Soc.* **2009**, *131*, 1646.
- [26] V. V. Guerrero, Y. Yoo, M. C. McCarthy and H.-K. Jeong, *J. Mater. Chem.* **2010**, *20*, 3938.
- [27] Y. Hu, X. Dong, J. Nan, W. Jin, X. Ren, N. Xu and Y. M. Lee, *Chem. Commun.* **2011**, *47*, 737.
- [28] Y. Liu, Z. Ng, E. A. Khan, H.-K. Jeong, C. Ching and Z. Lai, *Microporous Mesoporous Mater.* **2009**, *118*, 296.
- [29] Y. Yoo, Z. Lai and H.-K. Jeong, *Microporous Mesoporous Mater.* **2009**, *123*, 100.
- [30] Y. Liu, E. Hu, E. A. Khan and Z. Lai, *J. Membr. Sci.* **2010**, *353*, 36.
- [31] K. Li, D. H. Olson, J. Seidel, T. J. Emge, H. Gong, H. Zeng and J. Li, *J. Am. Chem. Soc.* **2009**, *131*, 10368.
- [32] S. R. Venna and M. A. Carreon, *J. Am. Chem. Soc.* **2010**, *132*, 76.
- [33] M. C. McCarthy, V. Varela-Guerrero, G. V. Barnett and H.-K. Jeong, *Langmuir*, **2010**, *26*, 14636.
- [34] E. V. Perez, K. J. Balkus, J. P. Ferraris and I. H. Musselman, *J. Membr. Sci.* **2009**, *328*, 165.
- [35] J. Hu, H. Cai, H. Ren, Y. Wei, Z. Xu, H. Liu and Y. Hu, *Ind. Eng. Chem. Res.* **2010**, *49*, 12605.
- [36] R. Adams, C. Carson, J. Ward. R. Tannenbaum and W. Koros, *Microporous Mesoporous Mater.* **2010**, *131*, 13.
- [37] M. J. C. Ordoñez, K. J. Balkus, J. P. Ferraris and I. H. Musselman, *J. Membr. Sci.* **2010**, *361*, 28.
- [38] K. Díaz, L. Garrido, M. López-González, L. F. del Castillo and E. Riande, *Macromolecules* **2010**, *43*, 316.
- [39] T.-H. Bae, J. S. Lee, W. Qiu, W. J. Koros, C. W. Jones and S. Nair, *Angew. Chem., Int. Ed.* **2010**, *49*, 9863.
-

- [40] B. Zornoza, A. Martinez-Joaristi, P. Serra-Crespo, C. Tellez, J. Coronas, J. Gascon and F. Kapteijn, *Chem. Commun.* **2011**, 47, 9522.
- [41] C.-X. Yang, Y.-J. Chen, H.-F. Wang and X.-P. Yan, *Chem. Eur. J.* **2011**, 17, 11734.
- [42] N. Chang, Z.-Y. Gu. and X.-P. Yan, *J. Am. Chem. Soc.* **2010**, 132, 13645.
- [43] V. Finsy, L. Ma, L. Alaerts, D. E. De Vos, G. V. Baron and J. F. M. Denayer, *Microporous Mesoporous Mater.* **2009**, 120, 221.
- [44] J.-R. Li, R. J. Kuppler and H.-C. Zhou, *Chem. Soc. Rev.* **2009**, 38, 1477.
- [45] L. J. Murray, M. Dincă and J. R. Long, *Chem. Soc. Rev.* **2009**, 38, 1294.
- [46] R. Banerjee, A. Phan, B. Wang, C. Knobler, H. Furukawa, M. O’Keeffe and O. M. Yaghi, *Science* **2008**, 319, 939.
- [47] W. Morris, B. Leung, H. Furukawa, O. K. Yaghi, N. He, H. Hayashi, Y. Houndonougbo, M. Asta, B. B. Laird and O. M. Yagh, *J. Am. Chem. Soc.* **2010**, 132, 11006.
- [48] R. Banerjee, H. Furukawa, D. Britt, C. Knobler, M. O’Keeffe and O. M. Yaghi, *J. Am. Chem. Soc.* **2009**, 131, 3875.
- [49] L. D. O’Neill, H. Zhang and D. Bradshaw, *J. Mater. Chem.* **2010**, 20, 5720.
- [50] S. Aguado, J. Canivet and D. Farrusseng, *Chem. Commun.* **2010**, 46, 7999.
- [51] S. Aguado, J. Canivet and D. Farrusseng, *J. Mater. Chem.* **2011**, 21, 7582.
- [52] P. Küsgens, S. Siegle and S. Kaskel, *Adv. Eng. Mater.* **2009**, 11, 93.
- [53] M. G. Schwab, I. Senkovska, M. Rose, M. Koch, J. Pahnke, G. Jonschker and S. Kaskel, *Adv. Eng. Mater.* **2008**, 10, 1151.
- [54] M. Rose, B. Böhringer, M. Jolly, R. Fischer and S. Kaskel, *Adv. Eng. Mater.* **2011**, 13, 356.
- [55] J. Lee, O. K. Farha, J. Roberts, K. A. Scheidt, S. T. Nguyen and J. T. Hupp, *Chem. Soc. Rev.* **2009**, 38, 1450.
- [56] D. Farrusseng, S. Aguado and C. Pinel, *Angew. Chem., Int. Ed.* **2009**, 48, 7502.
- [57] C. Chizallet and N Bats, *J. Phys. Chem. Lett.* **2010**, 1, 349.
- [58] U. P. N. Tran, K. K. A. Le and N. T. S. Phan, *ACS Catal.* **2011**, 1, 120.
- [59] C. Chizallet, S. Lazare, D. Bazer-Bachi, F. Bonnier, V. Lecocq, E. Soyer, A.-A. Quoineaud and N. Bats, *J. Am. Chem. Soc.* **2010**, 132, 12365.
- [60] S. Hermes, M.-K. Schröter, R. Schmid, L. Khodeir, M. Muhler, A. Tissler, R. W. Fischer and R. A. Fischer, *Angew. Chem., Int. Ed.* **2005**, 44, 6237.
-

- [61] D. Esken, S. Turner, O. I. Lebedev, G. Van Tendeloo and R. A. Fischer, *Chem. Mater.* **2010**, *22*, 6393.
- [62] H.-L. Jiang, B. Liu, T. Akita, M. Haruta, H. Sakurai and Q. Xu, *J. Am. Chem. Soc.* **2009**, *131*, 11302.
- [63] T. T. Isimjan, H. Kazemian, S. Rohani and A. K. Ray, *J. Mater. Chem.* **2010**, *20*, 10241.
- [64] S. B. Kalidindi, D. Esken and R. A. Fischer, *Chem. Eur. J.* **2011**, *17*, 6594.
- [65] M. D. Allendorf, C. A. Bauer, R. K. Bhakta and R. J. T. Houk, *Chem. Soc. Rev.* **2009**, *38*, 1330.
- [66] G. Lu and T. Hupp, *J. Am. Chem. Soc.* **2010**, *132*, 7832.
- [67] S. Liu, Z. Xiang, Z. Hu, X. Zheng and D. Cao, *J. Mater. Chem.* **2011**, *21*, 6649.
- [68] A. Demessence, C. Brossière, D. Grosso, P. Horcajada, C. Serre, G. Férey, G. J. A. A. Soler-Illia and C. Sanchez, *J. Mater. Chem.* **2010**, *20*, 7676.
- [69] A. C. McKinlay, R. E. Morris, P. Horcajada, G. Férey, R. Gref, P. Couvreur and C. Serre, *Angew. Chem., Int. Ed.* **2010**, *49*, 6260.
- [70] R. Ananthoji, J. F. Eubank, F. Nouar, H. Mouttaki, M. Eddaoudi and J. P. Harmon, *J. Mater. Chem.* **2011**, *21*, 9587.
- [71] R. E. Morris, *Chem. Commun.* **2009**, *21*, 2990.
- [72] P. J. Beldon, L. Fábíán, R. S. Stein, A. Thirumurugan, A. K. Cheetham and T. Frišćić, *Angew. Chem., Int. Ed.* **2010**, *49*, 9640.
- [73] S. Hausdorf, J. Wagler, R. Mossig and F. O. R. L. Mertens, *J. Phys. Chem. A* **2008**, *112*, 7567.
- [74] L. Huang, H. Wang, J. Chen, Z. Wang, J. Sun, D. Zhao and Y. Yan, *Microporous Mesoporous Mater.* **2003**, *58*, 105.
- [75] Z. Ni and R. I. Masel, *J. Am. Chem. Soc.* **2006**, *128*, 12394.
- [76] S. H. Jung, J.-H. Lee, J. W. Yoon, C. Serre, G. Férey and J.-S. Chang, *Adv. Mater.* **2007**, *19*, 121.
- [77] L.-G. Qui, Z.-Q. Li, Y. Wu, W. Wang, T. Xu and X. Jiang, *Chem. Commun.* **2008**, *31*, 3642.
- [78] W. J. Rieter, K. M. L. Taylor, H. An, W. Lin and W. Lin, *J. Am. Chem. Soc.* **2006**, *128*, 9024.
- [79] W. J. Rieter, K. M. L. Taylor and W. Lin, *J. Am. Chem. Soc.* **2007**, *129*, 9852.
-

- [80] C. Daguebonne, N. Kerbellec, O. Guillou, J.-C. Bünzli, F. Gumy, L. Catala, T. Mallah, N. Audebrand, Y. Gérault, K. Bernot and G. Calvez, *Inorg. Chem.* **2008**, *47*, 3700.
- [81] Y.-S. Li, H. Bux, A. Feldhoff, G.-L. Li, W.-S. Yang and J. Caro, *Adv. Mater.* **2010**, *22*, 3322.
- [82] T. Tsuruoka, S. Furukawa, Y. Takashima, K. Yoshida, S. Isoda and S. Kitagawa, *Angew. Chem., Int. Ed.* **2009**, *48*, 4739.
- [83] S. Hermes, T. Witte, T. Hikov, D. Zacher, S. Bahn Müller, G. Langstein, K. Huber and R. A. Fischer, *J. Am. Chem. Soc.* **2007**, *129*, 5324.
- [84] S. Diring, S. Furukawa, Y. Takashima, T. Tsuruoka and S. Kitagawa, *Chem. Mater.* **2010**, *22*, 4531.
- [85] A. Schaate, P. Roy, A. Godt, J. Lippke, F. Waltz, M. Wiebcke and P. Behrens, *Chem. Eur. J.* **2011**, *17*, 6643.
- [86] A. Schaate, P. Roy, T. Preuße, S. J. Lohmeier, A. Godt and P. Behrens, *Chem. Eur. J.* **2011**, *17*, 9320.
- [87] H. Guo, Y. Zhu, S. Qiu, J. A. Lercher and H. Zhang, *Adv. Mater.* **2010**, *22*, 4190.
- [88] W. Cho, H. J. Lee and M. Oh, *J. Am. Chem. Soc.* **2008**, *130*, 16943.
- [89] D. Zacher, R. Schmid, C. Wöll and R. A. Fischer, *Angew. Chem., Int. Ed.* **2011**, *50*, 176.
- [90] R. E. Morris, *ChemPhysChem* **2009**, *10*, 327.
- [91] J. A. Rood, W. C. Boggess, B. C. Noll and K. W. Henderson, *J. Am. Chem. Soc.* **2007**, *129*, 13675.
- [92] S. Surblé, F. Millange, C. Serre, G. Férey and R. I. Walton, *Chem. Commun.* **2006**, *14*, 1518.
- [93] D. Zacher, J. Liu, K. Huber and R. A. Fischer, *Chem. Commun.* **2009**, *9*, 1031.
- [94] E. Stavitski, M. Goesten, J. Juan-Alcañiz, A. Martinez-Joaristi, P. Serra-Crespo, A. V. Petukhov, J. Gascon and F. Kapteijn, *Angew. Chem., Int. Ed.* **2011**, *50*, 9624.
- [95] J. Juan-Alcañiz, M. Goesten, A. Martinez-Joaristi, E. Stavitski, A. V. Petukhov, J. Gascon and F. Kapteijn, *Chem. Commun.* **2011**, *47*, 8578.
- [96] F. Millange, M. I. Medina, N. Guillou, G. Férey, K. M. Golden and R. I. Walton, *Angew. Chem., Int. Ed.* **2010**, *49*, 763.
-

- [97] F. Millange, R. El Osta, M. E. Medina and R. I. Walton, *CrystEngComm* **2011**, *13*, 103.
- [98] T. Ahnfeldt, J. Moellmer, V. Guillerm, R. Staudt, C. Serre and N Stock, *Chem. Eur. J.* **2011**, *17*, 6462.
- [99] B. V. Erofe'ev, *Compt. Rend. Acad. Sci. USSR* **1946**, *52*, 511.
- [100] M. J. Avrami, *J. Chem. Phys.* **1941**, *9*, 177.
- [101] J. D. Sharp and J. H. Hancock, *J. Am. Ceram. Soc.* **1972**, *55*, 74.
- [102] A. F. Gualtieri, *Phys. Chem. Miner.* **2001**, *28*, 719.
- [103] S. R. Venna, J. B. Jasinski and M. A. Carreon, *J. Am. Chem. Soc.* **2010**, *132*, 18030.
- [104] N. S. John, C. Scherb, M. Shoaee, M. W. Anderson, M. P. Attfield and T. Bein, *Chem. Commun.* **2009**, *41*, 6294.
- [105] M. Shoaee, M. W. Anderson and M. P. Attfield, *Angew. Chem., Int. Ed.* **2008**, *47*, 8525.
- [106] K. Szelagowska-Kunstman, P. Cyganik, M. Goryl, D. Zacher, Z. Puterova, R. A. Fischer and M. Szymonski, *J. Am. Chem. Soc.* **2008**, *130*, 14446.
- [107] S. Aguado, C.-H. Nicolas, V. Moizan-Baslé, C. Nieto, H. Amrouche, N. Bats, N. Audebrand and D. Farrusseng, *New. J. Chem.* **2011**, *35*, 41.
- [108] A. van der Drift, *Philips Res. Repts.* **1967**, *22*, 267.
- [109] J. Yao, D. Dong, D. Li, L. He, G. Xu and H. Wang, *Chem. Commun.* **2011**, *47*, 2559.
-

3. Controlling Size and Shape of ZIF-8 Crystals

3.1 Summary

This chapter deals in two publications with the rapid synthesis of ZIF-8 nanocrystals at room temperature and the further control of their size and shape using auxiliary monodentate ligands (modulators). A significant point in this work was the use of methanol as solvent instead of DMF, which is commonly used for ZIF-8 synthesis. Removal of DMF from the microporous cages is difficult and high temperatures and vacuum are needed for activation. In contrast, methanol can pass the narrow pore windows quite easily. This allows activation at room temperature applying a slightly reduced pressure. Nanocrystals with a size of about 45 nm were obtained in methanol employing an excess of the bridging ligand 2-methylimidazole with respect to the zinc salt. The size of these nanocrystals could be further controlled by using modulators in addition to an excess of the bridging ligand, which modulate the coordination and deprotonation equilibria in the reaction solutions. Different modulators were tested. Monodentate carboxylates (e.g. formate) as well as *N*-heterocyclic molecules (e.g. 1-methylimidazole) yielded micrometer-sized crystals, while *n*-alkylamines (e.g. *n*-butylamine) resulted in the rapid formation of even smaller nanocrystals. The behavior of the modulators could be qualitatively explained on the basis of the pK_a values of the conjugate acids of the monodentate ligands. The size was tunable between about 10 and 1000 nm. In the case of microcrystal formation, intermediates and the final products were characterized using scanning and transmission electron microscopy. The crystal morphology changed with time from cubes via edge-truncated cubes to rhombic dodecahedra. In addition, the crystal growth was successfully monitored in-situ using time-resolved static light scattering, which gave significant insights into the crystal formation processes. It could for example be shown, that the modulators sodium formate and 1-methylimidazole decrease the nucleation rate (coordination modulation) in respect to the non modulated synthesis, resulting in the formation of comparatively large microcrystals with narrow size distributions. On the other hand, light scattering experiments showed that the non-modulated synthesis was characterized by persistent nucleation and fast crystal growth yielding 45 nm-sized nanocrystals.

The nano- and microcrystals exhibit high thermal stability in air and large surface areas that are comparable to those of well-crystalline macrocrystals. They can be easily activated due to the use of methanol as solvent and can, for example, be applied as seeds for membrane preparation by secondary growth.

3.2 Rapid Room-Temperature Synthesis and Characterization of Nanocrystals of a Prototypical Zeolitic Imidazolate Framework

Janosch Cravillon, Simon Münzer, Sven-Jare Lohmeier, Armin Feldhoff, Klaus Huber and Michael Wiebcke.

Chem. Mater. **2009**, *21*, 1410-1412.

DOI: 10.1021/cm900166h

Web: <http://pubs.acs.org/doi/abs/10.1021/cm900166h>

Supporting information: <http://pubs.acs.org/doi/suppl/10.1021/cm900166h>

Reprinted with permission from J. Cravillon, S. Münzer, S.-J. Lohmeier, A. Feldhoff, K. Huber and M. Wiebcke, *Chem. Mater.* **2009**, *21*, 1410-1412.

Copyright 2009 American Chemical Society.

Rapid Room-Temperature Synthesis and Characterization of Nanocrystals of a Prototypical Zeolitic Imidazolate Framework

Janosch Cravillon,[†] Simon Münzer,[†]
Sven-Jare Lohmeier,[†] Armin Feldhoff,[‡] Klaus Huber,[§]
and Michael Wiebcke^{*†}

*Institut für Anorganische Chemie, Leibniz Universität
Hannover, Callinstrasse 9, D-30167 Hannover, Germany,
Institut für Physikalische Chemie und Elektrochemie, Leibniz
Universität Hannover, Callinstrasse 3A,
D-30167 Hannover, Germany, and Department Chemie,
Universität Paderborn, Warburger Strasse 100,
D-33098 Paderborn, Germany*

Received January 19, 2009

Revised Manuscript Received March 16, 2009

We report here a rapid room-temperature colloidal chemistry route to produce nanocrystals with a narrow size distribution of a prototypical zeolitic imidazolate framework (ZIF) material, ZIF-8.^{1,2} ZIFs^{1–7} are a new subclass of porous metal-organic frameworks (MOFs)⁸ in which divalent metal cations are linked by imidazolate anions into tetrahedral frameworks that frequently possess a zeolite topology. Most interestingly, some guest-free ZIFs, e.g., ZIF-8, are reported to exhibit, besides a large intracrystallite surface area, exceptional chemical and thermal stability,¹ a combination of properties rarely to be found among other porous MOF materials. To further tune the properties of ZIFs for specific applications in gas storage, separation, or sensing as well as to make ZIFs available as novel building blocks for advanced nanotechnology devices, it is mandatory to develop synthetic routes for the production of monodisperse nanocrystals.⁹

The chemistry of nanoscale carboxylate-based MOF materials has started to be developed only recently. Direct

mixing,¹⁰ microwave,¹¹ ultrasound,¹² and microemulsion¹³ methods have been used for synthesis and some degree of size and shape control could be achieved. The formation of stable colloidal dispersions of MOF-5 nanocrystals in the presence of a stabilizing monocarboxylate ligand has been monitored in situ by time-resolved static light scattering.¹⁴ Also, nanocrystals of MOFs have been grown on functionalized self-assembled organic monolayers.¹⁵ However, this is the first report on the synthesis and characterization of a nanoscale ZIF material.

It is also remarkable, in comparison with previous syntheses of nanoscale carboxylate-based MOFs,^{10–15} that our simple method does not need any auxiliary stabilizing agents or activation (conventional heating, microwave or ultrasound irradiation) and yields well-shaped ZIF-8 nanocrystals in the form of powders or stable colloidal dispersions. The method relies on pouring at room temperature a methanol solution of Zn(NO₃)₂·6H₂O into a methanol solution of the imidazole derivative, 2-methylimidazole (Hmim). It is important to add Hmim in excess to the zinc source, contrary to reported protocols^{1,2} that were designed to produce large microcrystals and used the zinc salt and Hmim in a molar ratio ≤ 1:2. We obtained good results when employing Zn(NO₃)₂·6H₂O, Hmin, and methanol in a molar ratio of approximately 1:8:700 (details are provided in the Supporting Information).

Comparison of an X-ray diffraction (XRD) pattern taken from a powder sample with a pattern simulated from known structural data¹ (see Figure S1 in the Supporting Information) demonstrates that the product is single-phase ZIF-8 material. An average particle diameter of 46 nm is estimated from the broadening of the XRD peaks. Secondary electron micrographs (Figure 1a) reveal that the product consists of isometrical nanoparticles with sharp edges and a narrow size distribution. A statistical evaluation of 250 particles results in an average diameter of 40(3) nm. Considering that MOFs are easily damaged in the high-energy electron beam of a transmission electron microscope (TEM),¹⁶ a minimum dose exposure technique was applied for acquisition of high-

* Corresponding author. E-mail: Michael.Wiebcke@acb.uni-hannover.de.

[†] Institut für Anorganische Chemie, Leibniz Universität Hannover.

[‡] Institut für Physikalische Chemie and Elektrochemie, Leibniz Universität Hannover.

[§] Universität Paderborn.

- (1) Park, K. S.; Ni, Z.; Côté, A. P.; Choi, J. Y.; Huang, R.; Uribe-Romo, F. J.; Chae, H. K.; O'Keeffe, M.; Yaghi, O. M. *Proc. Natl. Acad. Sci., U.S.A.* **2006**, *103*, 10186.
- (2) Huang, X.-C.; Lin, Y.-Y.; Zhang, J.-P.; Chen, X.-M. *Angew. Chem., Int. Ed.* **2006**, *45*, 1557.
- (3) (a) Hayashi, H.; Côté, A. P.; Furukawa, H.; O'Keeffe, M.; Yaghi, O. M. *Nat. Mater.* **2007**, *6*, 501. (b) Banerjee, R.; Phan, A.; Wang, B.; Knobler, C.; Furukawa, H.; O'Keeffe, M.; Yaghi, O. M. *Science* **2008**, *319*, 939. (c) Wang, B.; Côté, A. P.; Furukawa, H.; O'Keeffe, M.; Yaghi, O. M. *Nature (London)* **2008**, *453*, 207. (d) Morris, W.; Doonan, C. J.; Furukawa, H.; Banerjee, R.; Yaghi, O. M. *J. Am. Chem. Soc.* **2008**, *130*, 12626.
- (4) Wu, H.; Zhou, W.; Yildirim, T. *J. Am. Chem. Soc.* **2007**, *129*, 5314.
- (5) Tian, Y.-Q.; Zhao, Y.-M.; Chen, Z.-X.; Zhang, G.-N.; Weng, L.-H.; Zhao, D.-Y. *Chem.-Eur. J.* **2007**, *13*, 4146.
- (6) (a) Wu, T.; Bu, X.; Liu, R.; Lin, Z.; Zhang, J.; Feng, P. *Chem.-Eur. J.* **2008**, *14*, 7771. (b) Wu, T.; Bu, X.; Zhang, J.; Feng, P. *Chem. Mater.* **2008**, *20*, 7377.
- (7) Baburin, I. A.; Leoni, S.; Seifert, G. *J. Phys. Chem. Soc.* **2008**, *112*, 9437.
- (8) Yaghi, O. M.; O'Keeffe, M.; Ockwig, N. W.; Chae, H. K.; Eddaoudi, M.; Kim, J. *Nature (London)* **2003**, *423*, 705.
- (9) Tosheva, L.; Valtchev, V. P. *Chem. Mater.* **2005**, *17*, 2494.
- (10) Huang, L.; Wang, H.; Chen, J.; Wang, Z.; Sun, J.; Zhao, D.; Yan, Y. *Microporous Mesoporous Mater.* **2003**, *58*, 105.
- (11) (a) Ni, Z.; Masel, R. I. *J. Am. Chem. Soc.* **2006**, *128*, 12394. (b) Jung, S. H.; Lee, J.-H.; Yoon, J. W.; Serre, C.; Férey, G.; Chang, J. S. *Adv. Mater.* **2007**, *19*, 121.
- (12) Qiu, L.-G.; Li, Z.-Q.; Wu, Y.; Wang, W.; Xu, T.; Jiang, X. *Chem. Commun.* **2008**, 3642.
- (13) Rieter, W. J.; Taylor, K. M. L.; An, H.; Lin, W.; Lin, W. *J. Am. Chem. Soc.* **2006**, *128*, 9024. (b) Rieter, W. J.; Taylor, K. M. L.; Lin, W. *J. Am. Chem. Soc.* **2007**, *129*, 9852. (c) Daigubonne, C.; Kerbellec, N.; Guillou, O.; Bünzli, J.-C.; Gumy, F.; Catala, L.; Mallah, T.; Audebrand, N.; Géraud, Y.; Bernot, K.; Clavez, G. *Inorg. Chem.* **2008**, *47*, 3700.
- (14) Hermes, S.; Witte, T.; Hikov, T.; Zacher, D.; Bahnmüller, S.; Langstein, G.; Huber, K.; Fischer, R. A. *J. Am. Chem. Soc.* **2007**, *129*, 5324.
- (15) (a) Hermes, S.; Schröder, F.; Chelmoski, R.; Wöll, C.; Fischer, R. A. *J. Am. Chem. Soc.* **2005**, *127*, 13744. (b) Biemmi, E.; Scherb, C.; Bein, T. *J. Am. Chem. Soc.* **2007**, *129*, 8054.
- (16) (a) Lebedev, O. I.; Millange, F.; Serre, C.; Van Tendeloo, G.; Férey, G. *Chem. Mater.* **2005**, *17*, 6525. (b) Turner, S.; Lebedev, O. I.; Schröder, F.; Esken, D.; Fischer, R. A.; Van Tendeloo, G. *Chem. Mater.* **2008**, *20*, 5622.

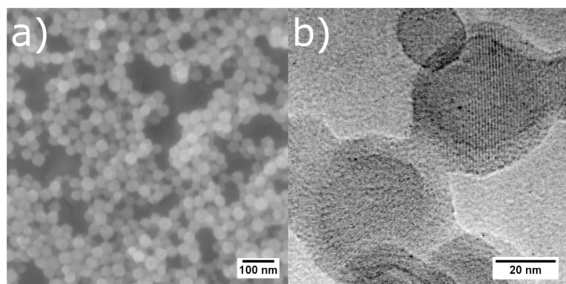


Figure 1. ZIF-8 nanocrystals prepared in methanol. (a) SEM micrograph, (b) HRTEM micrograph showing nanocrystals that exhibit lattice fringes of ca. 1.2 nm that correspond to the (110) family of planes.

resolution TEM (HRTEM) micrographs (Figure 1b). The nanocrystals were oriented on the TEM grid so that they exhibit predominantly (110) lattice fringes. Thus, the nanocrystals are approximately imaged almost along the [001] direction, and their approximate hexagonal envelope then indicates that the particles actually have the shape of a rhombic dodecahedron, that is a {110} crystal morphology (see Figure S3 in the Supporting Information).

Early stages of nanocrystal formation could be successfully monitored in situ by time-resolved static light scattering (TR-SLS). Because of the high refractive index of the nanoparticles and their rapid growth, the solutions had to be diluted for these experiments. As shown in Figure 2 for the 1:5:1000 Zn:Hmim:MeOH molar ratio, ca. 130 s after mixing the component solutions, particles with a radius of gyration R_g of ca. 20 nm had been formed. During the 170 s following, the weight averaged particle mass M_w increased further, whereas the corresponding size of the particles remained essentially constant in this growth period. This apparent contradiction can be explained by means of the different averages of the R_g and M_w values, respectively.

The radius of gyration R_g is a square root of the z-averaged squared radius of gyration $\langle S^2 \rangle_z$

$$R_g^2 = \langle S^2 \rangle_z = \frac{\sum_i n_i M_i^2 \langle S \rangle_i}{\sum_i n_i M_i^2}$$

and the molar mass value M_w is a weight averaged value.

$$M_w = \frac{\sum_i n_i M_i^2}{\sum_i n_i M_i}$$

In both averages, i denotes the number of elementary units forming a nanoparticle and n_i and M_i are the number and the molar mass of this nanoparticle, respectively. The scattering signals average over all species of nanoparticles with variable i including elementary units or monomers, which are not yet incorporated into particles. A situation with the size values staying constant but with mass values increasing is observed if single particles grow very fast compared to the duration of our time-resolved experiment. In such a case, the mass fraction of nanoparticles does not increase because of a growth of particles with time but because of an increase in the number of particles due to a

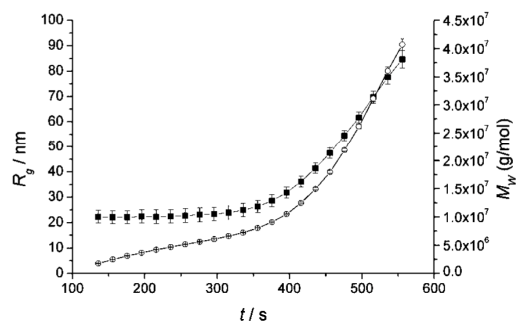


Figure 2. Growth of ZIF-8 nanocrystals in methanol (1: 5:1000 Zn:Hmim:MeOH). Radius of gyration R_g vs time (squares) and weight-averaged particle mass M_w vs time (spheres).

continuous nucleation. Such a process still affects the weight average of the mass, whereas the higher z-average of the squared size has already reached its final value. The results thus indicate the existence of an intermediate (primary) nanocrystal with $R_g \approx 20$ nm, which by assuming a spherical particle corresponds to a diameter of ~ 50 nm ($R_{\text{sphere}} = (5/3)^{1/2} R_g$). This nicely agrees with the XRD and TEM results.

Beyond 300 s, both the particle size and mass further increased, indicating an acceleration of the growth process, which likely is due to an agglomeration of primary nanocrystals. A correlation between the radius of gyration and the corresponding mass in this regime of agglomeration led to a power law behavior for $R_g \approx M_w^a$ with an exponent of $0.65 < a < 0.75$. This exponent is well above the value of a compact sphere or cube ($a = 1/3$) and indicates a fractal dimension $1/a$ that corresponds to a loose aggregate of constituent nanocrystal particles. During syntheses, it was observed that sedimentation from the milky synthesis mixtures occurred only very slowly.

Stable, slightly turbid colloidal dispersions were obtained by redispersing the nanocrystals in methanol and studied by dynamic light scattering (DLS) as well as small-angle X-ray scattering (SAXS). A hydrodynamic diameter of 49 nm and a polydispersity index (PDI) of 0.09 were obtained by DLS (see Figure S5 in the Supporting Information), whereas the SAXS data show that isometrical nanoparticles with an average $R_g = 20.4(7)$ nm are present (see Figure S6 in the Supporting Information).

Thermogravimetry (TG) performed on a nanoscale ZIF-8 powder sample (see Figure S7 in the Supporting Information) and temperature-dependent powder XRD (see Figure S8 in the Supporting Information) reveal that in air the nanocrystals are stable up to ca. 200 °C before decomposition of the framework structure takes place. Thus, nanoscale ZIF-8 exhibits considerable thermal stability although it is, as one would expect, of lower thermal stability than microscale ZIF-8 (up to ca. 400 °C in air,² and up to ca. 550 °C in N₂¹). Permanent microporosity of the nanoscale ZIF-8 powder is demonstrated by gas sorption analyses (see Figure S9 in the Supporting Information). From the N₂ sorption isotherms (Figure 3), an apparent specific surface area of 962 m²/g (BET method) and a micropore volume of 0.36 cm³/g are estimated for the evacuated nanocrystals. These values are

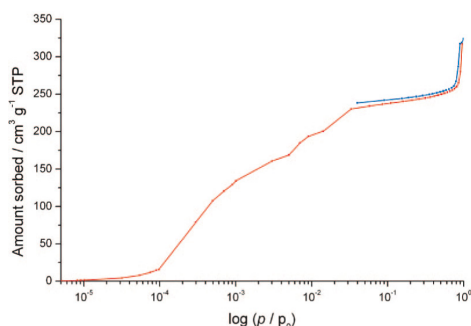


Figure 3. ZIF-8 nanocrystals prepared in methanol. Nitrogen sorption isotherms shown as linear–log plot in order to emphasize the low-pressure range. Adsorption and desorption branch are represented as red and blue curves, respectively.

lower than the highest values reported recently for microscale ZIF-8 (BET surface area: 1630 m²/g, micropore volume: 0.64 cm³/g).¹

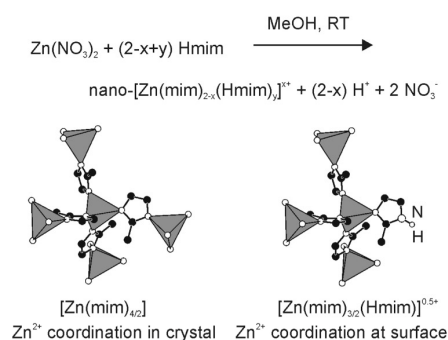
This possibly indicates that the as-synthesized nanoscale ZIF-8 still contains some residual species (e.g., unreacted Hmim) that could not be desorbed from the cavities of the nanocrystals during the activation step before the sorption measurements.

Taking together, our rapid and cheap (regarding chemicals and energy) synthetic protocol yields pure-phase nanoscale ZIF-8 material with a narrow size distribution, good thermal stability, and large accessible internal surface area. Such preformed nanocrystals should be excellent candidates for the preparation of supported ZIF films and membranes, as known for zeolites.¹⁷ Also, nanoscale microporous adsorbents and catalysts are favorable over microscale ones with regard to the mass and energy transport properties.⁹ This could be particularly beneficial for ZIF materials, which frequently possess large cavities that are connected by small apertures (as in the case of ZIF-8, ZIF-95, and ZIF-100), resulting in slow adsorption kinetics when microscale powders are used.^{3c}

We explain the formation of ZIF-8 nanocrystals with the excess of Hmim employed in the syntheses (Scheme 1).

Hmim can act both as a linker unit in its deprotonated form and as a stabilizing unit in its neutral form. If one takes

Scheme 1. Synthesis of ZIF-8 Nanocrystals Capped with Neutral 2-Methylimidazole (Hmim)



the $\text{p}K_{\text{a}1}$ (7.1) and $\text{p}K_{\text{a}2}$ (14.2) values for imidazole¹⁸ as a rough estimate for the acid–base properties of Hmim in methanol, one would expect that an equilibrium of the cationic (protonated) and neutral forms exists in solution and deprotonation of Hmim is only driven by the crystallization of ZIF-8 (gain of lattice energy). Enough neutral Hmim should then be available in solution for terminating growth and stabilizing positively charged nanocrystals. This is supported by the value (+55 mV) measured for the ζ potential of stable dispersions of ZIF-8 nanocrystals in methanol. This line of arguments suggests that our method of excess protic linker might be a general one and transferable to other ZIFs, and even carboxylate-based MOFs at low pH conditions.

Acknowledgment. Funding by the Deutsche Forschungsgemeinschaft (DFG) within the frame of the Priority Program 1362 (Porous Metal Organic Frameworks) is gratefully acknowledged.

Supporting Information Available: Experimental details as well as XRD, STEM, TR-SLS, DLS, SAXS, TG/DTA, temperature-dependent XRD, N₂, and Ar gas sorption data (PDF). This material is available free of charge via the Internet at <http://pubs.acs.org>.

CM900166H

(17) (a) Snyder, M. A.; Tsapatsis, M. *Angew. Chem., Int. Ed.* **2007**, *46*, 7560. (b) Caro, J.; Noack, M. *Microporous Mesoporous Mater.* **2008**, *115*, 215.

(18) Sundberg, R. J.; Martin, R. B. *Chem. Rev.* **1974**, *47*, 471.

3.3 Controlling Zeolitic Imidazolate Framework Nano- and Microcrystal Formation: Insight into Crystal Growth by Time-Resolved In Situ Static Light Scattering

Janosch Cravillon, Roman Nayuk, Sergej Springer, Armin Feldhoff, Klaus Huber and Michael Wiebcke.

Chem. Mater. **2011**, *23*, 2130-2141.

DOI: 10.1021/cm103571y

Web: <http://pubs.acs.org/doi/abs/10.1021/cm103571y>

Supporting information: <http://pubs.acs.org/doi/suppl/10.1021/cm103571y>

Reprinted with permission from J. Cravillon, R. Nayuk, S. Springer, A. Feldhoff, K. Huber and M. Wiebcke, *Chem. Mater.* **2011**, *23*, 2130-2141.

Copyright 2011 American Chemical Society.

Controlling Zeolitic Imidazolate Framework Nano- and Microcrystal Formation: Insight into Crystal Growth by Time-Resolved In Situ Static Light Scattering

Janosch Cravillon,[†] Roman Nayuk,[‡] Sergej Springer,[†] Armin Feldhoff,[§] Klaus Huber,^{*,†} and Michael Wiebcke^{*,†}

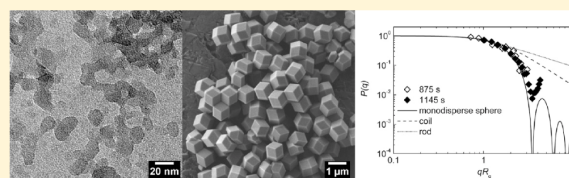
[†]Institut für Anorganische Chemie, Leibniz Universität Hannover, Callinstr. 9, 30167 Hannover, Germany

[‡]Department Chemie, Universität Paderborn, Warburger Str. 100, 33098 Paderborn, Germany

[§]Institut für Physikalische Chemie und Elektrochemie, Leibniz Universität Hannover, Callinstr. 3A, 30167 Hannover, Germany

S Supporting Information

ABSTRACT: We report on a simple and straightforward method that enables the rapid room-temperature production of nanocrystals (finely tuned in size between ~ 10 and 65 nm) and microcrystals ($\sim 1 \mu\text{m}$) of the prototypical microporous zeolitic imidazolate framework (ZIF) material ZIF-8. Control of crystal size is achieved in a novel approach by employing an excess of the bridging bidentate ligand and various simple auxiliary monodentate ligands with different chemical functionalities (carboxylate, *N*-heterocycle, alkylamine). The function of the monodentate ligands can be understood as a modulation of complex formation and deprotonation equilibria during crystal nucleation and growth. Using time-resolved static light scattering, the functioning of modulating ligands is monitored for the first time by in situ experiments, which offered significant insight into the crystal growth processes. Formation of nanocrystals is characterized by continuous, comparatively slow nucleation and fast crystal growth occurring on a time scale of seconds. Although nucleation and growth are not separated from each other, a significant narrowing of the particle size distribution during early stages results in rather monodisperse nanocrystals, before broadening of the particle size distribution occurs, as observed by complementary ex situ electron microscopy studies. Microcrystal growth is dominated by a particle–monomer addition mechanism, but indications for the operation of a coalescence process during early stages of growth have been also obtained. During later stages of microcrystal growth crystals change their shape from cubes to rhombic dodecahedra. The prepared phase-pure ZIF-8 nanoscale materials exhibit good thermal stability in air and large surface areas, which are comparable to those of large macrocrystals. Nanocrystal powders exhibit dual micro- and mesoporosity.



KEYWORDS: metal–organic framework, zeolitic imidazolate framework, nanomaterials, modulated synthesis, crystal growth, in situ static light scattering

INTRODUCTION

Zeolitic imidazolate framework (ZIF) materials¹ constitute a new distinctive, rapidly developing subclass of crystalline porous coordination polymers (PCPs) or metal–organic frameworks (MOFs).² For example, bulk ZIF materials³ and supported ZIF membranes and films⁴ have shown promising properties in the fields of CO₂ capture and storage, separation of light gases, sensing of vapors, and heterogeneous catalysis. The three-periodic tetrahedral framework structures of ZIFs are constructed from bivalent metal cations and bridging substituted imidazolate anions and frequently possess a zeolite topology.^{1,5} Numerous ZIFs combine the attractive features of MOFs (diversity of framework structures and pore systems, large surface areas, post-synthetically modifiable organic bridging ligands) with high thermal and chemical stability.⁶ It is this combination of properties which makes ZIFs very promising candidate materials for many technological applications. On the other hand, properties and performance of porous materials rely much

on their supply as nano- and microcrystals of well-defined size and shape, as is well-known for zeolites.⁷ Development of size- and shape-controlled syntheses, in turn, benefits considerably from a detailed understanding of the physicochemical fundamentals of the crystallization processes.⁸

These important issues have only scarcely been addressed in the field of porous MOFs. A limited number of carboxylate-based nanoscale MOFs have been prepared, for example, by reverse microemulsion methods and microwave- or ultrasound-assisted syntheses.^{9,10} A very attractive approach to controlling crystal size and shape that has been recently introduced is the coordination modulation method which employs an auxiliary monodentate ligand that acts in competition to the multidentate bridging ligand at surface-exposed metal centers of the forming

Received: December 15, 2010

Revised: February 24, 2011

Published: March 18, 2011

crystals.^{11,12} Such modulating ligands are usually monocarboxylates, having the same chemical functionality as the bridging polycarboxylate ligands. The power of this method has been very recently demonstrated by Kitagawa and co-workers^{12b} who were able to prepare $[\text{Cu}_3(\text{btc})_2]$ crystals (HKUST-1, btc = benzene-1,3,5-tricarboxylate) in the whole range from the small nanoscale (~ 20 nm) to the microscale (~ 2 μm). First insight into the mechanisms of carboxylate-based MOF crystallization has been obtained by a number of recent in situ investigations employing static light scattering,^{11a,13} surface plasmon resonance spectroscopy,¹⁴ atomic force microscopy,¹⁵ and energy-dispersive X-ray diffraction.¹⁶ Furthermore, the growth of nanorods of a carboxylate-based MOF by oriented attachment has been demonstrated in a remarkable ex situ electron microscopy study.^{12a}

Progress is still more limited for ZIFs. We have recently reported in a preliminary communication on a simple and rapid room-temperature solution-based synthesis of ~ 45 nm-sized ZIF-8 nanocrystals with a rhombic dodecahedral shape and a narrow size distribution.¹⁷ Such ZIF-8 nanocrystals have meanwhile been used to fabricate porous composite nanofibers by electrospinning,¹⁸ supported membranes with random¹⁹ and preferred crystal orientation for gas separation,²⁰ thin films with dual micro- and mesoporosity for selective adsorption and sensing of vapors,²¹ and capillary coatings for the chromatographic separation of alkanes,²² indicating the wide range of potential applications of nanoscale ZIF materials. Later, Thallapally and co-workers²³ have also prepared ~ 50 nm-sized ZIF-8 nanocrystals in a similar approach but with the addition of an organic polymer, claiming that the nanocrystals have a hexagonal shape. In addition, Li and co-workers²⁴ have recently reported on spherical ZIF-7 nanocrystals as well as ZIF-7 nano- and micro-rods. All these successful syntheses of nano- and microscale ZIF materials had to be developed empirically by exploratory synthetic work, since a detailed understanding of the crystallization processes is missing.

In order to gain a better understanding of the mechanisms of ZIF crystallization and thereby put the synthesis of ZIF materials on a more rational basis, we have combined systematic synthetic work with time-resolved experiments, namely, in situ static light scattering (SLS) and ex situ scanning electron microscopy (SEM). Herein, we demonstrate for the first time that various simple modulating monodentate ligands with different functionalities (sodium formate, 1-methylimidazole, *n*-butylamine) can be used in rapid room-temperature syntheses to tune the size of ZIF-8 crystals between ~ 10 nm and 1 μm . Along with this, significant insight is presented into ZIF-8 crystallization processes. We further demonstrate that the prepared nanoscale ZIF-8 materials are easily activated and exhibit good thermal stability in air as well as large surface areas.

■ EXPERIMENTAL SECTION

Materials. Commercially available chemicals were used without further purification (see Supporting Information). All syntheses were performed at ambient conditions.

Synthesis of ZIF-8 Nanocrystals in the Absence of a Modulating Ligand. Typically, 734.4 mg (2.469 mmol) of $\text{Zn}(\text{NO}_3)_2 \cdot 6\text{H}_2\text{O}$ and 810.6 mg (9.874 mmol) of 2-methylimidazole (Hmim) are each dissolved in 50 mL of MeOH. The latter clear solution is poured into the former clear solution under stirring with a magnetic bar. Stirring is stopped after combining the component solutions. After 24 h, the solid is separated from the milky colloidal dispersion by

centrifugation. Washing with fresh MeOH and centrifugation is repeated three times. The product is dried at room-temperature under reduced pressure.

Synthesis of ZIF-8 Microcrystals with Sodium Formate or 1-Methylimidazole As a Modulating Ligand. Typically, 734.4 mg (2.469 mmol) of $\text{Zn}(\text{NO}_3)_2 \cdot 6\text{H}_2\text{O}$ is dissolved in 50 mL of MeOH. A second solution is prepared by dissolving 810.6 mg (9.874 mmol) of Hmim and 810.6 mg (9.874 mmol) of 1-methylimidazole in 50 mL of MeOH. The latter clear solution is poured into the former clear solution under stirring with a magnetic bar. Stirring is stopped after combining the component solutions. After 24 h, the precipitate is recovered by filtration, washing with MeOH, and drying under reduced pressure. Syntheses in the presence of sodium formate is made similarly (see Supporting Information).

Synthesis of ZIF-8 Nanocrystals with *n*-Butylamine as a Modulating Ligand. Typically, 734.4 mg (2.469 mmol) of $\text{Zn}(\text{NO}_3)_2 \cdot 6\text{H}_2\text{O}$ is dissolved in 50 mL of MeOH. A second solution is prepared by dissolving 810.6 mg (9.874 mmol) of Hmim and 0.975 mL (9.874 mmol) of *n*-butylamine in 50 mL of MeOH. The latter clear solution is poured into the former clear solution under stirring with a magnetic bar. Stirring is stopped after combining the component solutions. After 24 h, the gel-like solid is recovered by centrifugation. Washing with fresh MeOH and centrifugation is repeated three times. The product is dried at room-temperature under reduced pressure. Syntheses with variation of the molar ratios were made similarly.

Methods of Characterization. Powder X-ray diffraction (XRD) at room temperature was performed in transmission mode on a STOE Stadi-P diffractometer using monochromatized $\text{Cu K}\alpha_1$ radiation of wavelength $\lambda = 1.54059$ Å. The instrumental peak broadening needed for Scherrer analysis was determined using a silicon reference standard (NIST 640c). For intensity data recording at variable temperatures in Debye–Scherrer geometry, the same diffractometer was equipped with a STOE high-temperature oven. Samples were filled into thin-walled silica glass capillaries (diameter 0.5 mm) which were left unsealed.

Small-angle X-ray scattering (SAXS) measurements were performed in transmission mode on a RIGAKU system consisting of a microfocus X-ray tube with Cu target and mirror optics ($\lambda = 1.541$ Å), a three-pinhole collimating system, and a 2D gas-filled multiwire detector. Colloidal solutions were filled into thin-walled glass capillaries (diameter 1.5 mm), while powder samples were kept between thin Kapton foils. SANS Analysis software²⁵ provided by the NIST Center for Neutron Research was used for model fitting of SAXS curves in reciprocal space. Indirect Fourier transformation was applied to obtain pair distance distribution functions (PDDFs)²⁶ in direct space from the SAXS data by using the program GNOM.²⁷

Thermogravimetry (TG) and difference thermal analysis (DTA) measurements were performed simultaneously on a NETZSCH 429 Thermoanalyzer. Samples were filled into alumina crucibles and heated in a flow of air with a ramp of 5 $^\circ\text{C} \cdot \text{min}^{-1}$ from room temperature up to 1000 $^\circ\text{C}$.

Nitrogen physisorption isotherms were measured at -196 $^\circ\text{C}$ on a QUANTACHROME Autosorb1-MP volumetric instrument. Samples were outgassed in vacuum at room temperature for at least 24 h before the sorption measurements. Surface areas were estimated by applying the Brunauer–Emmett–Teller (BET) equation. The Barrett–Joyner–Halenda (BJH) method was applied to determine mesopore size distributions.

Fourier-transform infrared (FT-IR) spectra were recorded on a BRUKER Tensor 27 spectrometer using the attenuated total reflection (ATR) technique.

Scanning electron micrographs (SEM) were taken in secondary electron contrast at an acceleration voltage of 2 keV using a JEOL JSM-6700F field-emission instrument. Samples were dispersed on a carbon sample holder. Transmission electron microscopy (TEM) micrographs

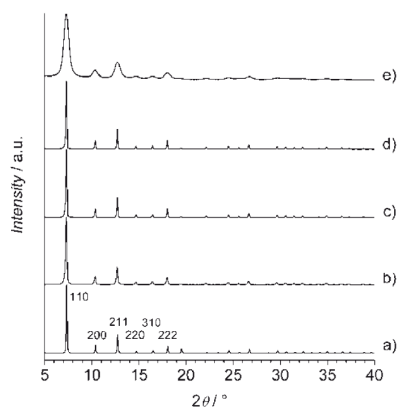


Figure 1. XRD patterns (a) simulated from crystal structure, (b) of 65 nm-sized nanocrystals prepared in the absence of a modulating ligand, (c) of microcrystals prepared in the presence of sodium formate, (d) of microcrystals prepared in the presence of 1-methylimidazole, and (e) of 18 nm-sized nanocrystals prepared in the presence of *n*-butylamine.

were taken using a JEOL JEM-2100F-UHR field-emission instrument at an acceleration voltage of 200 kV. The same instrument was used for taking selected area electron diffraction (SAED) patterns. Samples were collected with a syringe from the colloidal solutions and dispersed on a copper supported carbon film.

Time-Resolved in Situ Static Light Scattering (SLS). SLS measurements were performed at 25 °C with a home-built multi-angle goniometer described by Becker and Schmidt.²⁸ Cylindrical silica glass cuvettes with a diameter of 25 mm served as scattering cells. The goniometer was equipped with a He-Ne laser operating at a wavelength of 632.8 nm. It enabled simultaneous recording of the scattering intensity at 2 times 19 scattering angles arranged in pairs symmetrically on both sides of the beam in an angular regime of $25.84^\circ \leq \theta \leq 143.13^\circ$. Recording of an angular dependent curve was completed after 2 ms. 1000 successive recordings were added to form one measurement requiring 2 s in total. The time interval between the start of the successive measurements was 10 s. The component solutions (see syntheses) were cleaned by passing the solutions through 0.20 μm filters to remove dust particles and to combine them into the scattering cell. Addition of the second component solution determined the starting point ($t = 0$) of the experiment. Scattering curves were processed as the Rayleigh ratio ΔR_θ at variable scattering angle θ .²⁹ The scattering curves could be approximated by means of a Guinier plot,³⁰ which enabled the extraction from each scattering curve the accumulated weight-averaged molar mass, M_w , and the square root of the *z*-averaged squared radius of gyration, R_g (details are provided in the Supporting Information).

RESULTS AND DISCUSSION

Our approach to the size-controlled synthesis of nano- and microscale ZIF materials is an extension of the method we have recently developed for the production of ~ 45 nm-sized ZIF-8 nanocrystals. It employs an excess of the bridging 2-methylimidazole (Hmim) ligand with respect to the Zn(II) source, $\text{Zn}(\text{NO}_3)_2 \cdot 6\text{H}_2\text{O}$, in methanolic solutions.¹⁷ This simple method works already well at room temperature without the need of any activation, for example, by conventional or microwave heating. We have now added to such ZIF-8 synthesis solutions various monodentate ligands with different chemical functionalities (carboxylate, *N*-heterocycle, alkylamine). This is in contrast to related previous work, where the coordination modulation

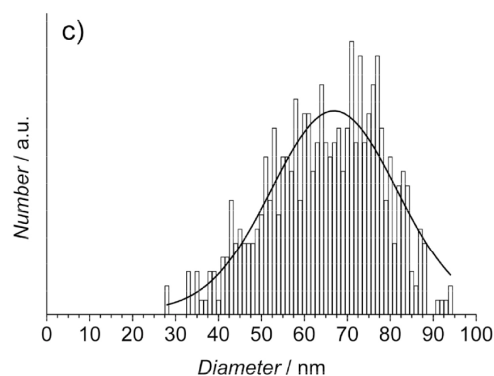
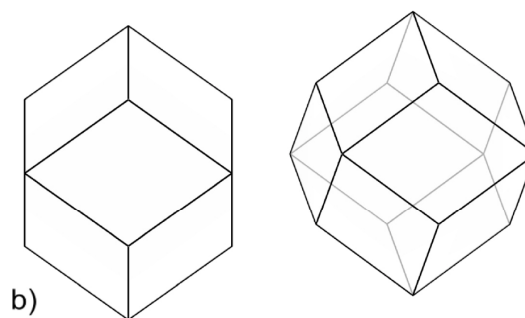
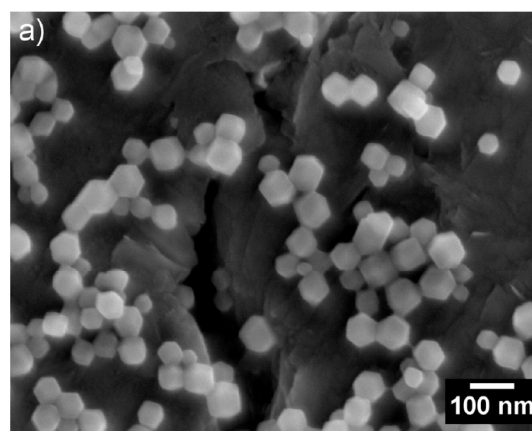


Figure 2. (a) SEM image of 65 nm-sized nanocrystals prepared in the absence of a modulating ligand, (b) drawings of a rhombic dodecahedron in two orientations, and (c) size distribution of 65 nm-sized nanocrystals (the line represents a Gaussian fit).

method has been employed in the synthesis of carboxylate-based MOFs with modulating ligands with only the same carboxylate functionality as the bridging ligands.^{11,12} We note that modulating ligands do not only act as competitive ligands at the metal centers but also as bases on the deprotonation of the bridging ligands. Thus, they may affect crystal nucleation and growth via both coordination and deprotonation equilibria. This combined effect has not been investigated and utilized before.

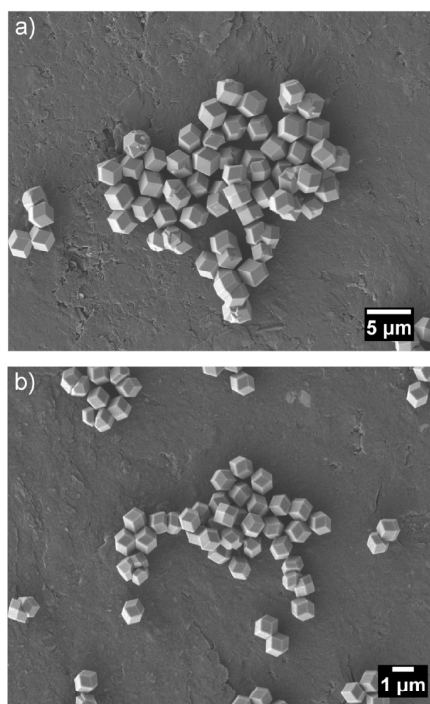


Figure 3. SEM images of (a) microcrystals prepared in the presence of sodium formate and (b) microcrystals prepared in the presence of 1-methylimidazole.

Synthesis of the Nano- and Microcrystals. We first investigated synthesis solutions with the total molar ratio $\text{Zn}/\text{Hmim}/\text{L}/\text{MeOH} = 1:4:x:1000$ (L = modulating ligand: sodium formate, 1-methylimidazole, n -butylamine). The products were isolated as described in the Experimental Section after 24 h of reaction at room temperature. The synthesis without addition of a modulating ligand ($x = 0$) yields pure-phase ZIF-8 nanocrystals (compare the XRD patterns in Figure 1a,b) with an average particle size of 64 nm, as estimated from the broadening of the Bragg reflections by applying Scherrer's equation. SEM images (Figure 2a) reveal that the well-defined nanocrystals have a rhombic dodecahedral shape (see Figure 2b for comparison) with 12 exposed $\{110\}$ faces. This is a special crystal form of the crystallographic point group $\bar{4}3m$ (in line with the cubic space group $I\bar{4}3m$ of crystalline ZIF-8).⁶ We note that rhombic dodecahedra, when viewed directly on a $\{110\}$ face, appear with a hexagonal cross-section (see drawing on the left-hand side of Figure 2b). Thus, care has to be taken not to mix up rhombic dodecahedral nanocrystals on SEM or TEM images with a hexagonal shape, which may have happened in recent work²³ (further comments on this point are given in the Supporting Information). A statistical evaluation of 500 particles results in an average size of 65 ± 13 nm (see size distribution in Figure 2c). The nanocrystals are redispersible in MeOH, yielding dispersions of nearly nonaggregated particles from which sedimentation occurs only very slowly. SAXS analysis results in an average size for the redispersed particles of 88 nm. A SAXS pattern taken from a dispersion along with a fitted curve obtained with a model of polydisperse spherical particles is provided in Figure S2 of the Supporting Information.

In the presence of formate or 1-methylimidazole as a modulating ligand at $x = 4$, pure-phase ZIF-8 microcrystals are obtained (see XRD patterns in Figure 1c,d). SEM images (Figure 3a,b) reveal a rhombic dodecahedral shape and a remarkable narrow size distribution. There is no significant difference between the products despite the quite different nature of the modulating ligands (anionic carboxylate vs neutral N-heterocyclic molecule). It should be noted that the narrow size distribution is only obtained when the synthesis solutions are not stirred. Stirring results in very broad size distributions, which may be due to secondary nucleation caused by turbulences.³¹

When n -butylamine is added as the modulating ligand at $x = 4$, nearly instantaneous formation of a solid is observed upon combining the component solutions, and pure-phase ZIF-8 nanocrystals are recovered after 24 h (see XRD pattern in Figure 1e). An average size of 18 nm is estimated from the broadening of the Bragg reflections. TEM images (Figure 4a) show roughly spherical particles being <20 nm in size, including some isolated particles and particles with sharp edges. It should be noted that the small ZIF nanocrystals are very sensitive to the high energy of the electron beam of a TEM.¹⁷ SAED patterns (Figure 4b) confirm that the particles are crystalline ZIF-8. The nanocrystals can be redispersed in MeOH. According to a SAXS analysis, the redispersed particles indicate the primary 18 nm-sized nanoparticles. Yet, they now form small secondary aggregates with a maximum size of ~ 88 nm and an average radius of gyration of $R_g = 27$ nm. A SAXS pattern along with the corresponding pair distance distribution function (PDDF) is provided in Figure S3 of the Supporting Information. The dispersions remain optically clear for a few hours, before a fine precipitate begins to form.

Then, we varied the molar ratios of the components in the system $\text{Zn}/\text{Hmim}/n\text{-butylamine}/\text{MeOH}$. Table 1 lists the compositions of the studied synthesis solutions and the average sizes of the obtained particles. XRD demonstrates that all products are pure-phase ZIF-8 (see Figure S5 of the Supporting Information). Particle sizes were determined from the powder samples by XRD (Scherrer's equation) and SAXS (PDDF), thus providing information on both the size of the crystalline domains (XRD) and the primary particles (SAXS). Compared to TEM, which is usually used to analyze primary particle size, SAXS has two advantages: (i) SAXS probes a much larger sample volume, which is therefore representative for the whole sample, and (ii) SAXS is nondestructive to ZIF nanocrystals. The PDDF, obtained by indirect Fourier transformation of a SAXS curve, is a representation of the intraparticle distance distribution, and in the case of homogeneous monodisperse spherical particles exhibits a maximum close to the radius of the spheres.²⁶ This behavior is preserved for powders consisting of spherical particles, where a maximum or shoulder is still observed at about the distance that corresponds to the radius of the primary particles.³² Representative SAXS patterns along with the corresponding PDDF curves are displayed in Figure 5 (the remaining SAXS and PDDF data are provided in Figure S4 of the Supporting Information). As can be seen from Table 1, the size values determined by XRD and SAXS are in good agreement for the products, confirming that the primary particles are crystalline ZIF-8. In addition, it can be also seen from Table 1 that by varying the compositions of the synthesis solutions, the nanocrystal size can be tuned between 9 and 65 nm. It should be noted that the volume of the smallest nanocrystals (diameter 9 nm) corresponds to only 78 unit cells of ZIF-8 (cubic cell constant $a = 1.7012$ nm).^{6b}

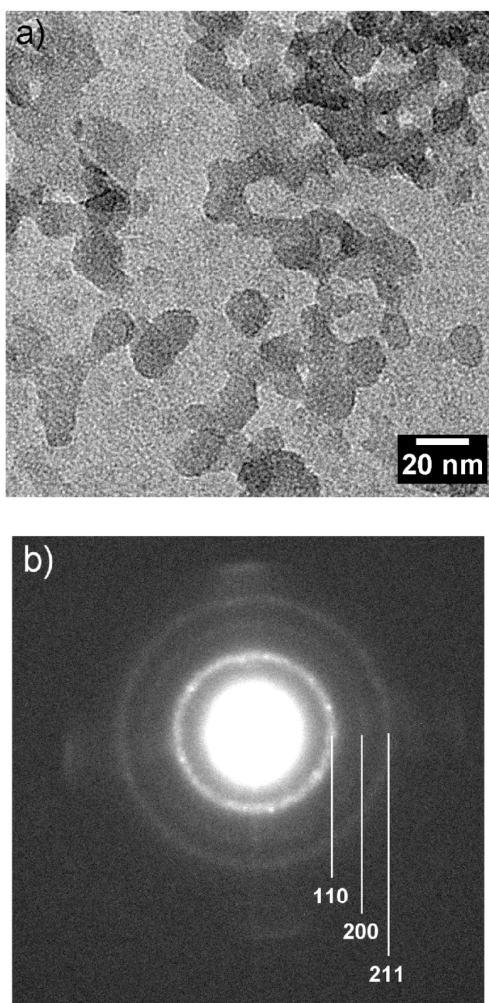


Figure 4. (a) TEM image and (b) SAED pattern of 18 nm-size nanocrystals prepared in the presence of *n*-butylamine.

By employing an excess of the bridging bidentate ligand together with different modulating ligands we have not only been able to achieve size control from the smallest nanoscale (~ 10 nm) to the microscale but, in addition, could gain new insight into the functioning of modulating ligands during MOF crystallization. In previous work,¹² only the effect of modulators on the coordination equilibria during nucleation and growth had been considered. In order to rationalize the outcome of our present syntheses we have to take deprotonation equilibria into consideration in addition to coordination equilibria. Scheme 1 summarizes in a simplified manner the basic reactions of ZIF-8 formation that have to be considered, namely, (i) complex formation, (ii) deprotonation, and (iii) ligand exchange. Due to the labile nature of Zn(II) complexes all equilibria are likely to be attained fast. Unfortunately, a complete set of the relevant complex formation constants is not available in the literature. We can, however, base a first qualitative discussion on the deprotonation constants of the conjugate acids of the ligands, which are provided in Scheme 1 in the form of pK_a values (for aqueous

Table 1. Compositions of Synthesis Solutions in the System Zn/Hmim/*n*-Butylamine/Methanol and Average Diameters of ZIF-8 Nanocrystals As Determined by XRD and SAXS

	composition	nanocrystal diameter	
	Zn/Hmim/ <i>n</i> -BuNH ₂ /MeOH	d_{XRD} , nm	d_{SAXS} , nm
(1)	1:4:4:1000	18	17
(2)	1:2:4:1000	45	39
(3)	1:4:2:1000	10	9
(4)	1:4:4:5000	24	20
(5)	1:2:4:5000	55	40
(6)	1:4:2:5000	9	9
(7)	1:4:4:500	16	16
(8)	1:2:4:500	43	42
(9)	1:4:2:500	10	8

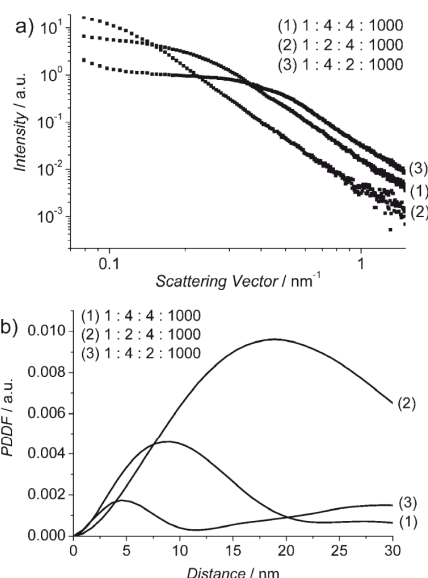
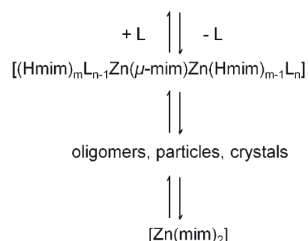
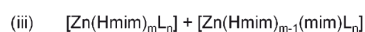
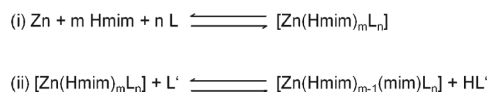


Figure 5. (a) Representative SAXS patterns and (b) inner parts of the corresponding PDDF curves of nanocrystals prepared in the presence of *n*-butylamine. Compositions of the synthesis solutions are indicated.

media, as an approximation for methanolic solutions). The list of pK_a values includes an estimate for the deprotonation constant of Hmim being bound to a Zn(II) cation, as taken from the work by Kimura et al.³³ Hereby, the following explanations can be given for the syntheses with constant total molar ratios Zn/Hmim/L/MeOH = 1:4:4:1000. An excess of Hmim in reaction (i) yields, at the beginning of ZIF-8 formation, a high concentration of $[\text{Zn}(\text{Hmim})_m\text{L}_n]$ species with $m > n$, which via deprotonation (ii) and ligand exchange (iii) results in a high nucleation rate and consequently in a small size of the final crystals (~ 65 nm in our case). Only the more basic modulating ligands with $pK_a > 10.3$ can deprotonate the $[\text{Zn}(\text{Hmim})_m\text{L}_n]$ species and thereby accelerate ligand exchange reactions, resulting in an even higher nucleation rate and consequently in a smaller final crystal size (~ 18 nm in our case). On the other hand, the less basic modulating ligands with $pK_a < 10.3$ cannot effectively deprotonate $[\text{Zn}(\text{Hmim})_m\text{L}_n]$ species but compete in reaction (i) with

Scheme 1. Basic Reactions of ZIF-8 Formation (Top) and pK_a Values for the Conjugate Acids of Relevant Ligands (Bottom)^a



ligand	pK_a
HCOOH	3.8
H ₂ mim ⁺	7.0
1-Methylimidazolium	7.2
[Zn(Hmim)] ²⁺	10.3
<i>n</i> -BuNH ₃ ⁺	10.7
Hmim	14.2

^a Charges of species are omitted in the reaction equations. L denotes all ligands that may be present: Auxiliary modulating ligands as well as NO₃⁻, H₂O, and MeOH.

Hmim, resulting in a low concentration of [Zn(Hmim)_{*m*}L_{*n*}] species with *m* > *n*, in a low nucleation rate and consequently in a large final crystal size (~1 μm in our case). The modulating ligands also affect crystal growth (see below), but their influence on nucleation appears to be more important. For a more detailed understanding, knowledge of the complex formation and deprotonation constants in methanol would be required. The results of the syntheses in the Zn/Hmim/*n*-butylamine/MeOH system at variable molar ratios (Table 1) suggest that, for targeting particular small nanocrystals, an excess of the bridging ligand is the dominating factor (e.g., compare compositions 1, 2, and 3 in Table 1). Increasing the content of the *n*-butylamine base obviously does not lead to a smaller particle size, because then its function as a competitive ligand comes into play (e.g., compare compositions 1 and 3 in Table 1).

Time-Resolved in Situ SLS and ex Situ SEM Investigations of Nanocrystal Formation. Particle formation could be successfully monitored by SLS with synthesis solutions of composition Zn/Hmim/MeOH = 1:4:1000, yielding 65 nm-sized nanocrystals. From each scattering pattern the accumulated weight-averaged molar mass, M_w , and the square root of the z-averaged squared radius of gyration, R_g , were extracted for the growing particles. The evolution with time of these parameters is displayed in Figure 6a. Nanoparticles with a radius of gyration of $R_g \approx 20$ nm (corresponding to $R_{\text{sphere}} = 26$ nm) become detectable for the first time after 130 s. The size of these particles corresponds to approximately 3/4 of the size of the final nanocrystals recovered after 24 h from the synthesis solution, and the particles are likely to be crystalline. During the following 670 s the total particle mass increases continuously, while the average particle size remains essentially constant. This apparent

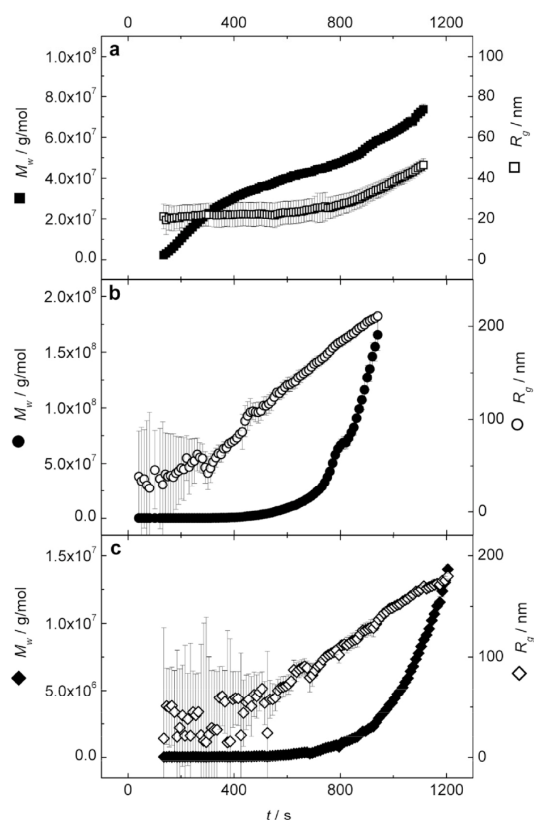


Figure 6. Weight-averaged particle mass, M_w , and radius of gyration, R_g , as they evolve with time for (a) the formation of 65 nm-sized nanocrystals in the absence of a modulating ligand, (b) the formation of microcrystals in the presence of sodium formate, and (c) the formation of microcrystals in the presence of 1-methylimidazole. Error bars are shown for R_g values.

inconsistency can be interpreted as follows. Single particles grow very fast compared to the time resolution of our experiment, and the individual growth becomes slow when a size close to $R_g = 20$ nm is attained. The increase in the averaged particle mass M_w (of a bimodal system composed of small building units and particles) is predominantly due to a continuous and comparatively slow nucleation, which increases the number of particles with time. The averaged squared size R_g^2 and the averaged mass values M_w are based on different averaging procedures. Whereas R_g^2 corresponds to the third moment, M_w is the second moment of the particle mass distribution. Thus, the average square of the size weights larger particles stronger than the average mass does. As a consequence, R_g^2 of an ever increasing ensemble of particles with similar size values approaches its final average value much earlier than M_w does.

After approximately 800 s the particle size and mass increases. This is due to a loose agglomeration of the primary nanoparticles which essentially keep their size, as evidenced by SEM investigations (see below). As can be seen from Figure 7a, this agglomeration stage is indicated by a steep upturn in the $\log(R_g)$ vs $\log(M_w)$ plot. The analysis during the agglomeration stage is impaired by an increasing turbidity of the dispersions causing multiple scattering. This results in mass values which increasingly

depart toward lower values, which prevents further quantitative interpretation of the upturn. Note that, after the beginning of the agglomeration stage, SLS can give no information anymore of whether nucleation still further continues or stops after some time.

For complementary SEM investigations, small amounts of liquid were taken from the synthesis solutions after 240 s (before the agglomeration stage) and after 1 h (during the agglomeration stage). After 240 s, spherical particles with an average size of 42 ± 11 nm and some amorphous material adhering to the particles are observed (see SEM image in Figure 8a). The particle size distribution (Figure 8c) is comparatively broad. This supports the above interpretation of the SLS data that slow, persistent nucleation and fast crystal growth take place in the early stages of nanoparticle formation. After 1 h, the nanoparticles still have nearly the same size, 38 ± 4 nm (see SEM image in Figure 8b).

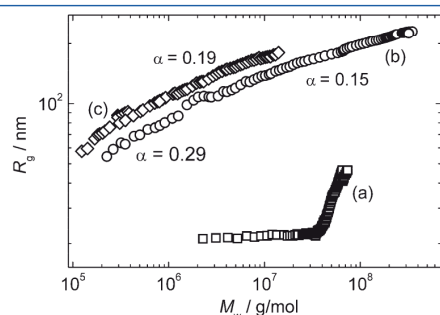


Figure 7. $\log(R_g)$ vs $\log(M_w)$ plot for (a) the formation of 65 nm-sized nanocrystals in the absence of a modulating ligand, (b) the formation of microcrystals in the presence of sodium formate, and (c) the formation of microcrystals in the presence of 1-methylimidazole.

This clearly proves that the steep increase in size and mass at 800 s observed by SLS is an agglomeration of primary nanocrystals with $R_g \approx 20$ nm. Importantly, the size distribution (Figure 8d) has become very narrow after 1 h. The nanoparticles with an age of 1 h are crystalline ZIF-8 and have a rhombic dodecahedral shape (see SEM image in Figure 8b and the detailed XRD and TEM characterization of similar nanocrystals presented elsewhere)¹⁷ as the final 65 nm-sized nanocrystals recovered after 24 h (see SEM image in Figure 2a). Note that the final nanocrystals (size 65 ± 13 nm) have a considerably broader size distribution (Figure 2c) as the nanocrystals with an age of 1 h.

Narrowing (“focusing”) of size distribution was first experimentally observed for semiconductor nanoparticles³⁴ and is reported here for the first time for a MOF. In this case, however, the narrowing of the size distribution of the primary nanocrystals at intermediate stages (after ~ 1 h) and, in particular, the very narrow size distribution at the size focusing point are rather surprising findings considering the observation by SLS that slow nucleation occurs together with fast growth at least for the first 800 s of the crystallization process. This means that nucleation and growth are not well separated from each other. Separation of both steps is usually believed to be necessary to obtain particles of low polydispersity (LaMer mechanism of burst nucleation and subsequent growth).^{8,34} The “focusing” may be explained by the termination of the fast particle growth at a size of $R_g \approx 20$ nm, due to colloidal stabilization of these intermediate particles by surface-coordinated neutral, nondeprotonated Hmim ligands that are present in excess and a corresponding build-up of positive surface charges and favorable interactions with the polar solvent. The effect of positive surface charges is supported experimentally by a zeta potential of $\xi = +55$ mV for ZIF-8 nanocrystals redispersed in MeOH.¹⁷ After supersaturation has sufficiently decreased and nucleation ceased, all nanoparticles

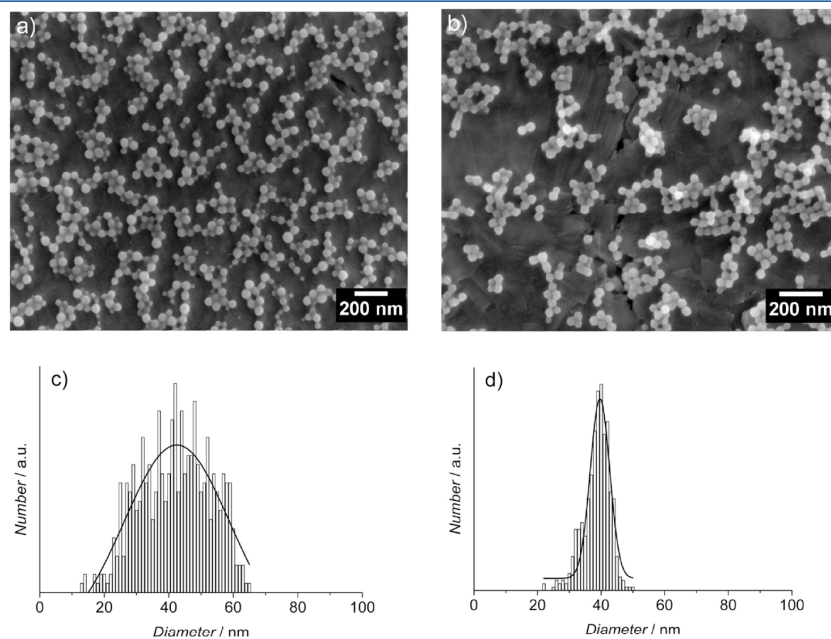


Figure 8. SEM images of intermediate particles during the formation of 65 nm-sized nanocrystals in the absence of a modulating ligand (a) after 240 s and (b) 1 h. Corresponding particle size distributions (c) after 240 s and (d) 1 h (the lines represent Gaussian fits).

terminate at nearly the same size, before “defocusing” of size distribution takes place in later stages due to growth of larger particles at the expense of smaller ones (Ostwald ripening).^{8,34} The observations clearly demonstrate that time is an important parameter to be considered when targeting monodisperse MOF nanocrystals.

Time-Resolved in Situ SLS and ex Situ SEM Investigations of Microcrystal Formation. SLS measurements were successfully performed with synthesis solutions of composition Zn/Hmim/L/MeOH = 1:4:4:1000 (L = formate and 1-methylimidazole), yielding microcrystals. The systems behave quite differently from those yielding nanocrystals. As can be seen from Figure 6b, in the case of microcrystal formation with formate as a modulating ligand, SLS enables the first significant size evaluation of particles ($R_g \approx 50$ nm) after approximately 350 s. The particle size rapidly increases with time, as does the total particle mass. Since the correlation of R_g with time is almost linear between 350 and 480 s, an estimate for the starting point of particle formation after mixing (induction time, t_{ind}) has been obtained as the intercept of the backward extrapolated curve with the abscissa ($t_{ind} = 280$ s). At 480 s, when the particles have grown to $R_g \approx 110$ nm, an abrupt change is clearly seen in the correlation of R_g with time, indicating a change in the mechanism of particle growth (see below). Beyond that point, growth in size and mass continues and could be safely monitored by SLS up to 950 s ($R_g \approx 220$ nm). Thereafter, sedimentation of larger particles was indicated by a beginning decrease of the scattering intensity.

Significant insight into the mechanism of particle growth can be obtained from the exponent α of the power law relation between R_g and M_w , $R_g \sim M_w^\alpha$. On the $\log(R_g)$ vs $\log(M_w)$ plot displayed in Figure 7b, the slope before and after 480 s corresponds to $\alpha = 0.29$ and $\alpha = 0.15$, respectively. Interestingly, these values are close to the values predicted recently by some of us²⁹ for spherical particles that grow by coalescence ($\alpha = 1/3$) or according to a monomer addition model ($\alpha = 1/6$). The same exponents are expected for particles with a cubic symmetry. The SEM investigations presented below support the assumption that intermediate particles in the course of ZIF-8 growth are isometrical. Thus, we may infer from the SLS data that ZIF-8 microcrystals grow, under the conditions studied here, by two consecutive mechanisms: (i) particle aggregation comparable to coalescence and (ii) particle–monomer attachment.

A similar pattern of growth is observed in the case of microcrystal formation with 1-methylimidazole as a modulating ligand (see Figure 6c). The first significant particle size values ($R_g \approx 50$ nm) are detected by SLS after approximately 500 s ($t_{ind} = 350$ s). The particles continuously grow in size and mass until 1200 s, corresponding to the last point shown in Figure 4c ($R_g \approx 180$ nm). However, a careful inspection of the $\log(R_g)$ vs $\log(M_w)$ plot displayed in Figure 7c reveals a bent curve, which only enables the estimate of a final slope after 800 s corresponding to $\alpha = 0.19$. Thus, we may infer from the SLS data that coalescence and monomer attachment simultaneously take place during early stages of growth, while monomer attachment dominates in later stages.

For larger particles ($R_g > 100$ nm), information on their shape can be obtained from the SLS curves. Scattering patterns with the intensity $I(q)$ in its normalized form $P(q) = I(q)/I(q=0)$ are displayed for selected intermediates of microcrystal formation in the presence of formate and 1-methylimidazole in Figure 9a,b, respectively. The data are compared with theoretically predicted

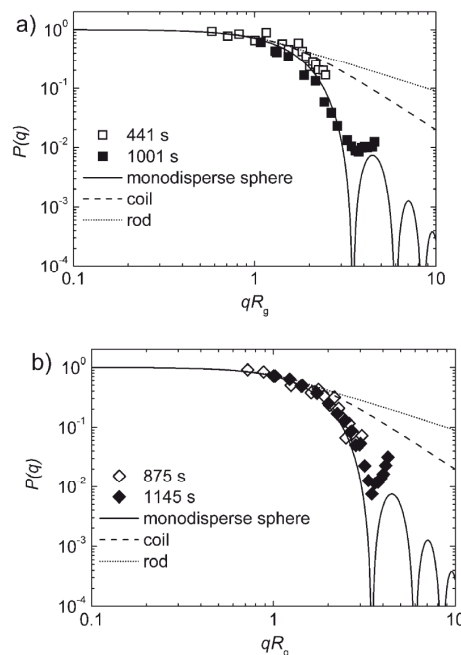


Figure 9. Normalized scattering intensity, $P(q)$, vs rescaled scattering vector modulus, $q \cdot R_g$, for two intermediates during the formation of microcrystals in the presence of (a) sodium formate and (b) 1-methylimidazole. Theoretical curves for monodisperse spheres, coils, and rods are shown for comparison.

curves for noninteracting particles of different morphologies, namely, monodisperse spheres,³⁵ coils,³⁶ and rods.³⁷ To better illustrate the shape selectivity, the scattering vector modulus q has been rescaled to the size of the particles according to $u = q \cdot R_g$. In this dimensionless representation, curves from self-similar structures fall on top of each other, if the structures differ in size only. For both modulating ligands, the individual experimental curves overlay and are close to the curve predicted for monodisperse spheres, suggesting that the particles are compact and isometrical. The first oscillation which is clearly seen in the experimental curves is a strong indication of a narrow size distribution, since increasing polydispersity results in blurring of such oscillations.¹³

Complementary SEM and TEM investigations were carried out for the synthesis with 1-methylimidazole as a modulating ligand. We were able to observe particles that are clear intermediates in the course of ZIF-8 formation after approximately 600 s, which apparently belong to the particle–monomer growth process. The first particles seen on the SEM images have the shape of a cube ($\{100\}$ crystal form) with rounded edges and a size of approximately 100 nm (see Figure 10a). After 2000 s, the particles still have the same shape but have grown to a size of 400 nm (see TEM image in Figure 10b), revealing that the relative growth rates of different faces are slowest along the $\langle 100 \rangle$ directions. The sharp spots seen on the ED pattern in Figure 10c, which is a view down a $\langle 100 \rangle$ zone axis with fourfold rotational symmetry, demonstrate that the cube-shaped particles are well crystalline ZIF-8. On the TEM image in Figure 10b, a thin rim around the nanocrystal with different electron density contrast is identified, which may, for example, indicate the presence of an

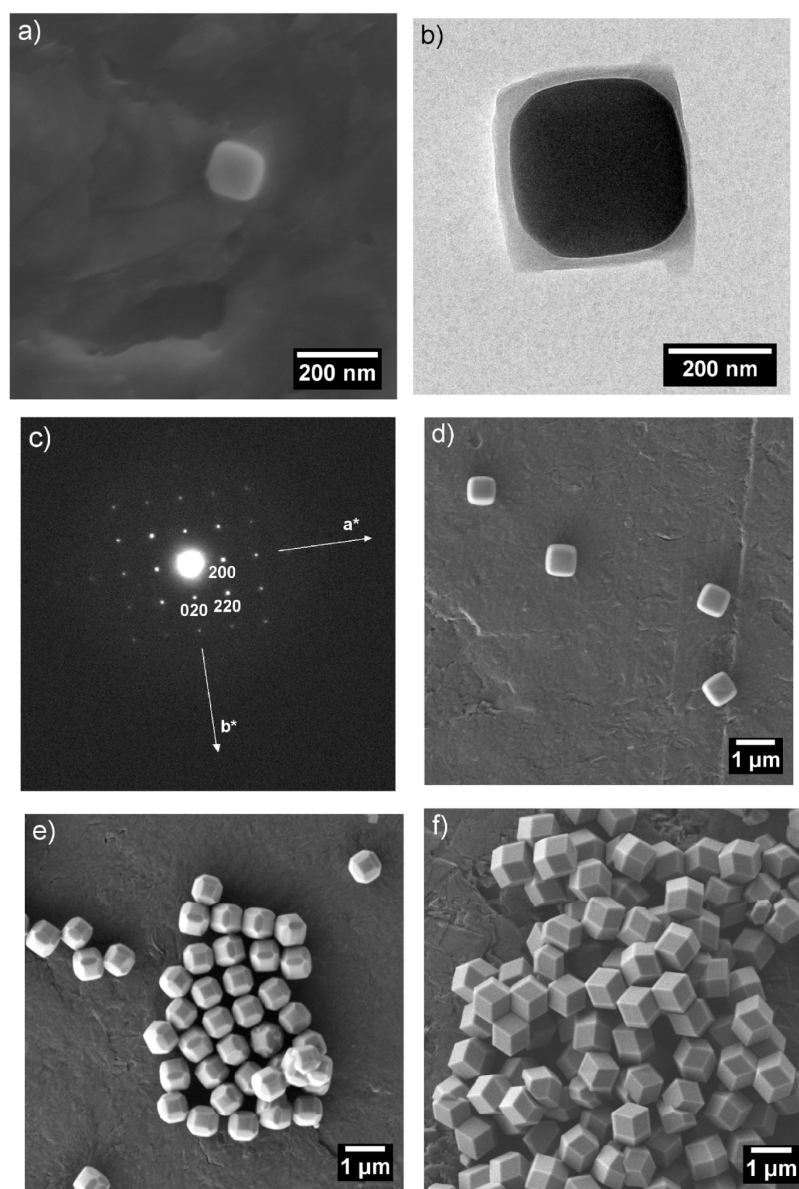


Figure 10. Intermediate particle during the formation of microcrystals in the presence of 1-methylimidazole: (a) SEM image of a particle after 600 s, (b) TEM image of a particle after 2000 s, (c) ED pattern of the particle after 2000 s, (d) SEM image of particles after 3000 s, (e) SEM image of particles after 5000 s, and (f) SEM image of particles after 24 h.

amorphous growth layer. The size distribution of the nanocrystals revealed by the SEM image taken after 3000 s (Figure 10d) appears to be rather narrow, in close agreement with the SLS data (oscillation in the scattering curve after 1145 s, Figure 9b). Beyond 4000 s, the nanocrystals change their shape due to a change in the relative growth rates, which are now slowest along $\langle 110 \rangle$ directions. On the SEM image taken after 5000 s, 500 nm-sized cubes with truncated edges that expose 6 $\{100\}$ and 12 $\{110\}$ faces are seen (Figure 10e). The micrometer-sized crystals recovered after 24 h have a rhombic dodecahedral shape with exposed $\{110\}$ faces (see SEM image in Figure 10f).

The formation of microcrystals in the presence of formate follows the same pattern of shape evolution from cubes with truncated edges to final rhombic dodecahedra (see the SEM images provided in Figure S7 of the Supporting Information). It should be noted here that SEM and TEM investigations on formate-containing systems are hampered much more seriously by species other than real ZIF-8 intermediates (e.g., sodium formate that deposits upon evaporating the dispersions prior to the SEM/TEM investigations) as is the case with 1-methylimidazole-containing systems. Due to uncertainty in the identity of species observed on SEM images taken during early stages of

ZIF-8 microcrystal formation (an example is provided in Figure S8 of the Supporting Information), we cannot up to now verify the coalescence mechanism suggested by our SLS data. Before unambiguous information can be obtained by SEM/TEM, specific procedures for separating impurities have to be developed first.

From a coordination chemistry point of view, 1-methylimidazole is expected to be a stronger coordinating ligand to Zn(II) than formate. In agreement with this, addition of 1-methylimidazole results in a lower nucleation rate, as judged from the longer induction time (350 vs 280 s), and a lower growth rate, as indicated by the slower increase of the R_g and M_W values with time. In addition, the change of shape from cubes to rhombic dodecahedra occurs at later times in the presence of 1-methylimidazole than of formate.

A comparison of the SLS data of the modulated and non-modulated syntheses points to an interesting difference between both types of crystallization processes. During the first 800 s, the apparent weight-averaged particle mass M_W recorded in the absence of a modulating ligand exceeds considerably the M_W values measured in the presence of either modulating ligand. As can be seen from Figures 6 and 7, the difference amounts to more than a magnitude. This is particularly intriguing as the particle size values are much smaller if modulating ligands are absent. However, in order to better judge this feature, the physical meaning and origin of the apparent mass values have to be briefly outlined. The values are directly taken from the intercepts of the scattering curves (see Supporting Information) and thus are proportional to the solid mass concentration times the apparent weight averaged solid mass. Now, this product can be looked at from two different perspectives:³⁹ (i) since the solid concentration in $\text{g}\cdot\text{L}^{-1}$ is a constant determined by weight and is not changing during the growth process, the intercept can be considered to be directly proportional to the weight averaged mass including all species, that is, monomers and growing particles, and (ii) the monomers can to a good approximation be considered as species with a negligible scattering contribution, which means that the intercept increases via the concentration of the generated and growing particles and/or via the growing particle mass (now excluding the monomer fraction). If we adopt the latter perspective, the discrepancy in apparent mass values for the two growth processes is immediately understandable: In the absence of modulating ligands, the increase of weight-averaged apparent mass values is due to a persisting nucleation during at least the first 800 s. In the presence of either modulating ligand, we observe a simultaneous growth of both the averaged size and the apparent mass values. Despite the much larger size values achieved in this case, the respective mass values are considerably lower because the number of particles and with it the mass concentration of particles are much lower in the latter case. This is due to the fact that the extent of nucleation has to be much lower and perhaps even ceases entirely before 800 s if modulating ligands are present. Thus, the SLS data provide clear direct evidence from in situ experiments that a function of modulating ligands of comparatively low basicity ($\text{p}K_a < 10.3$ in our case) is to slow down the nucleation rate, as proposed above and previously by Kitagawa and co-workers^{12b} on the basis of systematic synthetic work.

Investigation of Thermal Stability and Porosity. All prepared ZIF-8 materials exhibit good thermal stability in air, up to 250 °C in the case of the smaller 18 nm-sized nanocrystals, and up to 300 °C in the case of the larger nanocrystals and microcrystals. This is demonstrated by TG/DTA curves (see

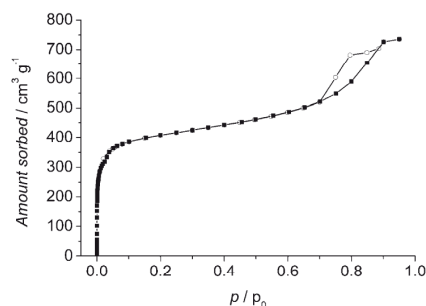


Figure 11. (a) Nitrogen sorption isotherms at $-196\text{ }^\circ\text{C}$ for the 18 nm-sized nanocrystals prepared in the presence of *n*-butylamine. Black squares: adsorption branch; open dots: desorption branch.

Figure S9 of the Supporting Information) as well as variable-temperature XRD patterns (see Figure S10 of the Supporting Information). Since nearly no mass loss is seen on the TG curves before the onset of the exothermic decomposition of the organic bridging ligand, it is clear that solvent (MeOH) and modulator molecules have already left the intracrystallite cavities during workup (drying) after synthesis. Hence, no further solvent exchange and/or heat treatment procedures are necessary for activation of the materials.

On the N_2 sorption isotherms of the 18 nm-sized nanocrystals (Figure 11), a first steep step at low relative pressure ($p/p_0 < 0.08$) is seen, revealing that the nanocrystals are microporous. The specific surface area estimated by the BET method amounts to $S_{\text{BET}} = 1617\text{ m}^2\cdot\text{g}^{-1}$. The value compares well with those reported recently for ZIF-8 macrocrystals ($S_{\text{BET}} = 1630\text{ m}^2\cdot\text{g}^{-1}$)^{6a} and ~ 30 nm-sized ZIF-8 nanocrystals ($S_{\text{BET}} = 1696\text{ m}^2\cdot\text{g}^{-1}$).²¹ This confirms that the 18 nm-sized nanocrystals are well crystalline, as already evidenced by XRD and SAED. The isotherms exhibit a second step at high relative pressure ($p/p_0 > 0.7$) with an adsorption–desorption hysteresis loop of type H2.³⁸ The step originates from interparticle mesopores, demonstrating the dual micro- and mesoporosity of the ZIF-8 nanocrystal powders. The mesopore size distribution estimated by the BJH method is centered at ~ 8 nm. Small crystal size and dual porosity are of interest for the development of advanced adsorbents and catalysts with fast mass transport kinetics. Indeed, a significant increase of adsorption rates of nanocrystals compared to microcrystals was recently demonstrated for ZIF-8 (~ 45 nm-sized nanocrystals)¹⁸ and the flexible MOF [Zn(ip)(bpy)] (CID-1, ip = isophthalate, bpy = 4,4'-bipyridyl).^{10f}

CONCLUSION

We have reported a novel synthetic approach to ZIF-8 nano- and microscale materials in which size-control between ~ 10 nm and $1\text{ }\mu\text{m}$ is achieved by employing an excess of the bridging bidentate ligand and three simple auxiliary modulating ligands that act as competitive ligands in coordination equilibria and bases in deprotonation equilibria during nucleation and growth. Time-resolved in situ SLS and ex situ SEM/TEM investigations have provided insight into the functioning of modulating ligands. Furthermore, the experiments have revealed that nanocrystal formation is characterized by continuous, comparatively slow nucleation and fast crystal growth. A focusing of the nanocrystal size distribution occurs with increasing time, resulting in a very narrow size distribution at the size focusing point, and is followed

by defocusing of the size distribution at later stages of the growth. The growth of microcrystals takes place by a particle–monomer attachment mechanism, and a change of crystal shape from cubes to rhombic dodecahedra occurs in later stages of growth. Furthermore, indications for the occurrence of a coalescence mechanism during early stages of the growth have been obtained. The prepared ZIF-8 materials are easily activated (due to the use of MeOH as the solvent) and exhibit good thermal stability in air as well as large surface areas, which are comparable to those of large macrocrystals. Nanocrystal powders exhibit dual micro- and mesoporosity.

The novel synthetic strategy and insight into the crystallization processes may help to put size- and shape-controlled syntheses of nano- and microscale bulk ZIF materials and supported ZIF membranes and films on a more rational basis. Indeed, the recent successful synthesis of ZIF-7 nanocrystals by employing an excess of the bridging benzimidazole ligand^{4b} indicates that the synthetic principles reported here may be transferable to other ZIF and possibly even to other MOF systems.

While the manuscript was under reviewing two papers appeared in the literature which are related to the work presented herein: Pan et al.⁴⁰ report the rapid synthesis of ZIF-8 nanocrystals being between ~50 and 85 nm in size. Their protocols differ from ours in the use of water (instead of MeOH) as the solvent and a much larger excess of the bridging Hmim ligand (Hmim/Zn \geq 70:1). Venna et al.⁴¹ report an ex situ XRD and TEM study of the formation of ZIF-8 nanocrystals at room temperature in the presence of an excess of the bridging Hmim ligand (Hmim/Zn = 8:1). They concluded that the crystallization process is nucleation-controlled. This is in general agreement with our findings by in situ SLS and ex situ SEM.

■ ASSOCIATED CONTENT

S Supporting Information. Details of syntheses, SLS measurements, comments on nanocrystal shape, SAXS/PDDF, SEM, XRD, TG/DTA, variable-temperature XRD, nitrogen physisorption, and FT-IR data (PDF). This material is available free of charge via the Internet at <http://pubs.acs.org>.

■ AUTHOR INFORMATION

Corresponding Author

*E-mail: michael.wiebecke@acb.uni-hannover.de (M.W.), klaus.huber@chemie.uni-paderborn.de (K.H.).

■ ACKNOWLEDGMENT

The authors thank G. Platz for performing the physisorption measurements. The work was supported by the Deutsche Forschungsgemeinschaft (DFG) within the frame of the Priority Program 1362 (Porous Metal–Organic Frameworks) organized by S. Kaskel. The authors gratefully acknowledge the funding by the DFG (Grants WI1156/2-1 and HU807/12-1).

■ REFERENCES

- (1) Phan, A.; Doonan, C. J.; Uribe-Romo, F. J.; Knobler, C. B.; O’Keeffe, M.; Yaghi, O. M. *Acc. Chem. Res.* **2010**, *43*, 58.
- (2) (a) Yaghi, O. M.; O’Keeffe, M.; Ockwig, N. W.; Chae, H. K.; Eddaoudi, M.; Kim, J. *Nature* **2003**, *423*, 705. (b) Kitagawa, S.; Kitaura,

R.; Noro, S. *Angew. Chem., Int. Ed.* **2004**, *43*, 2334. (c) Férey, G. *Chem. Soc. Rev.* **2008**, *37*, 191.

(3) (a) Banerjee, R.; Phan, A.; Wang, B.; Knobler, C.; Furukawa, H.; O’Keeffe, M.; Yaghi, O. M. *Science* **2008**, *319*, 939. (b) Banerjee, R.; Furukawa, H.; Britt, D.; Knobler, C.; O’Keeffe, M.; Yaghi, O. M. *J. Am. Chem. Soc.* **2009**, *131*, 3875. (c) Li, K.; Olson, D. H.; Seidel, J.; Emge, T. J.; Gong, H.; Zeng, H.; Li, J. *J. Am. Chem. Soc.* **2009**, *131*, 10368. (d) Morris, W.; Leung, B.; Furukawa, H.; Yaghi, O. K.; He, N.; Hayashi, H.; Houndonoubo, Y.; Asta, M.; Laird, B. B.; Yaghi, O. M. *J. Am. Chem. Soc.* **2010**, *132*, 11006. (e) Chizallet, C.; Lazare, S.; Bazar-Bachi, D.; Bonnier, F.; Lecocq, V.; Soyer, E.; Quoineaud, A.-A.; Bats, N. *J. Am. Chem. Soc.* **2010**, *132*, 12365.

(4) (a) Bux, H.; Liang, F.; Li, Y.; Cravillon, J.; Wiebecke, M.; Caro, J. *J. Am. Chem. Soc.* **2009**, *131*, 16000. (b) Li, Y.; Liang, F.; Bux, H.; Feldhoff, A.; Yang, W.-S.; Caro, J. *Angew. Chem., Int. Ed.* **2010**, *49*, 548. (c) McCarthy, M. C.; Varela-Guerrero, V.; Barnett, G. V.; Jeong, H.-K. *Langmuir* **2010**, *26*, 14636. (d) Huang, A.; Bux, H.; Steinbach, F.; Caro, J. *Angew. Chem., Int. Ed.* **2010**, *49*, 4958. (e) Lu, G.; Hupp, J. T. *J. Am. Chem. Soc.* **2010**, *132*, 7832. (f) Aguado, S.; Canivet, J.; Farrusseng, D. *Chem. Commun.* **2010**, *46*, 7999.

(5) (a) Tian, Y.-Q.; Cai, C.-X.; Ji, Y.; You, X.-Z.; Peng, S.-M.; Lee, G.-H. *Angew. Chem., Int. Ed.* **2002**, *41*, 1384. (b) Wu, T.; Zhang, J.; Zhou, C.; Wang, L.; Bu, X.; Feng, P. *J. Am. Chem. Soc.* **2009**, *131*, 6111. (c) Tian, Y.-Q.; Yao, S.-Y.; Gu, D.; Cui, K.-H.; Guo, D.-W.; Zhang, G.; Chen, Z.-X.; Zhao, D.-Y. *Chem.—Eur. J.* **2010**, *16*, 1137.

(6) (a) Park, K. S.; Ni, Z.; Côté, A. P.; Choi, J. Y.; Huang, R.; Uribe-Romo, F. J.; Chae, H. K.; O’Keeffe, M.; Yaghi, O. M. *Proc. Natl. Acad. Sci. U.S.A.* **2006**, *103*, 10186. (b) Huang, X.-C.; Lin, Y.-Y.; Zhang, J.-P.; Chen, X.-M. *Angew. Chem., Int. Ed.* **2006**, *45*, 1557.

(7) Tosheva, L.; Valtchev, V. P. *Chem. Mater.* **2005**, *17*, 2494.

(8) Park, J.; Joo, J.; Kwon, S. G.; Jang, Y.; Hyeon, T. *Angew. Chem., Int. Ed.* **2007**, *46*, 4630.

(9) (a) Spokoyny, A. M.; Kim, D.; Sumrein, A.; Mirkin, C. A. *Chem. Soc. Rev.* **2009**, *38*, 1218. (b) Lin, W.; Rieter, W. J.; Taylor, K. M. L. *Angew. Chem., Int. Ed.* **2009**, *48*, 650. (c) McKinlay, A. C.; Morris, R. E.; Horcajada, P.; Férey, G.; Gref, R.; Couvreur, P.; Serre, C. *Angew. Chem., Int. Ed.* **2010**, *49*, 6260.

(10) (a) Huang, L.; Wang, H.; Chen, J.; Wang, Z.; Sun, J.; Zhao, D.; Yan, Y. *Microporous Mesoporous Mater.* **2003**, *58*, 105. (b) Qiu, L.-G.; Li, Z.-Q.; Wu, Y.; Wang, W.; Xu, T.; Jiang, X. *Chem. Commun.* **2008**, 3642. (c) Taylor-Pashow, K. M. L.; Rocca, J. D.; Xie, Z.; Tran, S.; Lin, W. *J. Am. Chem. Soc.* **2009**, *131*, 14261. (d) Horcajada, P.; Chalati, T.; Serre, C.; Gillet, B.; Sebrie, C.; Baati, T.; Eubank, J. F.; Heurtaux, D.; Clayette, P.; Kreuz, C.; Chang, J.-S.; Hwang, Y. K.; Marsaud, V.; Bories, P.-N.; Cynober, L.; Gil, S.; Férey, G.; Couvreur, P.; Gref, R. *Nat. Mater.* **2010**, *9*, 172. (e) Guillemin, V.; Gross, S.; Serre, C.; Devic, T.; Bauer, M.; Férey, G. *Chem. Commun.* **2010**, *46*, 767. (f) Tanaka, D.; Henke, A.; Albrecht, K.; Moeller, M.; Nakagawa, K.; Kitagawa, S.; Groll, J. *Nat. Chem.* **2010**, *2*, 410.

(11) (a) Hermes, S.; Witte, T.; Hikov, T.; Zacher, D.; Bahn Müller, S.; Langstein, G.; Huber, K.; Fischer, R. A. *J. Am. Chem. Soc.* **2007**, *129*, 5324. (b) Horcajada, P.; Serre, C.; Grosso, D.; Boissière, C.; Perruchas, S.; Sanchez, C.; Férey, G. *Adv. Mater.* **2009**, *21*, 1931.

(12) (a) Tsuruoka, T.; Furukawa, S.; Takashima, Y.; Yoshida, K.; Isoda, S.; Kitagawa, S. *Angew. Chem., Int. Ed.* **2009**, *48*, 4739. (b) Diring, S.; Furukawa, S.; Takashima, Y.; Tsuruoka, T.; Kitagawa, S. *Chem. Mater.* **2010**, *22*, 4531.

(13) Zacher, D.; Lin, J.; Huber, K.; Fischer, R. A. *Chem. Commun.* **2009**, 1031.

(14) Shekhan, O.; Wang, H.; Zacher, D.; Fischer, R. A.; Wöll, C. *Angew. Chem., Int. Ed.* **2009**, *48*, 5038.

(15) John, N. S.; Scherb, C.; Shöàèè, M.; Anderson, M. W.; Atfield, M. P.; Bein, T. *Chem. Commun.* **2009**, 6294.

(16) Millange, F.; Medina, M. I.; Guillou, N.; Férey, G.; Golden, K. M.; Walton, R. I. *Angew. Chem., Int. Ed.* **2010**, *49*, 763.

(17) Cravillon, J.; Münzer, S.; Lohmeier, S.-J.; Feldhoff, A.; Huber, K.; Wiebecke, M. *Chem. Mater.* **2009**, *21*, 1410.

- (18) Ostermann, R.; Cravillon, J.; Weidmann, C.; Wiebcke, M.; Smarsly, B. M. *Chem. Commun.* **2010**, 47, 442.
- (19) Venna, S. R.; Carreon, M. A. *J. Am. Chem. Soc.* **2010**, 132, 76.
- (20) Bux, H.; Feldhoff, A.; Cravillon, J.; Wiebcke, M.; Li, Y.; Caro, J. *Chem. Mater.* **2011**, accepted.
- (21) Demessence, A.; Boissière, C.; Grosso, D.; Horcajada, P.; Serre, C.; Férey, G.; Soler-Illia, G. J. A. A.; Sanchez, C. *J. Mater. Chem.* **2010**, 20, 7676.
- (22) Chang, N.; Gu, Z.-Y.; Yan, X.-P. *J. Am. Chem. Soc.* **2010**, 132, 13645.
- (23) Nune, S. K.; Thallapally, P. K.; Dobnalkova, A.; Wang, C.; Liu, J.; Exarbos, G. J. *Chem. Commun.* **2010**, 46, 4878.
- (24) Li, Y.; Bux, H.; Feldhoff, A.; Li, G.-L.; Yang, W.-S.; Caro, J. *Adv. Mater.* **2010**, 22, 3322.
- (25) Kline, S. R. *J. Appl. Crystallogr.* **2006**, 39, 895.
- (26) Glatter, O.; Kratky, O. *Small Angle X-ray Scattering*; Academic Press: London, 1982.
- (27) Konarev, P. V.; Petoukhov, M. V.; Volkov, V. V.; Svergun, D. I. *J. Appl. Crystallogr.* **2006**, 39, 277.
- (28) Becker, A.; Schmidt, M. *Macromol. Chem. Macromol. Symp.* **1991**, 50, 249.
- (29) Liu, J.; Rieger, J.; Huber, K. *Langmuir* **2008**, 24, 8262.
- (30) Guinier, A.; Fournet, G. *Small-Angle Scattering of X-Rays*; Wiley: New York, 1955.
- (31) Mullin, J. W. *Crystallization*, 4th ed.; Butterworth-Heinemann: Oxford, 2001.
- (32) Rath, T.; Kunert, B.; Resel, R.; Fritz-Popovski, G.; Saf, R.; Trimmel, G. *Inorg. Chem.* **2008**, 47, 3014.
- (33) Kimura, E.; Kurogi, Y.; Shionoya, M.; Shiro, M. *Inorg. Chem.* **1991**, 30, 4524.
- (34) Peng, X.; Wickham, J.; Alivisatos, A. P. *J. Am. Chem. Soc.* **1998**, 120, 5343.
- (35) Rayleigh, L. *Proc. R. Soc. London, Ser. A* **1914**, 90, 219.
- (36) Debye, P. *J. Phys. Colloid Chem.* **1947**, 51, 18.
- (37) Neugebauer, T. *Ann. Phys.* **1943**, 434, 509.
- (38) Sing, K. S. W.; Everett, D. H.; Haul, R. A. W.; Moscou, L.; Pierotti, R. A.; Rouquérol, J.; Siemieniowska, T. *Pure Appl. Chem.* **1985**, 57, 603.
- (39) Liu, J.; Pancera, S.; Boyko, V.; Shukla, A.; Narayanan, T.; Huber, K. *Langmuir* **2010**, 26, 17405.
- (40) Pan, Y.; Liu, Y.; Zeng, G.; Zhao, L.; Lai, Z. *Chem. Commun.* **2011**, 47, 2071.
- (41) Venna, S. R.; Jasinski, J. B.; Carreon, M. A. *J. Am. Chem. Soc.* **2010**, 132, 18030.

4. Monitoring ZIF-8 Syntheses by Time-Resolved In-Situ Synchrotron X-ray Scattering Experiments

4.1 Summary

The results of time-resolved in-situ synchrotron X-ray scattering experiments on room temperature and solvothermal syntheses of ZIF-8 are reported in this chapter in two publications. Using small-angle and wide-angle X-ray scattering (SAXS and WAXS) at beamline ID02 of the ESRF (European Synchrotron Radiation Facility), it was possible to monitor the early stages of nucleation and growth of the non-modulated ZIF-8 nanoparticle synthesis in methanol at room temperature with a one-second time resolution. Because of the very fast reaction, a stopped-flow device was used to rapidly mix the two component solutions of zinc salt and bridging ligand before injection into a quartz glass capillary, which served as scattering cell. Instantaneously after mixing, amorphous particles (denoted prenucleation clusters) with a size of about 2 nm were observed. The number density of these clusters started to decrease after 15 seconds, while at the same time simultaneous formation and growth of ZIF-8 nanoparticles began. The number density of the ZIF-8 particles increased constantly indicating that new nanoparticles continued to nucleate. Information about the mechanism of nanocrystal growth could be inferred from the power law relation between the radius of gyration and the weight-averaged molar mass of the particles, which suggested a monomer addition mechanism in favor over particle coalescence. The earliest nanoparticles seemed to be amorphous, since Bragg reflections in the WAXS patterns were first observed after 35 seconds, that is 20 seconds after the first detection of particles. Explanations for the “missing” Bragg reflections before 35 seconds are a reorganization mechanism of the particles (the first amorphous particles might transfer into crystalline ZIF-8 domains via internal reorganization) and / or too weak reflections caused by the low amount and small size of the first crystalline domains.

The second article deals with the in-situ monitoring of the formation of big ZIF-8 macrocrystals in the presence of sodium formate as a modulator in methanol under solvothermal conditions. Time-resolved in-situ energie-dispersive X-ray diffraction (EDXRD) experiments were carried out at beamline F3 of DORIS III at the

HASYLAB (Hamburger Synchrotronstrahlungslabor) at DESY (Deutsches Elektronen-Synchrotron) with variation of the amount of added formate and the temperature. From the integrated Bragg peak intensities the extent of crystallization as a function of time was derived for each experiment. The resulting crystallization curves were evaluated applying the Avrami-Erofe'ev and the Gualtieri equations. The kinetic analyses indicated that formate acted to increase the nucleation rate which in turn suggested that formate primary acted as a base to deprotonate the bridging ligand (deprotonation modulation) instead as a competitive ligand (coordination modulation). This behavior is different from the coordination modulation function of formate in room temperature ZIF-8 syntheses. Additional time-resolved ex-situ SEM investigations revealed that the crystal morphology evolved from cubes with truncated edges via rhombic dodecahedra with truncated corners to rhombic dodecahedra.

4.2 Fast Nucleation and Growth of ZIF-8 Nanocrystals Monitored by Time-Resolved In Situ Small-Angle and Wide-Angle X-Ray Scattering

Janosch Cravillon, Christian A. Schröder, Roman Nayuk, Jeremie Gummel, Klaus Huber and Michael Wiebcke.

Angew. Chem. Int. Ed. **2011**, *50*, 8067-8071.

DOI: 10.1002/anie.201102071

Web: <http://onlinelibrary.wiley.com/doi/10.1002/anie.201102071/abstract>

Supporting information:

<http://onlinelibrary.wiley.com/doi/10.1002/anie.201102071/suppinfo>

Reprinted by permission of Wiley VCH.

Copyright 2011 WILEY-VCH Verlag GmbH & Co. KGaA, Weinheim.

Metal–Organic Frameworks**Fast Nucleation and Growth of ZIF-8 Nanocrystals Monitored by Time-Resolved In Situ Small-Angle and Wide-Angle X-Ray Scattering*****Janosch Cravillon, Christian A. Schröder, Roman Nayuk, Jeremie Gummel, Klaus Huber,* and Michael Wiebcke**

Porous coordination polymers (PCPs) or metal–organic frameworks (MOFs) are a novel fascinating class of crystalline porous inorganic–organic hybrid materials, with many potential applications in gas storage, separation, sensing, catalysis, and medical diagnostics.^[1] MOFs are usually synthesized from solution under mild conditions. At present, the synthesis of new MOFs is guided by choosing metal cations and polydentate organic bridging ligands with known coordination preferences that assemble with some degree of predictability into a particular three-dimensional framework,^[2] which may allow further modification by post-synthetic methods.^[3] One limitation of this kind of designing MOF synthesis is set by the poor understanding of the molecular-scale mechanisms of MOF crystallization.^[4–6] Detailed knowledge of the physicochemical fundamentals of MOF nucleation and growth could also enable better control over crystal size and shape, an issue that is of particular relevance in the emerging field of advanced nanoscale MOF materials.^[6,7] There are as yet only few experimental studies of the mechanisms of MOF crystallization. For example, ex situ extended X-ray absorption fine structure (EXAFS) spectroscopy^[8] and electrospray ionization mass spectrometry (ESI-MS)^[9] have been used to detect multinuclear metal complexes (secondary building units) in solution, whereas in situ static light scattering (SLS)^[10] and in situ energy-dispersive X-ray diffraction (EDXRD)^[5,11] have provided time-resolved information about the evolution of particles and crystalline phases, respectively. The growth of MOF nanorods by oriented attachment has also been investigated by ex situ transmission electron microscopy (TEM).^[12] However, direct observations of MOF nucleation processes in homogeneous solution have as yet not been reported.

Herein we present combined time-resolved in situ small-angle and wide-angle X-ray scattering (SAXS/WAXS) experiments that enabled for the first time monitoring the fast nucleation and growth of nanocrystals of a MOF material, the zeolitic imidazolate framework 8 (ZIF-8). Combining SAXS and WAXS is a powerful method that provides detailed information about particle size and shape and crystalline phase, as has been demonstrated previously by excellent in situ studies on the formation of zeolite,^[13] CaCO₃,^[14] Fe₃O₄,^[15] and Au particles.^[16]

ZIFs are a distinctive, rapidly developing subclass of MOFs.^[17] Their tetrahedral framework structures consist of divalent metal cations (such as Zn²⁺, Co²⁺) and bridging substituted imidazolate anions, and frequently possess a zeolite topology. The prototypical ZIF-8 of composition [Zn(mim)₂]_nG (Hmim = 2-methylimidazole, G = guest) crystallizes with a cubic sodalite-related framework.^[18] We have previously reported a procedure for the rapid production at room temperature of 45 nm sized ZIF-8 nanocrystals with a narrow size distribution.^[19] An excess of the bridging Hmim ligand with respect to the zinc salt was employed to increase the nucleation rate. An in situ SLS study of the synthesis revealed that particle formation is generally characterized by comparatively slow nucleation occurring together with fast particle growth on a timescale of a few seconds, which was too fast for monitoring details of the very early crystallization events. Furthermore, SLS does not allow the detection of very small particles and crystallinity. This becomes possible by using SAXS/WAXS.

The SAXS/WAXS experiments were performed at the undulator beam line ID02 of the European Synchrotron Radiation Facility (Grenoble, France). The high brilliance of the X-ray source enabled monitoring ZIF-8 nanocrystal formation with a time resolution of 1 s. To define the onset of the fast reaction as precisely as possible, a stopped-flow device was used for rapid turbulent mixing of the methanolic component solutions before injection into a glass capillary that served as the scattering cell (experimental details are provided in the Supporting Information). The total molar ratio of Zn(NO₃)₂·6H₂O:Hmim:MeOH was set to 1:4:1000, in analogy to previous preparations and SLS studies employing usual mixing methods.^[19]


Figure 1a and Figure 1c show plots of the experimental SAXS and WAXS patterns, respectively. Two features can be identified in the SAXS patterns. The feature of a residual intensity at the momentum transfer q of more than about 0.9 nm⁻¹ is already observed in the first measurement and originates from very small particles (denoted clusters hereafter); that is, these clusters form spontaneously upon mixing

[*] J. Cravillon, C. A. Schröder, Dr. M. Wiebcke
Institut für Anorganische Chemie, Leibniz Universität Hannover
Callinstrasse 9, 30167 Hannover (Germany)
E-mail: michael.wiebcke@aci.uni-hannover.de

R. Nayuk, Prof. Dr. K. Huber
Department Chemie, Universität Paderborn
Warburger Strasse 100, 33098 Paderborn (Germany)
E-mail: klaus.huber@chemie.uni-paderborn.de

Dr. J. Gummel
European Synchrotron Radiation Facility
38043 Grenoble Cedex (France)

[**] Financial support by the DFG Priority Program 1362 “Porous Metal–Organic Frameworks” (WI1156/2-1, HU807/12-1) and provision of beam time at ID02 by ESRF is gratefully acknowledged. We thank Dr. T. Narayanan for fruitful discussions.

 Supporting information for this article is available on the WWW under <http://dx.doi.org/10.1002/anie.201102071>.

Communications

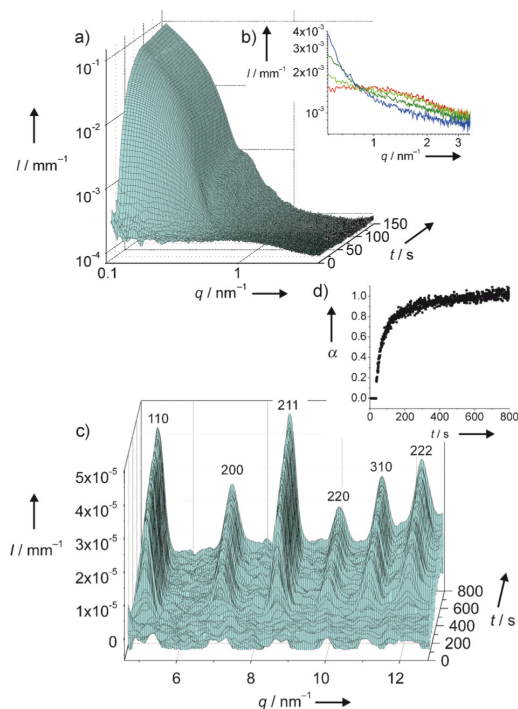


Figure 1. Time-resolved scattering patterns during ZIF-8 nanocrystal formation: a) SAXS patterns for the first 150 s. The time interval between succeeding patterns is 1 s. b) High- q region of selected SAXS patterns originating from the small particles (clusters). The time at which each pattern was measured is indicated by color: red 10 s, light green 30 s, dark green 50 s, blue 70 s. c) WAXS patterns between 1 and 800 s. The time interval between succeeding patterns is 1 s. d) Plot of the extent of crystallization α versus time t as produced from the integrated intensity of the 211 reflections in the WAXS patterns.

the component solutions. The feature at q less than about 0.9 nm^{-1} is first detected after 15 s and originates from the formation of particles. While the intensity corresponding to the particles increases with time, a simultaneous decrease of the intensity corresponding to the clusters is observed, indicating that the formation of particles is correlated with a depletion of clusters (Figure 1b). All Bragg reflections that appear in the WAXS patterns belong to the cubic body-centered lattice of ZIF-8 (space group $I\bar{4}3m$, $a = 1.7012 \text{ nm}$),^[18a] revealing that pure-phase ZIF-8 nanocrystals are generated without the occurrence of any other transient crystalline phase.

Figure 1d shows a plot of the extent of crystallization versus time that was produced by normalization of the integrated intensity of the 211 reflections in the WAXS patterns at various times to the intensity at 800 s. The fast crystallization process slows down at about 300 s and is followed by a slower process (most likely Ostwald ripening),^[19b] which may even extend beyond our last measurement at 800 s, where a maximum in intensity (and the end of

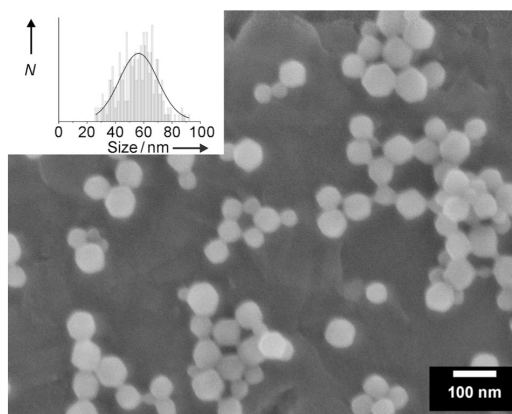


Figure 2. SEM micrograph of ZIF-8 nanocrystals obtained after turbulent mixing and 1 h reaction time. The mixing unit of a stopped-flow device was used for reproducing as close as possible the mixing conditions of the SAXS/WAXS experiments. Inset: Size distribution of the nanocrystals.

reaction) has not yet been reached. A value of about 25 nm was estimated for the diameter d of the nanocrystals with an age of 800 s from the first oscillation minimum at $q \approx 0.35 \text{ nm}^{-1}$ in the SAXS pattern ($d = 4.493 q^{-1}$).^[20] A SEM micrograph (Figure 2) taken after turbulent mixing of the component solutions and 1 h reaction time reveals spherical particles with indications of a rhombic dodecahedral shape ($\{110\}$ crystal form)^[19] and a diameter of $(55 \pm 12) \text{ nm}$. This size is probably larger than the final size of the nanocrystals generated in the thin scattering capillary under stopped-flow conditions.

An evaluation of the SAXS data based on the Guinier approximation and the Porod invariant that is independent from any assumption of particle shape^[21] has been performed after subtraction of the scattering contribution of the clusters for the period from 22 to 60 s (details of data evaluation are provided in the Supporting Information). Figure 3a and Figure 3b show the radius of gyration, weight-averaged molar mass, and number density for the particles obtained accordingly as a function of time. The increase of the values of all these parameters with time can only be interpreted with a particle growth accompanied by a continuous nucleation of new particles. Further information about the particle growth process may be obtained from the power law relation between the radius of gyration and the particle mass, $R_g \approx M_p^\beta$ (Figure 3c). The value of 0.35 determined for the exponent β is in close agreement with the theoretically expected value for spherical (isometric) particles of $\beta = 1/3$. A correlation of the same radii with the weight average mass of all ZIF-8 species including particles and clusters and/or small units resulted in an experimental value of 0.17. It is this division of the exponent by two that is predicted for a monomer addition mechanism.^[21] Hence, particles grow by the addition of monomers (clusters and/or smaller units) but not by coalescence. This result is also in line with the increase of the

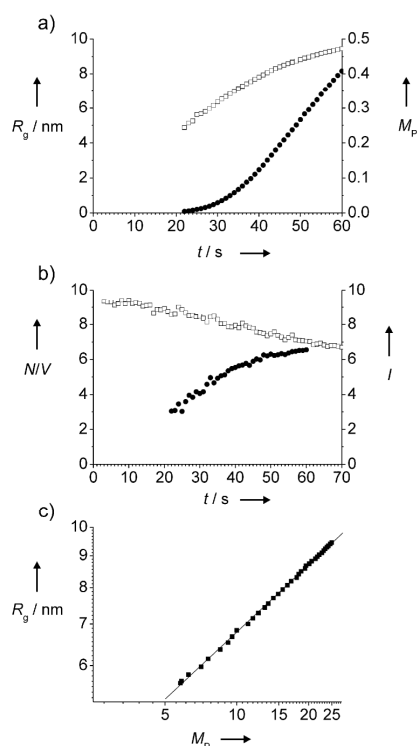


Figure 3. Parameters of ZIF-8 nanoparticles as obtained by SAXS data evaluation: a) Radius of gyration R_g and weight-averaged molar mass M_p as a function of time (\square R_g , \bullet M_p). b) Number density N/V of particles and scattering intensity I at $q = 1.1502 \text{ nm}^{-1}$ taken as an estimate for the mass concentration of clusters as a function of time (\bullet N/V , \square I). c) Correlation of R_g and M_p , revealing a power-law behavior: $R_g \approx M_p^\beta$. The slope of the straight line gives the exponent $\beta = 0.35$.

particle number density with time, as coalescence would decrease the number density of the particles.

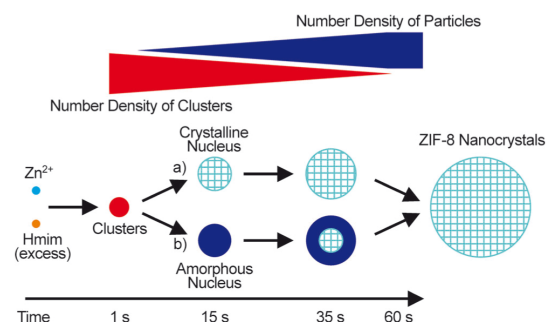
To further demonstrate that nucleation and/or growth of the particles occur at the expense of clusters, the mass concentration of clusters as a function of time was estimated by taking the scattering intensity at a fixed q value (Figure 3b). The intensity starts to decrease with the first observation of particles in the SAXS pattern at 15 s. At about 60 s, the clusters are nearly consumed, while the particle number density appears to approach a constant value, indicating that the nucleation process ceases by this time. At the same time, the extent of crystallization α is about 0.5 (Figure 1d). The fact that the gradual disappearance of clusters is parallel with the approach of a constant number of particles suggests that the clusters are involved in the particle nucleation process.

The SAXS patterns before the appearance of particles could be fitted with a model of monodisperse homogeneous spheres, yielding a radius for the clusters of 1.1 nm. This value should be taken as an average size estimate, as the clusters may be polydisperse. Thus, the volume of a cluster corre-

sponds to about 1.1 unit cells of ZIF-8. After the appearance of particles, that is, after 22 s, the SAXS patterns could be fitted with a bimodal model consisting of polydisperse spheres (modeling the contribution of the particles) and monodisperse spheres or an additive Lorentzian function for random fluctuations (modeling the contribution of the clusters). Examples of model fits and the values obtained for the radius and polydispersity of the particles are provided in the Supporting Information. The values support the above model-independent data analysis.

The first point in time at which the ZIF-8 structure is established in the particles cannot be determined from the WAXS data because a few unit cells are needed for the generation of Bragg reflections and the sensitivity of WAXS is lower than that of SAXS. Thus, we cannot say whether the first particles are already crystalline or amorphous and then reorganize into the ZIF-8 structure. Extrapolation of the experimental extent of crystallization versus time (Figure 1d) to $\alpha = 0$ yields a time of about 22 s (7 s after the first appearance of particles), which may be taken as the time where the periodic ZIF-8 structure emerges.

Scheme 1 summarizes the species detected by SAXS/WAXS during the fast nucleation and growth of ZIF-8 nanocrystals under conditions of high supersaturation that are



Scheme 1. Species occurring during nucleation and growth of ZIF-8 nanocrystals under conditions of high supersaturation. Two possible alternative crystallization pathways (a) and (b) are considered.

generated by the excess of the Hmim ligand. Clusters with a diameter of about 2 nm form in solution from the Zn^{2+} and Hmim precursors and transform into ZIF-8 particles. The nucleation of particles continues while the existing particles grow by attachment of monomers until the clusters are consumed. The following questions remain to be answered. First, do the clusters merely constitute a reservoir of monomers or are they actively involved in the particle nucleation process? As already mentioned, the gradual disappearance of clusters while approaching a final number of particles (Figure 3b) may support the alternative suggestion of an involvement of the clusters in nucleation. Second, if the clusters merely act as reservoir, how do the clusters contribute to the growing particles (by direct attachment and/or by dissolution into smaller building units)? Finally, if the clusters are involved in nucleation, do the clusters possess a structural

Communications

preorganization that is specific for ZIF-8 or not and by which pathway do they contribute to particle nucleation (by aggregation or growth)?

The clusters are of a similar size as the prenucleation particles that have been previously observed during the crystallization of some zeolites from clear solutions.^[13,22] Strong evidence exists for an internal structural evolution towards a zeolite-related structure and aggregation of the particles during nucleation^[22] and the transformation of amorphous into crystalline zeolite particles.^[23] There might be similarities between ZIFs and zeolites not only in the framework topologies but also in the mechanisms of crystallization. Another question concerns the influence of the turbulent mixing. We believe that the observed ZIF-8 nanocrystal formation is valid under usual mixing conditions as well, as we have observed the same overall characteristics of the crystallization process by in situ SLS under conditions of usual mixing^[19] as well as of turbulent mixing (Supporting Information, Figures S8, S9). In both cases, continuous, comparatively slow nucleation and fast crystal growth run parallel over an extended period of time.

Very recently, Venna et al.^[24] reported the results of an XRD and TEM study of ZIF-8 nanocrystal formation from solutions with similar compositions (excess of Hmim) at room temperature, yet the time resolution of their ex situ experiments was too low to resolve any details of the fast crystallization process at early stages. From a classical Avrami analysis of the extent of crystallization as a function of time, they inferred that the crystallization process is nucleation-controlled and suggested the occurrence of an intermediate metastable amorphous phase. The much larger size of their nanocrystals ((230 ± 20) nm, 1 h) compared to ours may be explained by differences in experimental conditions (composition, stirring, mixing). Unfortunately, Venna et al. did not discuss the additional Bragg reflections (besides those of ZIF-8) that are clearly seen in all of their time-dependent XRD patterns. It appears likely that these additional reflections originate from an impurity phase that was generated during sample preparation for the invasive ex situ techniques, as we did not detect by our in situ experiments any other crystalline phase than ZIF-8.

In summary, we have performed in situ SAXS/WAXS investigations of a fast ZIF crystallization process with high time resolution at various length scales. This method allowed us to gain direct insight for the first time into homogeneous nucleation and early growth events. The observed prenucleation clusters and nanoparticles/nanocrystals hint at a complex crystallization process that may not follow classical nucleation theory and exhibits similarities with crystallization processes of other chemical systems, such as zeolites. It is clear that further experiments combining complementary techniques that probe different length scales, preferably under in situ conditions,^[25] are needed to gain a more comprehensive picture of ZIF and MOF crystallization.

Received: March 23, 2011
Published online: July 11, 2011

Keywords: crystal growth · metal–organic frameworks · microporous materials · nanoparticles · zeolite analogues

- [1] a) S. Kitagawa, R. Kitaura, S. Noro, *Angew. Chem.* **2004**, *116*, 2388; *Angew. Chem. Int. Ed.* **2004**, *43*, 2334; b) G. Férey, *Chem. Soc. Rev.* **2008**, *37*, 191.
- [2] a) D. J. Tranchemontagne, J. L. Mendoza-Cortés, M. O’Keeffe, O. M. Yaghi, *Chem. Soc. Rev.* **2009**, *38*, 1257; b) J. J. Perry IV, J. A. Perman, M. J. Zaworotko, *Chem. Soc. Rev.* **2009**, *38*, 1400.
- [3] Z. Wang, S. M. Cohen, *Chem. Soc. Rev.* **2011**, *40*, 498.
- [4] R. E. Morris, *ChemPhysChem* **2009**, *10*, 327.
- [5] F. Millange, M. I. Medina, N. Guillou, G. Férey, K. M. Golden, R. I. Walton, *Angew. Chem.* **2010**, *122*, 775; *Angew. Chem. Int. Ed.* **2010**, *49*, 763.
- [6] D. Zacher, R. Schmid, C. Wöll, R. A. Fischer, *Angew. Chem.* **2011**, *123*, 184; *Angew. Chem. Int. Ed.* **2011**, *50*, 176.
- [7] a) W. Lin, W. J. Rieter, K. M. L. Taylor, *Angew. Chem.* **2009**, *121*, 660; *Angew. Chem. Int. Ed.* **2009**, *48*, 650; b) A. C. McKinlay, R. E. Morris, P. Horcajada, G. Férey, R. Gref, P. Couvreur, C. Serre, *Angew. Chem.* **2010**, *122*, 6400; *Angew. Chem. Int. Ed.* **2010**, *49*, 6260.
- [8] S. Surblé, F. Millange, C. Serre, G. Férey, R. I. Walton, *Chem. Commun.* **2006**, 1518.
- [9] J. A. Rood, W. C. Boggess, B. C. Noll, K. W. Henderson, *J. Am. Chem. Soc.* **2007**, *129*, 13675.
- [10] a) S. Hermes, T. Witte, T. Hikov, D. Zacher, S. Bahn Müller, G. Langstein, K. Huber, R. A. Fischer, *J. Am. Chem. Soc.* **2007**, *129*, 5324; b) D. Zacher, J. Liu, K. Huber, R. A. Fischer, *Chem. Commun.* **2009**, 1031.
- [11] F. Millange, R. El Osta, M. E. Medina, R. I. Walton, *CrystEngComm* **2011**, *13*, 103.
- [12] T. Tsuruoka, S. Furukawa, Y. Takashima, K. Yoshida, S. Isoda, S. Kitagawa, *Angew. Chem.* **2009**, *121*, 4833; *Angew. Chem. Int. Ed.* **2009**, *48*, 4739.
- [13] a) P.-P. E. A. de Moor, T. P. M. Beelen, B. U. Komanschek, L. W. Beck, P. Wagner, M. E. Davis, R. A. van Santen, *Chem. Eur. J.* **1999**, *5*, 2083; b) W. Fan, M. Ogura, G. Sankar, T. Okubo, *Chem. Mater.* **2007**, *19*, 1906.
- [14] a) J. Bolze, B. Peng, N. Dingenouts, P. Panine, T. Narayanan, M. Ballauff, *Langmuir* **2002**, *18*, 8364; b) D. Pontoni, J. Bolze, N. Dingenouts, T. Narayanan, M. Ballauff, *J. Phys. Chem. B* **2003**, *107*, 5123.
- [15] M. Bremholm, M. Felicissimo, B. B. Iversen, *Angew. Chem.* **2009**, *121*, 4882; *Angew. Chem. Int. Ed.* **2009**, *48*, 4788.
- [16] B. Abécassis, F. Testard, O. Spalla, P. Barboux, *Nano Lett.* **2007**, *7*, 1723.
- [17] a) A. Phan, C. J. Doonan, F. J. Uribe-Romo, C. B. Knobler, M. O’Keeffe, O. M. Yaghi, *Acc. Chem. Res.* **2010**, *43*, 58; b) J. C. Tan, T. D. Bennett, A. K. Cheetham, *Proc. Natl. Acad. Sci. USA* **2010**, *107*, 9938; c) C. Chizallet, S. Lazare, D. Bazer-Bachi, F. Bonnier, V. Lecocq, E. Soyer, A.-A. Quoineaud, N. Bats, *J. Am. Chem. Soc.* **2010**, *132*, 12365; d) D. Esken, S. Turner, O. I. Lebedev, G. van Tendeloo, R. A. Fischer, *Chem. Mater.* **2010**, *22*, 6393; e) A. Huang, H. Bux, F. Steinbach, J. Caro, *Angew. Chem.* **2010**, *122*, 5078; *Angew. Chem. Int. Ed.* **2010**, *49*, 4958; f) T. D. Bennett, D. A. Keen, J.-C. Tan, E. R. Barney, A. L. Goodwin, A. K. Cheetham, *Angew. Chem.* **2011**, *123*, 3123; *Angew. Chem. Int. Ed.* **2011**, *50*, 3067; g) Q. Shi, Z. Chen, Z. Song, J. Li, J. Dong, *Angew. Chem.* **2011**, *123*, 698; *Angew. Chem. Int. Ed.* **2011**, *50*, 672; h) P. J. Beldon, L. Fábrián, R. S. Stein, A. Thirumurugan, A. K. Cheetham, T. Friščić, *Angew. Chem.* **2010**, *122*, 9834; *Angew. Chem. Int. Ed.* **2010**, *49*, 9640; i) Y.-Q. Tian, S.-Y. Yao, D. Gu, K.-H. Cui, D.-W. Guo, G. Zhang, Z.-X. Chen, D.-Y. Zhao, *Chem. Eur. J.* **2010**, *16*, 1137.
- [18] a) X.-C. Huang, Y.-Y. Lin, J.-P. Zhang, X.-M. Chen, *Angew. Chem.* **2006**, *118*, 1587; *Angew. Chem. Int. Ed.* **2006**, *45*, 1557;

- b) K. S. Park, Z. Ni, A. P. Côté, J. Y. Choi, R. Huang, F. J. Uribe-Romo, H. K. Chae, M. O'Keeffe, O. M. Yaghi, *Proc. Natl. Acad. Sci. USA* **2006**, *103*, 10186.
- [19] a) J. Cravillon, S. Münzer, S.-J. Lohmeier, A. Feldhoff, K. Huber, M. Wiebcke, *Chem. Mater.* **2009**, *21*, 1410; b) J. Cravillon, R. Nayuk, S. Springer, A. Feldhoff, K. Huber, M. Wiebcke, *Chem. Mater.* **2011**, *23*, 2130.
- [20] O. Glatter in *Neutrons, X-rays and Light: Scattering Methods Applied to Soft Condensed Matter* (Eds.: P. Lindner, T. Zemb), North-Holland Delta Series, Amsterdam, **2002**, p. 84.
- [21] J. Liu, S. Pancera, V. Boyko, A. Shukla, T. Narayanan, K. Huber, *Langmuir* **2010**, *26*, 17405.
- [22] a) S. Kumar, Z. Wang, R. L. Penn, M. Tsapatsis, *J. Am. Chem. Soc.* **2008**, *130*, 17284; b) A. Aerts, M. Haouas, T. P. Caremans, L. R. A. Follens, T. S. van Erp, F. Taulelle, J. Vermant, J. A. Martens, C. E. A. Kirschhock, *Chem. Eur. J.* **2010**, *16*, 2764.
- [23] S. Mintova, N. H. Olson, V. Valtchev, T. Bein, *Science* **1999**, 283, 958.
- [24] S. R. Venna, J. B. Jasinski, M. A. Carreon, *J. Am. Chem. Soc.* **2010**, *132*, 18030.
- [25] N. Pienack, W. Bensch, *Angew. Chem.* **2011**, *123*, 2062; *Angew. Chem. Int. Ed.* **2011**, *50*, 2014.
-

4.3 Formate Modulated Solvothermal Synthesis of ZIF-8 Investigated Using Time-Resolved In-Situ X-ray Diffraction and Scanning Electron Microscopy

Janosch Cravillon, Christian A. Schröder, Helge Bux, André Rothkirch, Jürgen Caro and Michael Wiebcke.

CrystEngComm **2012**, accepted.

DOI: 10.1039/c1ce06002c

Web: <http://pubs.rsc.org/en/content/articlelanding/2012/ce/c1ce06002c>

Supporting informations:

<http://www.rsc.org/suppdata/ce/c1/c1ce06002c/c1ce06002c.pdf>

Reproduced by permission of The Royal Society of Chemistry.

Copyright 2011.

Cite this: DOI: 10.1039/c1ce06002c

www.rsc.org/crystengcomm

PAPER

Formate modulated solvothermal synthesis of ZIF-8 investigated using time-resolved *in situ* X-ray diffraction and scanning electron microscopy†

Janosch Cravillon,^{*a} Christian A. Schröder,^a Helge Bux,^b André Rothkirch,^c Jürgen Caro^b
and Michael Wiebcke^{*a}

Received 4th August 2011, Accepted 29th September 2011

DOI: 10.1039/c1ce06002c

Time-resolved investigations using *in situ* energy-dispersive X-ray diffraction in tandem with *ex situ* scanning electron microscopy revealed that solvothermal crystallisation of ZIF-8 in methanol solvent and in the presence of sodium formate as a simple monodentate ligand (modulator) is a rapid process yielding big, high-quality single crystals in short time (<4 h). Kinetic analysis of crystallisation curves was performed by applying the Avrami–Erofe'ev and Gualtieri models. The analyses revealed that the weakly basic formate modulator acts as a base in deprotonation equilibria (deprotonation of the bridging 2-methylimidazole ligand) rather than as a competitive ligand in coordination equilibria at the metal (Zn²⁺) centres. This is in contrast to the coordination modulation function of formate in ZIF-8 synthesis at room temperature. Crystal shape evolves with time in the presence of formate from cubes with truncated edges to rhombic dodecahedra. The latter shape represents most likely the stable equilibrium morphology of ZIF-8.

Introduction

Zeolitic imidazolate framework (ZIF) materials¹ constitute a novel distinctive subclass of crystalline porous coordination polymers (PCPs) or metal–organic frameworks (MOFs).² The three-dimensional framework structures of ZIFs are formally obtained from those of aluminosilicate zeolites by replacement of the tetrahedral Al/Si centres and bridging O atoms by divalent metal cations (M = Zn, Co) and substituted imidazolate anions (im), respectively. Similarity of the angles sustained at the Al–O–Si and M–im–M bridges (~145°) gives rise to topological related tetrahedral networks. For example, ZIF-8 of composition [Zn(mim)₂]_nG (Hmim = 2-methylimidazole, G = guest) crystallises with a cubic sodalite-related framework.³ Recent research has revealed that ZIFs are very promising materials for many applications in fields such as gas storage,⁴ separation,⁵ catalysis⁶ and sensing.⁷

However, to tune ZIFs for particular applications, methods have to be developed that enable the controlled synthesis of crystals with well-defined size and shape.⁸ To reach this goal our

current understanding of the crystallisation processes has to be significantly improved,⁹ although recent time-resolved investigations using static light scattering (SLS),¹⁰ small-angle and wide-angle X-ray scattering (SAXS/WAXS),¹¹ and transmission electron microscopy and X-ray diffraction (TEM/XRD)¹² have provided first insight into ZIF-8 nucleation and growth at room temperature by revealing the occurrence of transient clusters, nanoparticles and nanocrystals.

A very attractive method to control size and shape that has been recently introduced to prepare carboxylate-based MOF crystals from the nanoscale to the macroscale is the coordination modulation method.^{13–15} An auxiliary monodentate carboxylate ligand is added that acts in competition to the bridging multi-dentate ligands in coordination equilibria at the metal centres and thereby controls (slows) the nucleation and growth rates. Similarly, we used various simple monodentate ligands with different chemical functionalities to prepare at room temperature ZIF-8 crystals ranging in size from ~10 nm to 1 μm.¹⁰ The role of the various modulators could be qualitatively rationalised as modulating coordination and/or deprotonation equilibria (deprotonation of the Hmim ligand). Furthermore, we could provide direct experimental evidence by *in situ* SLS that modulators of comparatively low basicity (e.g. formate) act indeed as competitive ligands to retard nucleation and growth. Formate (sodium salt) was also used as a modulator to prepare big ZIF-8 macrocrystals and gas separating supported ZIF-8 membranes,^{16,17} yet under solvothermal conditions using the same solvent (methanol) but a different metal salt (ZnCl₂ instead of Zn(NO₃)₂·6H₂O) and Hmim/Zn ratio (Hmim/Zn ≤ 2 instead of Hmim/Zn ≥ 4). The high-quality ZIF-8 crystals enabled

^aInstitut für Anorganische Chemie, Leibniz Universität Hannover, Callinstr. 9, 30167 Hannover, Germany. E-mail: michael.wiebcke@acb.uni-hannover.de; Fax: +49-511-7623006; Tel: +49-511-7623698; janosch.cravillon@acb.uni-hannover.de; +49-511-7623006; +49-511-7628064

^bInstitut für Physikalische Chemie und Elektrochemie, Leibniz Universität Hannover, Callinstr. 3A, 30167 Hannover, Germany

^cDeutsches Elektronen-Synchrotron (DESY), Notkestr. 85, 22607 Hamburg, Germany

† Electronic supplementary information (ESI) available: Powder XRD, data of kinetic analyses, SEM micrographs, TG/DTA, and nitrogen sorption isotherm. See DOI: 10.1039/c1ce06002c

experimental determination of adsorption and diffusion data by IR microscopy and, in combination with theoretical studies using GCMC simulation methods, reliable estimation of ZIF-8 membrane permeation selectivities.^{17,18}

It appeared interesting to us to investigate also the mechanism of ZIF-8 crystallisation under solvothermal conditions and clarify the role of the formate modulator (coordination or deprotonation modulation). For this purpose we performed time-resolved *in situ* energy-dispersive X-ray diffraction (EDXRD) and *ex situ* scanning electron microscopy (SEM) investigations of the synthesis with various formate concentrations and temperatures. EDXRD is a diffraction method of low *d*-spacing resolution utilising the high intensity of a synchrotron-generated white X-ray beam that can penetrate common laboratory reaction vessels and enable kinetic and mechanistic studies with high time resolution.¹⁹ The EDXRD and SEM studies and the results are reported below.

Results and discussion

Fig. 1 shows plots of time-resolved EDXRD spectra recorded at intervals of 2 min during a ZIF-8 synthesis at 130 °C. The molar ratio of the starting solution was ZnCl₂/Hmim/NaHCO₂ (sodium formate)/MeOH = 1 : 2 : 2 : 333. Three *hkl* Bragg reflections of ZIF-8 emerge after a short induction time of $t_0 \approx 6$ min and continuously increase in intensity, reaching a constant maximum intensity after ~ 100 min which corresponds to the end of the crystallisation process. Other crystalline phases were not detected, neither as intermediate phases nor as by-products. The product was pure-phase ZIF-8 as demonstrated by the high-resolution XRD pattern taken from the solid recovered after synthesis (Fig. S1, ESI†). Similarly, syntheses were monitored *in situ* (i) at different temperatures ($120 \leq T \leq 140$ °C) with constant composition (Zn/Hmim/NaHCO₂/MeOH = 1 : 2 : 2 : 333) and (ii) at constant temperature ($T = 130$ °C) with varying amounts of sodium formate (Zn/Hmim/NaHCO₂/MeOH = 1 : 2 : x : 333 with $0.5 \leq x \leq 4.0$). Fig. 2 shows the corresponding crystallisation curves (extent of crystallisation $\alpha(t)$

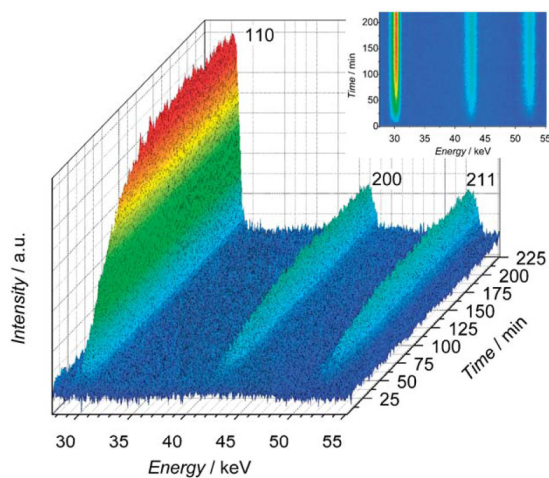


Fig. 1 Time-resolved *in situ* EDXRD spectra of ZIF-8 crystallisation at 130 °C for the composition Zn/Hmim/NaHCO₂/MeOH = 1 : 2 : 2 : 333.

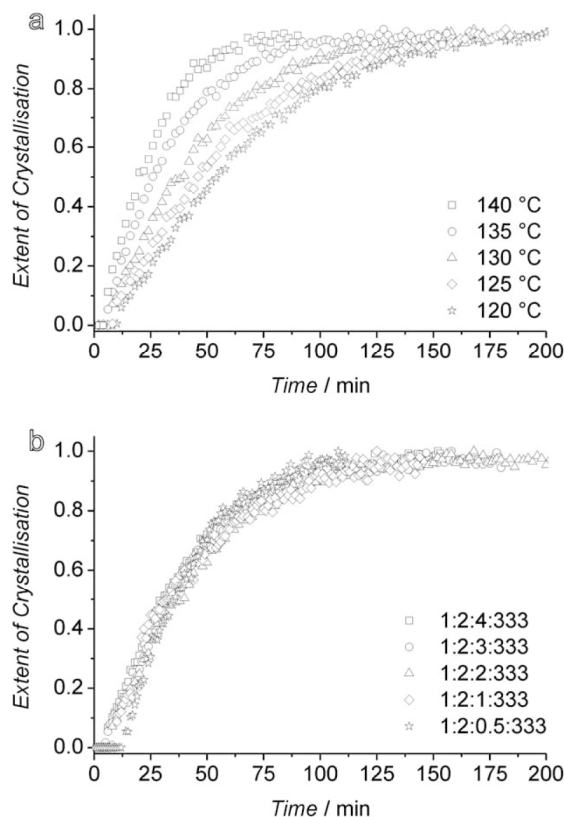


Fig. 2 Extent of crystallisation vs. time: (a) for the composition Zn/Hmim/NaHCO₂/MeOH = 1 : 2 : 2 : 333 at different temperatures as indicated and (b) for different compositions Zn/Hmim/NaHCO₂/MeOH = 1 : 2 : x : 333 ($T = 130$ °C) as indicated.

vs. time t) as obtained from the most intense 110 reflection after normalising the integrated intensities at various times to the respective integrated maximum intensities. Each synthesis yielded pure-phase ZIF-8 as demonstrated by XRD (Fig. S1, ESI†).

To obtain kinetic and mechanistic information, EDXRD data recorded during the solvo-/hydrothermal crystallisation of various materials,²⁰ including some carboxylate-based MOFs,^{21–23} were most frequently evaluated applying the Avrami–Erofe’ev (abbreviated AE) equation.²⁴ Following that former work kinetic analysis was performed applying the method of Sharp and Hancock²⁵ (abbreviated SH) which is based on a linearisation of the AE equation to extract from the slope and intercept of so-called SH plots the Avrami exponent n and overall rate constant k , respectively (see Experimental section for details). Values of n and k were also determined using a non-linear least-squares procedure to fit the experimental EDXRD data with the AE equation. Fig. S2 (ESI†) shows the SH plots of the monitored syntheses, while Tables 1 and 2 list the obtained values of t_0 , n and k .

Each SH plot is linear for the range $0.10 \leq \alpha(t) \leq 0.95$, indicating that mechanistic changes do not occur during a crystallisation process which is also reflected by the fits of the EDXRD data with the AE equation (Fig. S3 and S4, ESI†). The two methods of analysis yielded slightly deviating values of n and k .

Table 1 Kinetic parameters for different temperatures obtained by the Sharp–Hancock (SH) method and non-linear least-squares fitting (NLF) with the Avrami–Erofe'ev equation

$T/^\circ\text{C}$	t_0/min	n_{SH}	$k_{\text{SH}}/\text{min}^{-1}$	n_{NLF}	$k_{\text{NLF}}/\text{min}^{-1}$
140	4	1.00	0.046	1.33	0.012
135	4	1.06	0.032	1.23	0.012
130	6	1.03	0.024	1.26	0.007
125	8	1.02	0.020	1.30	0.005
120	10	1.11	0.017	1.41	0.003

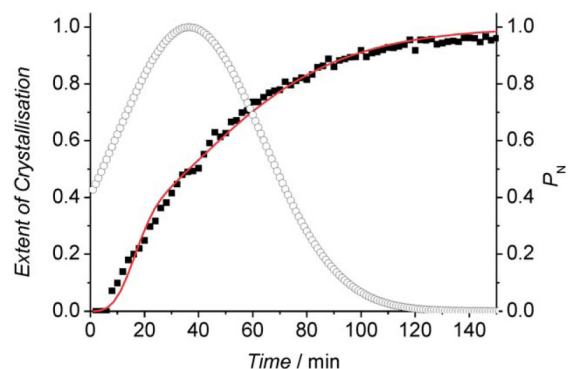
Table 2 Kinetic parameters for the compositions Zn/Hmim/NaHCO₂/MeOH = 1 : 2 : x : 333 obtained by the Sharp–Hancock (SH) method and non-linear least-squares fitting (NLF) with the Avrami–Erofe'ev equation

x	t_0/min	n_{SH}	$k_{\text{SH}}/\text{min}^{-1}$	n_{NLF}	$k_{\text{NLF}}/\text{min}^{-1}$
4.0	5	0.99	0.027	1.23	0.010
3.0	5	1.08	0.021	1.28	0.008
2.0	6	1.03	0.024	1.25	0.008
1.0	9	0.86	0.029	1.20	0.010
0.5	14	0.98	0.036	1.67	0.002

Such differences have been observed previously.²⁶ Nevertheless, the n values are close to 1.0 (SH analysis) or 1.3 (non-linear fitting, NLF) independent of the synthesis conditions. Values of $n \approx 1$ have been taken as an indication that crystallisation processes are rate-limited by a surface reaction²⁵ and it appears to be generally accepted that the importance of nucleation processes increases with increasing n . The k values increase with temperature as expected and from Arrhenius plots (Fig. S5, ESI†) the following apparent activation energies have been determined: $E_A = 66.9 \text{ kJ mol}^{-1}$ (k values from SH analysis) and $E_A = 113.4 \text{ kJ mol}^{-1}$ (k values from NLF).

As pointed out by Finney and Finke²⁷ a serious limitation of an AE analysis is that no differentiation is made between nucleation and growth, rather both processes are convoluted in the same parameters (n and k). Accordingly, Millange *et al.*²² have recently successfully applied a kinetic model that separates both processes for evaluating EDXRD data of solvothermal carboxylate-based MOF crystallisations. The kinetic model was originally introduced by Gualtieri.²⁸ We also applied the Gualtieri model to analyse our EDXRD data (see Experimental section for details). An example of a crystallisation curve with the corresponding Gualtieri fit is shown in Fig. 3, while the remaining fitted crystallisation curves are shown in Fig. S6 and S7 (ESI†). Tables 3 and 4 list the values obtained for different parameters of the Gualtieri model which include in particular values for separate rate constants of nucleation (k_n) and growth (k_g). The model also allows extracting from the k_n values dimensionless probability curves (Gaussian function) which represent the nucleation behaviour and give some illustration on how the nucleation process extends into the growth regime (Fig. 3, S6 and S7, ESI†).

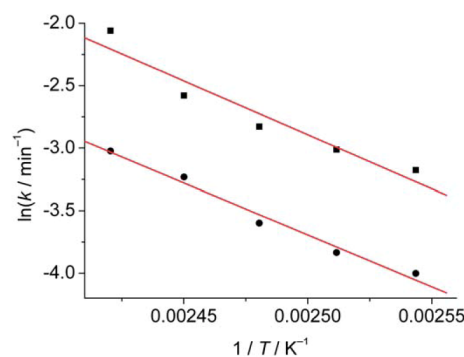
The k_n and k_g values vary only slightly with the synthesis conditions investigated. In every case k_n is smaller than k_g , suggesting that the nucleation process is rate-limiting, in contrast to what the above AE analysis indicates. The k_n and k_g values

**Fig. 3** Extent of crystallisation vs. time (black squares) for the composition Zn/Hmim/formate/MeOH = 1 : 2 : 2 : 333 ($T = 130 \text{ }^\circ\text{C}$) and corresponding non-linear least-squares fit with the Gualtieri equation (red curve) as well as probability curve of nucleation P_N (open circles).**Table 3** Kinetic parameters for different temperatures obtained by non-linear least-squares fitting with the Gualtieri equation

$T/^\circ\text{C}$	a/min	b/min	k_g/min^{-1}	k_n/min^{-1}
140	20.6(3)	12.3(3)	0.128(6)	0.0486(8)
135	25.3(6)	21.3(6)	0.076(3)	0.0395(9)
130	36.6(7)	27.3(7)	0.059(2)	0.0274(6)
125	46.3(7)	31.9(7)	0.049(2)	0.0216(4)
120	54.7(5)	33.1(5)	0.042(1)	0.0183(2)

Table 4 Kinetic parameters for the compositions Zn/Hmim/NaHCO₂/MeOH = 1 : 2 : x : 333 obtained by non-linear least-squares fitting with the Gualtieri equation

x	a/min	b/min	k_g/min^{-1}	k_n/min^{-1}
4.0	30.0(5)	25.2(5)	0.066(2)	0.0333(6)
3.0	27.7(9)	29.8(7)	0.048(1)	0.036(1)
2.0	36.6(7)	27.3(7)	0.059(2)	0.0274(6)
1.0	30.6(6)	30.0(5)	0.059(1)	0.0326(7)
0.5	33.8(5)	19.9(5)	0.047(1)	0.030(1)

**Fig. 4** Arrhenius plots for the temperature-dependent rate constants of nucleation (black circles) and growth (black squares) from the Gualtieri model.

increase with temperature and from Arrhenius plots (Fig. 4) separate activation energies and pre-exponential factors for nucleation ($E_{An} = 69.0 \text{ kJ mol}^{-1}$, $A_n = 2.56 \times 10^7 \text{ min}^{-1}$) and growth ($E_{Ag} = 71.8 \text{ kJ mol}^{-1}$, $A_g = 1.31 \times 10^8 \text{ min}^{-1}$) have been determined. The activation energies are almost equal and effects expressed by the pre-exponential factors such as collision frequencies of reactive species obviously cause the different rate constants of nucleation and growth. The kinetic parameters obtained here by the AE/SH and Gualtieri methods are comparable to those reported by Millange *et al.*^{21,22} for the crystallisation of HKUST-1 ($[\text{Cu}_3(\text{btc})_2]$, btc = benzene-1,3,5-tricarboxylate) which occurred in a similar alcoholic solvent and at similar temperatures but in the absence of a modulator. However, an induction period was not observed for HKUST-1 crystallisation and the activation energies exhibit a greater difference ($E_{An} > E_{Ag}$).

An important question to be answered is the role of formate in the coordination and deprotonation equilibria during nucleation and growth of ZIF-8. The following information can be obtained from the data in Tables 2 and 4 regarding this question. First, the induction time t_0 , defined as the time where the Bragg peaks were first observed, is longer for the smallest amount of formate ($x = 0.5$) than for the other amounts where t_0 values are significantly shorter. Second, the n value obtained by the non-linear fitting of the AE equation for $x = 0.5$ is larger than for the other cases. Finally, the k_n value for $x = 0.5$ is smaller than for the other cases with one exception ($x = 2.0$). Taken together, these observations suggest that formate acts to accelerate nucleation leading to a larger number of nuclei. This conclusion is further experimentally supported by the maximum size of the final crystals produced in the monitored syntheses. The maximum size decreases with increasing amount of formate because a larger number of nuclei can only grow to a smaller individual crystal size (Fig. S8 and Table S1, ESI†).

The above findings suggest that the primary role of formate is to deprotonate the bridging Hmim ligand (deprotonation modulation) and not to act as a competitive ligand (coordination modulation). In the latter case an increasing amount of formate is expected to retard nucleation and growth.¹⁰ Further experimental evidence of the deprotonation modulation function of formate is the observation that solvothermal reactions in the absence of formate under otherwise similar conditions did not yield solid material even after prolonged periods of time (3 months). Similar observations were made recently by McCarthy *et al.*³⁰ during systematic synthetic work on ZIF-8 membrane fabrication. The key to successfully prepare big ZIF-8 crystals is to add only a small amount of weakly basic formate that thermodynamically drives the crystallisation process while keeping the nucleation rate low.

The deprotonation modulation function of formate is a surprising finding when considering the low basicity of a formate ion (as expressed by $\text{p}K_a[\text{HCO}_2\text{H}] = 3.8$ for the corresponding acid in water) compared to the basicity of a mim (deprotonated Hmim) ligand being coordinated to a Zn^{2+} ion ($\text{p}K_a[\text{Zn}(\text{Hmim})]^{2+} \approx \text{p}K_a[\text{Zn}(\text{Him})]^{2+} = 10.3$ in water (Him = imidazole), data taken from the work of Kimura *et al.*).²⁹ Indeed, the role of formate in the present solvothermal syntheses (Hmim/Zn ≤ 2) is in contrast to its coordination modulation role in room temperature syntheses. The different behaviour of formate

at room temperature may be explained with the higher Hmim/Zn ratio (≥ 4) which generates a high nucleation rate and formate acts to slow it.¹⁰ However, the simple explanation based solely on the Hmim/Zn ratio neglects other possible factors such as the nature of the counter-anion (chloride vs. nitrate), the concentration of the reactants and the temperature.

For complementary SEM investigations solutions of the composition Zn/Hmim/NaHCO₂/MeOH = 1 : 2 : 2 : 333 were treated at 120 °C and quenched to room temperature in a water bath after various periods of time. The solutions were kept in the same glass tubes under similar heating conditions as for the EDXRD experiments. During the EDXRD experiments the solutions had to be stirred vigorously to avoid sedimentation of solid material out of the X-ray beam. However, SEM micrographs taken from solid material separated from stirred solutions revealed crystals with very inhomogeneous morphologies and broad size distributions and definite morphological information could hardly be obtained (Fig. S9, ESI†). It was therefore decided to continue the SEM investigations with samples taken from unstirred solutions which showed crystals with much more homogeneous morphologies. In addition, solvothermal syntheses

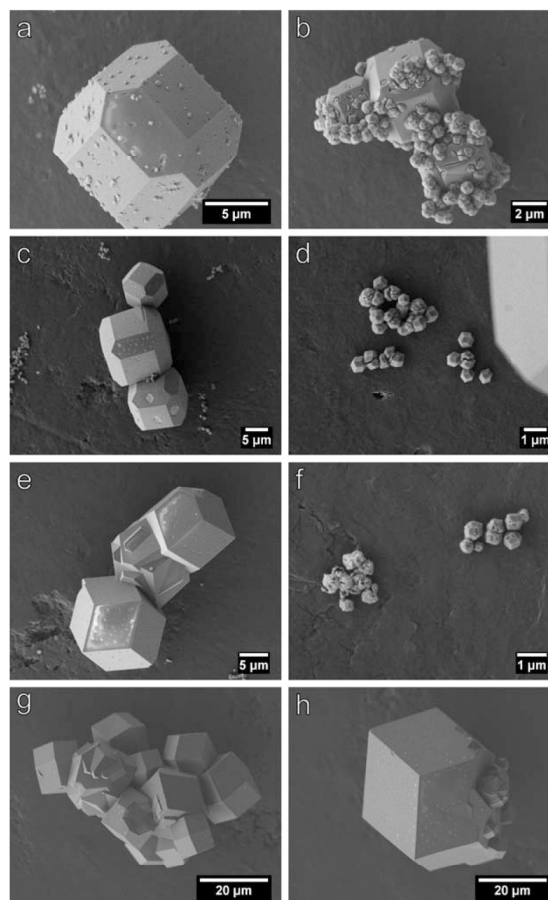


Fig. 5 SEM micrographs taken after 15 min (a and b), 20 min (c and d), 45 min (e and f) and 240 min (g and h).

are usually performed without stirring. Fig. 5 shows a series of typical SEM micrographs thus obtained.

On SEM micrographs taken after 15 min (Fig. 5a and b) comparatively large crystals together with many considerably smaller crystals are seen. Both the larger and smaller crystals exhibit the shape of a cube with truncated edges exposing 6 {100} and 12 {110} faces. The smaller crystals mostly adhere to the surfaces of the larger ones. Furthermore, indentations on the surfaces of the larger crystals can be identified that seem to be the former locations of smaller crystals which had been detached during work up. The indentations on the larger crystal's surfaces are more clearly seen on micrographs taken after 20 min (Fig. 5c and d) which still show larger and smaller crystals. The indentations indicate that the smaller crystals did not nucleate in the course of the quenching procedure, *i.e.* they are most likely not an artefact. Thus, SEM reveals that during crystal growth heterogeneous nucleation of new crystals at the surfaces of existing crystals took place. Similar heterogeneous nucleation was recently also observed during solvothermal growth of a carboxylate-based MOF (MOF-14).²¹ The micrographs after 20 min also show that the larger crystals still exhibit the shape of a cube with truncated edges, while most of the smaller crystals have changed their shape to a rhombic dodecahedron exposing 12 {110} faces. After 45 min SEM micrographs (Fig. 5e and f) show that most of the larger crystals have also developed a rhombic dodecahedral shape and still exhibit indentations on the surfaces. The relative number of smaller crystals has considerably decreased and many of the smaller crystals exhibit holes, indicating that they are in a stage of dissolution. Thus, Ostwald ripening has likely taken place. After 240 min smaller crystals cannot be seen anymore (Fig. 5g, h) and all crystals have the shape of a rhombic dodecahedron, suggesting that this is the stable equilibrium morphology of ZIF-8 crystals. Fig. 6 illustrates the most probable morphology evolution during solvothermal ZIF-8 growth. It appears likely that cube-shaped crystals are formed in early stages but have a short lifetime and could therefore not be detected by SEM. An analogous sequence of morphologies was observed during modulated ZIF-8 growth at room temperature even including cubes (with rounded edges) at early stages.¹⁰ However, heterogeneous nucleation was not observed at room temperature.

Finally, we mention that the above EDXRD studies revealed that formate modulated solvothermal crystallisation of ZIF-8 is

a rapid process running to completion within <4 h. This finding allowed us to optimise our former synthesis protocols¹⁷ with respect to efficiency (see Experimental section).

Experimental

Synthesis

An optimised formate modulated solvothermal ZIF-8 synthesis protocol is as follows: a clear solution is prepared by dissolving 30.3 mg (0.22 mmol) of ZnCl₂ (Sigma-Aldrich, ≥98.0%), 36.5 mg (0.44 mmol) of Hmim (Sigma-Aldrich, 99.0%) and 30.3 mg (0.44 mmol) of NaHCO₂ (Sigma-Aldrich, ≥99.0%) in 3 mL of MeOH (Sigma-Aldrich, ≥99.8%). The solution with a molar ratio Zn/Hmim/NaHCO₂/MeOH = 1 : 2 : 2 : 333 is treated without stirring at 130 °C for 4 h in a sealed glass tube under homogeneous heating in a convection oven. The crystals are recovered by filtration, washed with MeOH and dried under reduced pressure. Yield is 63% based on Zn. The rhombic dodecahedral crystals have a size up to 180 μm (Fig. 7). A thermogravimetric (TG) analysis curve (Fig. S10) and a nitrogen sorption isotherm (Fig. S11) are reported in the ESI†.

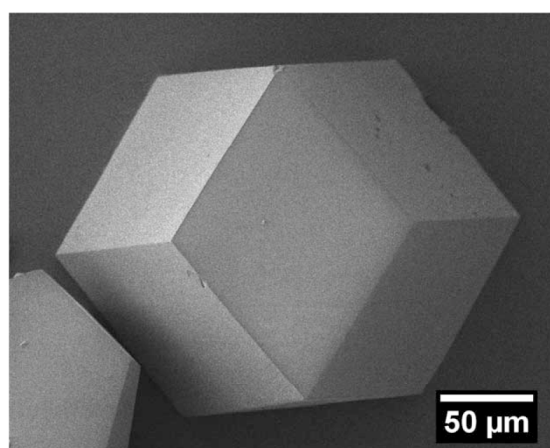


Fig. 7 SEM micrograph of a crystal from the optimised solvothermal synthesis.

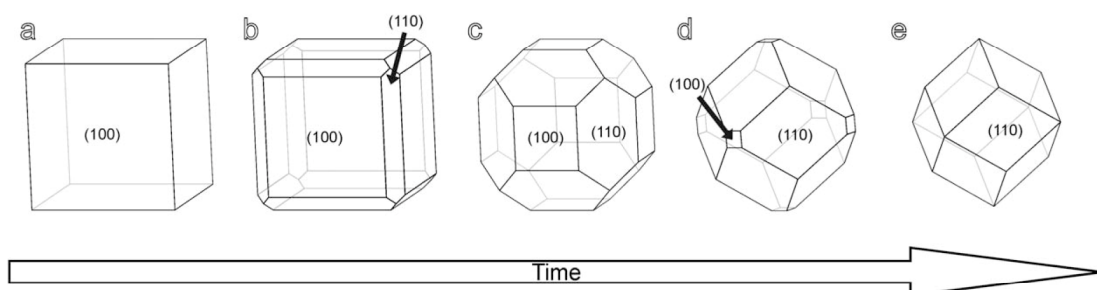


Fig. 6 Illustration of the crystal morphology evolution with time: cube (a), cube with truncated edges (b), rhombic dodecahedron with truncated corners (truncated rhombic dodecahedron) (c and d) and rhombic dodecahedron (e). Miller indices are given only for one representative face out of the different sets of symmetry-equivalent faces (crystals forms); cubic point group $43m$.³

It should be emphasised that the above homogeneous heating in a convection oven without temperature gradient deviates from the heating method used for the EDXRD and SEM investigations. In the latter cases only the lower parts ($\approx 3/4$) of the glass tubes containing the synthesis solutions were heated. The temperature gradient caused refluxing of the volatile solvent (MeOH). Under these conditions smaller crystals are produced (Fig. S8†).

EDXRD investigations

Time-resolved *in situ* EDXRD experiments were performed at beam line F3 at light source DORIS III at DESY (Hamburg, Germany). The beam line receives white synchrotron radiation from a bending magnet with an energy of 8–56 keV, exhibiting a maximum photon flux at 16 keV. Diffracted radiation was recorded using a fixed angle solid-state germanium detector. The detector angle was set at $\sim 1^\circ$ in order to place the most intense 110 Bragg peak of ZIF-8 close to the maximum flux of the beam. Silver behenate powder was used for detector angle calibration. Solvothermal reactions were performed in sealed borosilicate glass tubes with an inner diameter of 9 mm and a volume of 7 mL. The tubes were placed in an aluminium block that was pre-heated to the desired temperature using a circulating oil heater and equipped with a magnetic stirring device. The time between placement of the tubes and start of a diffraction experiment was ~ 30 s. EDXRD spectra were recorded at intervals of 60 s or 120 s. The d -spacing ($d/\text{\AA}$) of a Bragg peak is calculated from the recorded energy (E/keV) by

$$d = \frac{6.19921}{E \sin(\theta)} \quad (1)$$

Data were normalised to the incident beam intensity by using the logged synchrotron radiation current. The profiles of Bragg peaks were fitted with a Gaussian function.

The extent of crystallisation $\alpha(t)$ was obtained as the ratio of the integrated intensities $I(t)$ at various times to the maximum integrated intensity I_{max} at the end of the reaction by

$$\alpha(t) = \frac{I(t)}{I_{\text{max}}} \quad (2)$$

For kinetic analysis experimental EDXRD data were directly fitted with the AE equation

$$\alpha(t) = 1 - e^{-(kt)^n} \quad (3)$$

with n and k being the Avrami exponent and an overall rate constant, respectively. For SH analysis the reduced time $t_{\text{red}} = (t - t_0)$ was introduced considering the induction time t_0 and the AE equation was converted to

$$\ln[-\ln(1 - \alpha)] = n \ln(k) + n \ln(t_{\text{red}}) \quad (4)$$

The Gualtieri model considers nucleation and growth as separate processes in the following equation

$$\alpha(t) = \frac{1}{1 + e^{-(t-a)/b}} \left[1 - e^{-(k_g t)^n} \right] \quad (5)$$

with k_g and n being the rate constant and dimension of growth, respectively. We set $n = 3$ (three-dimensional growth) as proved by SEM investigations (isometric crystal shapes).

Nucleation is represented by the first term in eqn (5). From the parameters a and b the dimensionless probability of nucleation (Gaussian function) can be calculated by

$$P_N = e^{-(t-a)^2/2b^2} \quad (6)$$

with a and b being the position of the peak and the variance of the Gaussian distribution, respectively. The rate constant of nucleation is calculated by

$$k_n = \frac{1}{a} \quad (7)$$

Further methods of characterisation

High-resolution XRD patterns were recorded at room temperature using a Stoe STADI P transmission diffractometer using monochromatised $\text{CuK}_{\alpha 1}$ radiation (wavelength: 1.54060 Å). SEM micrographs were taken in secondary contrast at an acceleration voltage of 2 kV using a Jeol JSM-6700F field-emission instrument. Samples were dispersed on a carbon sample holder.

Conclusions

Using *in situ* EDXRD and *ex situ* SEM we showed that formate modulated solvothermal ZIF-8 crystallisation is a rapid process yielding big, high-quality single crystals within short time (< 4 h). Analysis of crystallisation curves allowed disclosing the role of the weakly basic formate modulator. It acts as a base in deprotonation equilibria (deprotonation modulation) rather than as a competitive ligand in coordination equilibria (coordination modulation). This is in contrast to the role formate takes in room temperature ZIF-8 syntheses¹⁰ and demonstrates that the function of simple monodentate ligands in dynamic coordination and deprotonation equilibria critically depends on a number of parameters such as basicity, complex formation constants, kind of counter-anions, ratio of metal ion to bridging ligand and temperature. It appears that coordination modulation only occurs in situations with high nucleation rates as induced, for example, by an excess of the bridging ligand,¹⁰ rapid microwave heating¹⁴ or low solubility of the MOF.¹⁵ The morphology of the growing ZIF-8 crystals evolves with time in the presence of simple monodentate ligands from cubes *via* intermediate shapes to rhombic dodecahedra. The latter shape is most likely the stable equilibrium morphology of ZIF-8. The results presented here may help to put size- and shape-controlled ZIF and MOF synthesis on a more rational basis.

Acknowledgements

We thank DESY for provision of beam time at F3, Prof. W. Bensch for providing the heating device used at F3 and Beatrix Seidlhofer, Elena Antonova and Mark Freyand (Christian-Albrechts-Universität zu Kiel) for support. The work was financially supported by the DFG-SPP 1362 (Porous Metal-Organic Frameworks) organised by Prof. S. Kaskel.

Notes and references

- 1 A. Phan, C. J. Doonan, F. J. Uribe-Romo, C. B. Knobler, M. O'Keeffe and O. M. Yaghi, *Acc. Chem. Res.*, 2010, **43**, 58.

- 2 (a) G. Férey, *Chem. Soc. Rev.*, 2008, **37**, 191; (b) S. Kitagawa, R. Kitaura and S. Noro, *Angew. Chem., Int. Ed.*, 2004, **43**, 2334; (c) H. Furukawa, N. Ko, Y. B. Go, N. Aratani, S. B. Choi, E. Choi, A. Ö. Yazaydin, R. Q. Snurr, M. O'Keeffe, J. Kim and O. M. Yaghi, *Science*, 2010, **329**, 424.
- 3 (a) X.-C. Huang, Y.-Y. Lin, J.-P. Zhang and X.-M. Chen, *Angew. Chem., Int. Ed.*, 2006, **118**, 1587; (b) K. S. Park, Z. Ni, A. P. Côté, J. Y. Choi, R. Huang, F. J. Uribe-Romo, H. K. Chae, M. O'Keeffe and O. M. Yaghi, *Proc. Natl. Acad. Sci. U. S. A.*, 2006, **103**, 10186.
- 4 R. Banerjee, A. Phan, B. Wang, C. Knobler, H. Furukawa, M. O'Keeffe and O. M. Yaghi, *Science*, 2008, **319**, 939.
- 5 (a) Y.-S. Li, F.-Y. Liang, H. Bux, A. Feldhoff, W.-S. Yang and J. Caro, *Angew. Chem., Int. Ed.*, 2010, **49**, 548; (b) C. Gücüyener, J. van den Bergh, J. Gascon and F. Kapteijn, *J. Am. Chem. Soc.*, 2010, **132**, 17704; (c) Y. Pan and Z. Lai, *Chem. Commun.*, 2011, **47**, 10275.
- 6 C. Chizallet, S. Lazane, D. Bazer-Bachi, F. Bonnier, V. Lecocq, E. Soyer, A.-A. Quoineaud and N. Bats, *J. Am. Chem. Soc.*, 2010, **132**, 12365.
- 7 (a) G. Lu and J. T. Hupp, *J. Am. Chem. Soc.*, 2010, **132**, 7832; (b) A. Demessence, C. Boissière, D. Grosso, P. Horcajada, C. Serre, G. Férey, G. J. A. A. Soler-Illia and C. Sanchez, *J. Mater. Chem.*, 2010, **20**, 7676.
- 8 (a) J. Cravillon, S. Münzer, S.-J. Lohmeier, A. Feldhoff, K. Huber and M. Wiebcke, *Chem. Mater.*, 2009, **21**, 1410; (b) Y.-S. Li, H. Bux, A. Feldhoff, G.-L. Li, W.-S. Yang and J. Caro, *Adv. Mater.*, 2010, **22**, 3322.
- 9 (a) R. E. Morris, *ChemPhysChem*, 2009, **10**, 327; (b) D. Zacher, R. Schmid, C. Wöll and R. A. Fischer, *Angew. Chem., Int. Ed.*, 2011, **50**, 176.
- 10 J. Cravillon, R. Nayuk, S. Springer, A. Feldhoff, K. Huber and M. Wiebcke, *Chem. Mater.*, 2011, **23**, 2130.
- 11 J. Cravillon, C. A. Schröder, R. Nayuk, J. Gummel, K. Huber and M. Wiebcke, *Angew. Chem., Int. Ed.*, 2011, **50**, 8067.
- 12 S. R. Venna, J. B. Jasinski and M. A. Carreon, *J. Am. Chem. Soc.*, 2010, **132**, 18030.
- 13 T. Tsuruoka, S. Furukawa, Y. Takashima, K. Yoshida, S. Isoda and S. Kitagawa, *Angew. Chem., Int. Ed.*, 2009, **48**, 4739.
- 14 S. Diring, S. Furukawa, Y. Takashima, T. Tsuruoka and S. Kitagawa, *Chem. Mater.*, 2010, **22**, 4531.
- 15 A. Schaate, P. Roy, A. Godt, J. Lippke, F. Waltz, M. Wiebcke and P. Behrens, *Chem.-Eur. J.*, 2011, **17**, 6643.
- 16 (a) H. Bux, F. Liang, Y. Li, J. Cravillon, M. Wiebcke and J. Caro, *J. Am. Chem. Soc.*, 2009, **131**, 16000; (b) H. Bux, A. Feldhoff, J. Cravillon, M. Wiebcke, Y.-S. Li and J. Caro, *Chem. Mater.*, 2011, **23**, 2262.
- 17 H. Bux, C. Chmelik, R. Krishna and J. Caro, *J. Membr. Sci.*, 2011, **369**, 284.
- 18 H. Bux, C. Chmelik, J. M. van Baten, R. Krishna and J. Caro, *Adv. Mater.*, 2010, **22**, 4741.
- 19 R. I. Walton and D. O'Hare, *Chem. Commun.*, 2000, **23**, 2283.
- 20 (a) R. I. Walton, T. Loiseau, D. O'Hare and G. Férey, *Chem. Mater.*, 1999, **11**, 3201; (b) R. I. Walton, F. Millange, D. O'Hare, A. T. Davies, G. Sankar and C. R. A. Catlow, *J. Phys. Chem. B*, 2001, **105**, 83; (c) L. Engelke, M. Schaefer, M. Schnur and W. Bensch, *Chem. Mater.*, 2001, **13**, 1383.
- 21 F. Millange, M. I. Medina, N. Guillou, G. Férey, K. M. Golden and R. I. Walton, *Angew. Chem., Int. Ed.*, 2010, **49**, 763.
- 22 F. Millange, R. El Osta, M. E. Medina and R. I. Walton, *CrystEngComm*, 2011, **13**, 103.
- 23 T. Ahnfeldt, J. Moellmer, V. Guillerme, R. Staudt, C. Serre and N. Stock, *Chem.-Eur. J.*, 2011, **17**, 6462.
- 24 (a) M. J. Avrami, *J. Chem. Phys.*, 1941, **9**, 177; (b) B. V. Erofe'ev, *Compt. Rend. Acad. Sci. USSR*, 1946, **52**, 511.
- 25 J. D. Sharp and J. H. Hancock, *J. Am. Ceram. Soc.*, 1972, **55**, 74.
- 26 E. E. Finney and R. G. Finke, *Chem. Mater.*, 2009, **21**, 4692.
- 27 E. E. Finney and R. G. Finke, *J. Colloid Interface Sci.*, 2008, **317**, 351.
- 28 A. F. Gualtieri, *Phys. Chem. Miner.*, 2001, **28**, 719.
- 29 E. Kimura, Y. Kurogi, M. Shionoya and M. Shiro, *Inorg. Chem.*, 1991, **30**, 4524.
- 30 M. C. McCarthy, V. Varela-Guerrero, G. V. Barnett and H.-K. Jeong, *Langmuir*, 2010, **26**, 14636.

5. Syntheses of Supported ZIF-8 Membranes

5.1 Summary

Syntheses of supported ZIF-8 membranes were carried out in cooperation with Dr. Helge Bux and Prof. Dr. Jürgen Caro (Leibniz University Hannover). The preparation of non-oriented and oriented membranes by in-situ crystallization and secondary growth, respectively, are presented in this chapter in two papers. All membrane preparations were based on the formate-modulated solvothermal approach discussed in section 4.3.

Using microwave-assisted solvothermal treatment it was possible to synthesize a 30 μm thick ZIF-8 membrane with random crystal orientation on a porous titania support. The membrane exhibited molecular sieving properties and selectivity for H_2 with respect to other gases. Nevertheless, the H_2 flux through such a thick ZIF-8 membrane was only about 50% in comparison to zeolite membranes with the same selectivity. This could be improved using secondary growth under otherwise similar solvothermal conditions. By using ZIF-8 nanoparticles as seeds on a porous alumina support the polycrystalline layer was significantly thinner (12 μm) than the one obtained by in-situ crystallization. The nanocrystals were attached to the support surface using the polymer PEI (polyethyleneimine). In a following reaction step, the growth of the seeds was established by microwave heating, resulting in a columnar growth of the seed crystals perpendicular to the support. The layer ended up with a high crystal orientation in [100] direction, which could be explained by the evolutionary selection model of van der Drift. The lower thickness of the membrane compared to the one obtained by in-situ crystallization resulted in a doubled H_2 permeance. All ZIF-8 membranes did not show a sharp cutoff for the molecular sieve effect at a kinetic diameter of 3.4 \AA , which corresponds to the crystallographically estimated pore size. This indicates that the ZIF-8 crystal structure is comparatively flexible.

5.2 Zeolitic Imidazolate Framework Membrane with Molecular Sieving Properties by Microwave-Assisted Solvothermal Synthesis

Helge Bux, Fangyi Liang, Yanshuo Li, Janosch Cravillon, Michael Wiebcke and Jürgen Caro.

J. Am. Chem. Soc. **2009**, *131*, 16000-16001.

DOI: 10.1021/ja907359t

Web: <http://pubs.acs.org/doi/abs/10.1021/ja907359t>

Supporting information: <http://pubs.acs.org/doi/suppl/10.1021/ja907359t>

Reprinted with permission from H. Bux, F. Liang, Y. Li, J. Cravillon, M. and J. Caro, *J. Am. Chem. Soc.* **2009**, *131*, 16000-16001.

Copyright 2009 American Chemical Society.

Zeolitic Imidazolate Framework Membrane with Molecular Sieving Properties by Microwave-Assisted Solvothermal Synthesis

Helge Bux,[†] Fangyi Liang,[†] Yanshuo Li,^{†,§} Janosch Cravillon,[‡] Michael Wiebcke,[‡] and Jürgen Caro^{*,†}

Institute of Physical Chemistry and Electrochemistry, Leibniz University Hannover, Callinstr. 3A, D-30167 Hannover, Germany, Institute of Inorganic Chemistry, Leibniz University Hannover, Callinstr. 9, D-30167 Hannover, Germany, and Dalian Institute of Chemical Physics, Chinese Academy of Sciences, Zhong-Shan Road 457, Dalian 116023, China

Received August 31, 2009; E-mail: juergen.caro@pci.uni-hannover.de

Metal–organic frameworks (MOFs) are new microporous inorganic–organic hybrid materials.^{1,2} Their remarkable properties allow their utilization in various applications.^{3–9} The large diversity in structures and pore sizes as well as the high surface areas and adsorption affinities make MOFs attractive as advanced separation media.¹⁰ Supported microporous membranes possess significant potential for the development of methods for energy-efficient and environmentally benign separation of gas mixtures. Although there have been attempts to synthesize MOF layers on porous supports,^{9,11,12} only a very few have reported dense coatings.^{13–17} For membrane synthesis, not only the problems with growing a dense polycrystalline layer on porous ceramic or metal supports but also the thermal and chemical stability of a MOF have to be considered. Among the zeolitic imidazolate frameworks (ZIFs), a new subclass of MOFs, there are ZIFs that exhibit exceptionally high thermal and chemical stability.^{18–22} Therefore, we focused on ZIF-8, having the formula $\text{Zn}(\text{mim})_2$ ($\text{mim} = 2\text{-methylimidazolate}$), which crystallizes with a sodalite-related structure (Figure 1).^{18,19} ZIF-8 not only is highly stable but also shows adsorption affinity toward hydrogen and methane.^{23–25} Because of the narrow size of the six-membered-ring pores ($\sim 3.4 \text{ \AA}$), it can be anticipated that a ZIF-8 membrane should be able to separate H_2 (kinetic diameter $\sim 2.9 \text{ \AA}$) from larger molecules. Another important feature of ZIF-8 is its hydrophobic behavior, whereas ultramicroporous zeolites are usually hydrophilic. This should give a ZIF-8 membrane an advantage over zeolites in the separation of H_2 from a mixture with steam.

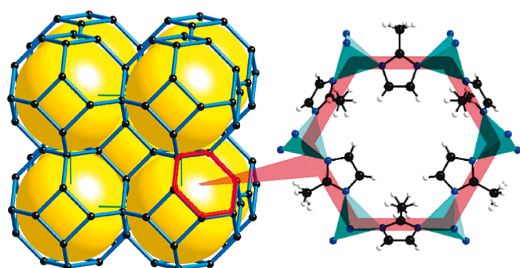


Figure 1. (left) Sodalite topology and (right) narrow six-membered-ring opening through which molecules have to pass.

Recently, we succeeded in preparing ZIF-8 nanocrystals at room temperature by modifying reported synthetic protocols^{18,19} in replacing the solvents dimethylformamide (DMF) and aqueous methanol with pure methanol.²⁶ Methanol has a much smaller

kinetic diameter than DMF. The ZIF-8 adsorption isotherm of methanol exhibits an unusual s shape,¹⁹ indicating that polar methanol only weakly interacts with the ZIF-8 framework. Therefore, methanol can be removed much more easily from the pore network than DMF, and importantly for membrane synthesis, the stress to the crystals is strongly reduced. By further modifying the synthesis in adding sodium formate and using solvothermal conditions, we were able to obtain in methanol pure-phase ZIF-8 material containing large crystals with sizes of up to $300 \mu\text{m}$ (Figure S1 in the Supporting Information). The time of synthesis could be substantially reduced to 4 h by using microwave-assisted heating.

By applying this improved synthetic protocol in membrane preparation (see the Supporting Information), we were able to obtain a crack-free, dense polycrystalline layer of ZIF-8 on a porous titania support (Figure 2). The cross section of the membrane shows a continuous, well-intergrown layer of ZIF-8 crystals on top of the support. Energy-dispersive X-ray spectroscopy (EDXS) revealed that there is a sharp transition between the ZIF-8 layer (Zn signal) and the titania support (Ti signal). A comparison of the X-ray diffraction (XRD) patterns of the ZIF-8 layer and the corresponding crystal powder sedimented during membrane synthesis indicated that the membrane layer consists of randomly oriented crystallites (Figure S2). In thermogravimetric (TG) analysis of the sedimented powder in air, no mass loss was observed at temperatures up to $\sim 360 \text{ }^\circ\text{C}$, where decomposition of the framework structure starts (Figure S3). This proves that in air, methanol has readily escaped completely from the cavities even at room temperature, yielding guest-free, activated ZIF-8.

The volumetric flow rates of the single gases H_2 , CO_2 , O_2 , N_2 , and CH_4 and of a 1:1 mixture of H_2 and CH_4 through the membrane were measured using the Wicke–Kallenbach technique (Figure S4). The permeation measurements were performed both with and without activation of the ZIF-8 membrane in fine vacuum. Nearly the same flow rates were observed in those two cases, confirming the TG results that methanol readily escapes from the pores and clearly demonstrating the advantage of replacing the DMF solvent by methanol in the synthesis.

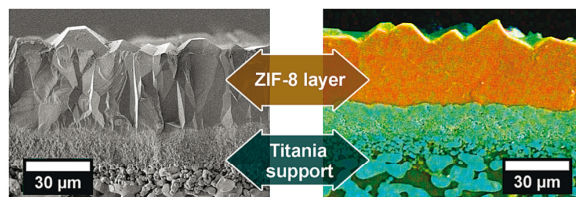


Figure 2. (left) SEM image of the cross section of a simply broken ZIF-8 membrane. (right) EDXS mapping of the sawn and polished ZIF-8 membrane (color code: orange, Zn; cyan, Ti).

[†] Institute of Physical Chemistry and Electrochemistry, Leibniz University Hannover.

[‡] Institute of Inorganic Chemistry, Leibniz University Hannover.

[§] Dalian Institute of Chemical Physics.

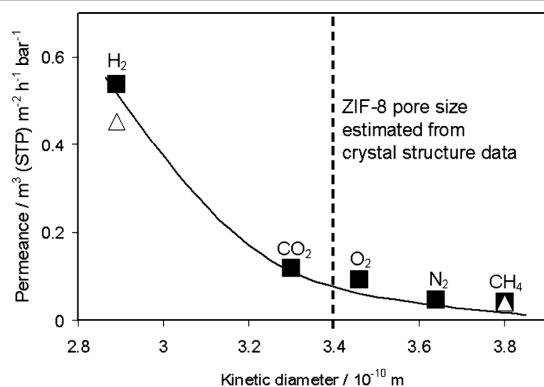


Figure 3. Single (squares) and mixed (triangles) gas permeances for a ZIF-8 membrane vs kinetic diameters.

The permeances calculated from the volumetric flow rates through the ZIF-8 membrane are presented in Figure 3 and Table S1. From both it can be seen that the permeances clearly depend on the molecular size of the gases. Although the pore size of ZIF-8 is estimated from crystallographic data to be ~ 3.4 Å, even larger molecules like CH₄ (kinetic diameter ~ 3.8 Å) can (only slowly) pass through the pore network, and consequently, there exists no sharp cutoff at 3.4 Å. This indicates that the framework structure of ZIF-8 is in fact more flexible rather than static in its nature, in accordance with recent findings by inelastic neutron scattering.²⁷

Comparison of the H₂ single-gas permeance with the H₂/CH₄ mixed-gas one revealed only a small difference, meaning that the larger CH₄ only slightly influences the permeation of the mobile H₂. This experimental finding is different from the results for mixture diffusion in zeolites, where an immobile component usually reduces the mobility of a coadsorbed, more mobile component. As an example, the presence of isobutane reduces the self-diffusivity of *n*-butane in MFI zeolites by orders of magnitude.²⁸ Our observation can be understood by considering that the pore size of ZIF-8 is narrow but the cages are large (~ 11.4 Å in diameter). Thus, although a CH₄ molecule can block the pore entrance for an H₂ molecule, as soon as it has entered the cage, it does not restrict the H₂ diffusion any more.

The separation factor $\alpha_{i,j}$ of a binary mixture is defined as the molar ratio of the components *i* and *j* in the permeate divided by the molar ratio of *i* and *j* in the retentate.²⁹ From the Wicke–Kallenbach permeation studies with gas-chromatographic control of a 1:1 H₂/CH₄ mixture, the value of α at 298 K and 1 bar was determined to be 11.2, which considerably exceeds the Knudsen separation factor for H₂/CH₄ (~ 2.8). In comparison, Guo et al.¹⁶ reported a H₂/CH₄ separation factor of ~ 6 for a supported Cu₃(btc)₂ membrane (btc = benzene-1,3,5-tricarboxylate). Very recently, Ranjan and Tsapatsis¹⁷ reported a high ideal H₂/N₂ selectivity (~ 23) but relatively low fluxes for a Cu(hfipbb)(H₂hfipbb)_{0.5} membrane [H₂hfipbb = 4,4'-(hexafluoroisopropylidene)bis(benzoic acid)].

In conclusion, we have obtained by a novel microwave-assisted solvothermal process a gas-separating ZIF membrane with selectivity for H₂ with respect to other gases. The membrane achieves a fine balance between flux and selectivity relative to other MOF membranes reported to date.^{16,17} The hydrogen permeance of our still relatively thick ZIF-8 membrane is $\sim 50\%$ of the hydrogen permeances of zeolite membranes of the same selectivity.³⁰ It is

expected that the membrane permeance can be improved by reducing the membrane thickness through further optimization of the synthesis parameters. Our ZIF-8 membrane has the additional advantage of high thermal and chemical stability, which provides the possibility of increasing the permeance at high temperature. Our work demonstrates that it is generally possible to prepare highly gas-selective MOF membranes on ceramic supports by in situ crystallization. There is some optimism that MOF membranes can represent a new generation of advanced molecular sieving membranes for gas separation.

Acknowledgment. We thank O. M. Yaghi and B. Wang for permission to use their ZIF-8 structure drawing. We thank A. Feldhoff and F. Steinbach for support in electron microscopy and F. Brieler for adsorption measurements. Y.L. thanks the Alexander von Humboldt Foundation. This work is part of DFG Priority Program 1362 (Porous Metal–Organic Frameworks).

Supporting Information Available: Synthesis protocol, measured flow rates, permeance calculation, numeric permeance data, XRD patterns of the ZIF-8 membrane and ZIF-8 crystal powder, and TG and Ar physisorption data. This material is available free of charge via the Internet at <http://pubs.acs.org>.

References

- Yaghi, O. M.; O'Keeffe, M.; Ockwig, N. W.; Chae, H. K.; Eddaoudi, M.; Kim, J. *Nature* **2003**, *423*, 705.
- Feréy, G. *Chem. Soc. Rev.* **2008**, *37*, 191.
- Kitagawa, S.; Kitaura, R.; Noro, S. *Angew. Chem., Int. Ed.* **2004**, *43*, 2334.
- Murray, L. J.; Dinca, M.; Long, J. R. *Chem. Soc. Rev.* **2009**, *38*, 1294.
- Lee, J.; Farha, O. K.; Roberts, J.; Scheidt, K. A.; Nguyen, S. T.; Hupp, J. T. *Chem. Soc. Rev.* **2009**, *38*, 1450.
- Ma, L.; Abney, C.; Lin, W. *Chem. Soc. Rev.* **2009**, *38*, 1248.
- Czaja, A. U.; Trukhan, N.; Müller, U. *Chem. Soc. Rev.* **2009**, *38*, 1284.
- Spokoyny, A. M.; Kim, D.; Sumrein, A.; Mirkin, C. A. *Chem. Soc. Rev.* **2009**, *38*, 1218.
- Zacher, D.; Shekhan, O.; Wöll, C.; Fischer, R. A. *Chem. Soc. Rev.* **2009**, *38*, 1418.
- Li, J.-R.; Kuppler, R. J.; Zhou, H.-C. *Chem. Soc. Rev.* **2009**, *38*, 1477.
- Arnold, M.; Kortunov, P.; Jones, D. J.; Nedellec, Y.; Kärger, J.; Caro, J. *Eur. J. Inorg. Chem.* **2007**, 60.
- Yoo, Y.; Jeong, H.-K. *Chem. Commun.* **2008**, 2441.
- Gascon, J.; Aguado, S.; Kapteijn, F. *Microporous Mesoporous Mater.* **2008**, *113*, 132.
- Liu, Y.; Ng, Z.; Khan, E. A.; Jeong, H.-K.; Ching, C.; Lai, Z. *Microporous Mesoporous Mater.* **2009**, *118*, 296.
- Yoo, Y.; Lai, Z.; Jeong, H.-K. *Microporous Mesoporous Mater.* **2009**, *123*, 100.
- Guo, H.; Zhu, G.; Hewitt, I. J.; Qiu, S. *J. Am. Chem. Soc.* **2009**, *131*, 1646.
- Ranjan, R.; Tsapatsis, M. *Chem. Mater.* [Online early access]. DOI: 10.1021/cm902032y. Published Online: Sept 1, 2009.
- Park, K. S.; Ni, Z.; Côté, A. P.; Choi, J. Y.; Huang, R.; Uribe-Romo, F. J.; Chae, H. K.; O'Keeffe, M.; Yaghi, O. M. *Proc. Natl. Acad. Sci. U.S.A.* **2006**, *103*, 10186.
- Huang, X.-C.; Lin, Y.-Y.; Zhang, J.-P.; Chen, X.-M. *Angew. Chem., Int. Ed.* **2006**, *45*, 1557.
- Banerjee, R.; Phan, A.; Wang, B.; Knobler, C.; Furukawa, H.; O'Keeffe, M.; Yaghi, O. M. *Science* **2008**, *319*, 939.
- Banerjee, R.; Furukawa, H.; Britt, D.; Knobler, C.; O'Keeffe, M.; Yaghi, O. M. *J. Am. Chem. Soc.* **2009**, *131*, 3875.
- Wu, T.; Zhang, J.; Zhou, C.; Wang, L.; Bu, X.; Feng, P. *J. Am. Chem. Soc.* **2009**, *131*, 6111.
- Wu, H.; Zhou, W.; Yildirim, T. *J. Am. Chem. Soc.* **2007**, *129*, 5314.
- Zhou, W.; Wu, H.; Hartman, M. R.; Yildirim, T. *J. Phys. Chem. C* **2007**, *111*, 16131.
- Wu, H.; Zhou, W.; Yildirim, T. *J. Phys. Chem. C* **2009**, *113*, 3029.
- Cravillon, J.; Münzer, S.; Lohmeier, S.-J.; Feldhoff, A.; Huber, K.; Wiebcke, M. *Chem. Mater.* **2009**, *21*, 1410.
- Zhou, W.; Wu, H.; Udovic, T. J.; Rush, J. J.; Yildirim, T. *J. Phys. Chem. A* **2008**, *112*, 12602.
- Fernandez, M.; Kärger, J.; Freude, D.; Pampel, A.; van Baten, J. M.; Krishna, R. *Microporous Mesoporous Mater.* **2007**, *105*, 124.
- Koros, W. J.; Ma, Y. H.; Shimidzu, T. *Pure Appl. Chem.* **1996**, *68*, 1479.
- Caro, J.; Noack, M. *Microporous Mesoporous Mater.* **2008**, *115*, 215.

JA907359T

5.3 Oriented Zeolitic Imidazolate Framework-8 Membrane with Sharp H₂/C₃H₈ Molecular Sieve Separation

Helge Bux, Armin Feldhoff, Janosch Cravillon, Michael Wiebcke, Yan-Shuo Li and Jürgen Caro.

Chem. Mater. **2011**, *23*, 2262-2269.

DOI: 10.1021/cm200555s

Web: <http://pubs.acs.org/doi/abs/10.1021/cm200555s>

Supporting information: <http://pubs.acs.org/doi/suppl/10.1021/cm200555s>

Reprinted with permission from H. Bux, A. Feldhoff, J. Cravillon, M. Wiebcke, Y.-S. Li and J. Caro, *Chem. Mater.* **2011**, *23*, 2262-2269.

Copyright 2009 American Chemical Society.

Oriented Zeolitic Imidazolate Framework-8 Membrane with Sharp H₂/C₃H₈ Molecular Sieve Separation

Helge Bux,^{†,*} Armin Feldhoff,^{†,*} Janosch Cravillon,[‡] Michael Wiebcke,[‡] Yan-Shuo Li,[§] and Juergen Caro[†]

[†]Institute of Physical Chemistry and Electrochemistry, Leibniz University Hannover, Callinstr. 3A, D-30167 Hannover, Germany

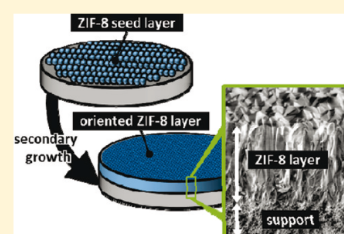
[‡]Institute of Inorganic Chemistry, Leibniz University Hannover, Callinstr. 9, D-30167 Hannover, Germany

[§]Dalian Institute of Chemical Physics, Chinese Academy of Sciences, Zhong-Shan Road 457, Dalian 116023, China

S Supporting Information

ABSTRACT: A highly oriented zeolitic imidazolate framework 8 (ZIF-8) composite membrane was prepared by seeding and secondary growth. By dip-coating, preformed ZIF-8 nanocrystals were attached to the surface of a porous α -alumina support using polyethyleneimine as the coupling agent. After solvothermal treatment, a continuous and well-intergrown ZIF-8 layer was obtained. X-ray diffraction analysis of the membrane showed preferred orientation of the {100} plane parallel to the support. Further time-dependent investigations by scanning and transmission electron microscopy as well as X-ray diffraction indicated that the preferred orientation develops during an evolutionary growth process. In gas mixture permeation experiments, the membrane showed good performance in H₂/hydrocarbon separation. A sharp molecular sieve separation is observed for an equimolar H₂/C₃H₈ mixture with a separation factor above 300.

KEYWORDS: metal–organic frameworks, zeolitic imidazolate frameworks, membrane, oriented growth



INTRODUCTION

In the past 10 years, porous metal–organic frameworks (MOFs) have established themselves in materials science.^{1–3} The 3-D framework structures are formed by metal clusters or cations connected by organic linker molecules. On the basis of the organic–inorganic hybrid character, MOFs have promise in a wide range of applications, e.g., gas storage,^{4,5} medical applications,^{6–8} catalysis,⁹ sensor technology,^{10,11} and molecular separation.^{12–14}

Basically, there are three options to use MOFs for molecular separation of liquid or gas mixtures: (i) by retaining one or more species from the liquid or gas phase by preferential adsorption in the pores, (ii) by different diffusivities of the species in the MOF, which is in the extreme case steric size exclusion (molecular sieving) of one or more species, and (iii) the combination of (i) and (ii). One of the primary features that makes MOFs highly interesting for molecular separation is the so-called isorecticular design.¹⁵ Linker molecules can be modified with functional groups or even completely substituted, maintaining the basic framework structure while altering adsorption and diffusion properties.¹⁶

Membranes in general represent a cost and energy effective solution for industrial gas and liquid separation modified support. The mixture separation performance of membranes is characterized by the separation factor α_{ij} , which is defined after IUPAC as the ratio of the molar fraction of species i and j in the permeate, divided by the ratio of the molar fraction of species i and j in the retentate.¹⁷ Currently, there are increasing numbers of successful attempts to prepare molecular sieving MOF membranes as thin, polycrystalline layers on top of macroporous support materials, showing separation factors up to 25.^{18–27}

For the preparation of MOF membranes, usually two basic techniques known from zeolite membrane fabrication are applied: (i) secondary growth crystallization, where in a first step a seed layer is attached to the support and, subsequently, in a second step, grown to a continuous polycrystalline layer under solvothermal conditions, and (ii) in situ crystallization, where the polycrystalline layer is grown on the bare or chemically modified support in a one-step one-pot solvothermal synthesis. In situ crystallizations seem to be simple and, thus, the favored preparation route. However, they have the disadvantage of critically depending on high rates of heterogeneous nucleation on the support surface to successfully obtain continuous, well-intergrown MOF layers. Whether or not a high surface nucleation rate occurs depends on various factors, e.g., the surface chemistry of the support material (zeta potential, surface acidity, etc.). In secondary growth crystallizations, nucleation and crystal growth are decoupled, and hence, high nucleation rates and chemical interactions with the support material are less crucial.

Recently, we reported on the preparation of ceramic-supported zeolitic imidazolate framework (ZIF) membranes. ZIF-type MOFs frequently crystallize within zeolite-like tetrahedral framework structures, e.g., ZIF-7 and ZIF-8 with sodalite (SOD) and ZIF-22 with Linde type A (LTA) topologies.^{28–30} A number of ZIFs show excellent chemical and thermal stabilities, which is advantageous for membrane applications. ZIF-8 (Zn(mim)₂, mim = 2-methylimidazolate) membranes^{31,32} and ZIF-22 (Zn(Sabim)₂, Sabim = 5-azabenzimidazolate) membranes³³ were prepared by in situ crystallization,

Received: February 22, 2011

Revised: March 1, 2011

Published: March 22, 2011

while secondary growth was used for the preparation of ZIF-7 ($\text{Zn}(\text{bim})_2$, bim = benzimidazolate) membranes.^{34–36} The ZIF-7 and ZIF-22 membranes (both with pore sizes of ~ 3.0 Å) showed in the separation of an equimolar H_2/CO_2 mixture (kinetic diameters: 2.9 Å/3.3 Å)³⁷ separation factors of $\alpha = 13.6$ at 220 °C and $\alpha = 7.2$ at 50 °C, respectively. Because the pores of ZIF-8, as determined from crystallographic data, are larger (3.4 Å),²⁸ the membrane had a lower H_2/CO_2 separation factor ($\alpha = 4.5$ at 25 °C) compared to that of the above-mentioned narrow-pore ZIF membranes, but performed very well in the separation of H_2 from CH_4 (kinetic diameters: 2.9/3.8 Å)³⁷ with $\alpha = 11.2$ at 25 °C.

Under certain synthesis conditions, ZIF-7 (hexagonal space group $R\bar{3}$) with its structural anisotropy forms needle-like crystals.³⁶ Thus, a ZIF-7 membrane with preferred crystal orientation relative to the support could be obtained by secondary growth of a ZIF-7 seed layer on top of an alumina support. In contrast, the ZIF-8 and ZIF-22 (cubic space groups $I\bar{4}3m$ and $Fm\bar{3}m$, respectively) with their isotropic structures resulted in supported layers of only randomly orientated crystals by in situ crystallization. Here, we report on the preparation of a continuous and well-intergrown polycrystalline ZIF-8 layer formed by secondary growth from a nanocrystal³⁸ seed layer on top of a porous alumina support. Contrary to the previously reported in situ crystallization, a highly oriented crystal growth is observed, although the seeds are randomly oriented. We will report the detailed preparation route and discuss a possible mechanism of oriented crystal growth that is supported by time-dependent electron microscopy and X-ray diffraction studies. We further report on the H_2/CO_2 and $\text{H}_2/\text{C}_1\text{--C}_3$ hydrocarbon gas separation performance of the newly developed ZIF-8 membrane.

EXPERIMENTAL SECTION

Membrane Synthesis. Asymmetric porous $\alpha\text{-Al}_2\text{O}_3$ discs (Fraunhofer IKTS) with a diameter of 18 mm were used as supports. ZIF-8 ($\text{Zn}(\text{mim})_2$) nanocrystals were prepared as previously reported.³⁸ The seeding solution was prepared as follows: 1.210 g freshly synthesized ZIF-8 nanocrystals (still wet and in gel-like state) were dispersed into a water/polyethyleneimine (PEI) solution, which consisted of 0.120 g sodium bicarbonate (Roth, > 99.5%), 1.506 g PEI ($\sim 50\%$ solution in H_2O , Fluka), and 30 mL water.^{34,35} Addition of PEI to the seeding solution is vital to ensure that the seed crystals adhere to the support surface. As proposed by Ranjan and Tsapatsis,²¹ PEI may form hydrogen bonds with both the ZIF seed crystals and free hydroxyl groups of the support surface. In addition, PEI may form Zn–N coordination bonds to zinc cations on the surface of the nanocrystals. To generate a sufficiently high concentration of surface hydroxyl groups, the alumina supports were pretreated with $\sim 6\%$ hydrochloric acid and extensively washed with water afterward. For high reproducibility, the seeds were attached to the alumina discs using an automatic dip-coating device with a defined dipping and withdrawing speed of 300 and 100 mm/min, respectively. The discs were immediately removed after dip-coating and air-dried in an oven at 80 °C for 4 h. For subsequent solvothermal secondary growth solutions of low concentration were used, typically containing 0.532 g (3.95 mmol) zinc chloride (>99% Merck), 0.487 g (5.92 mmol) 2-methylimidazole (>99%, Sigma-Aldrich), and 0.272 g (3.95 mmol) sodium formate (>99%, Sigma-Aldrich) dissolved in 80 mL methanol (99.9%, Roth). The seeded alumina discs were placed vertically in PTFE holders to avoid sedimentation of crystals, which eventually nucleated from the homogeneous solution during membrane synthesis. In addition, the holders covered the back side of the supports to prevent crystallization on the coarse side of the asymmetric supports. The holders with mounted alumina supports were placed in autoclaves so that their top layer (70 nm $\alpha\text{-Al}_2\text{O}_3$) faced the synthesis solution. The autoclaves were heated in a microwave oven to 100 °C within 10 min typically for 2 h. In further experiments, the

synthesis time was varied from 0.5 h to 4 h. After cooling to room temperature, the membranes were carefully removed from the holder, intensively washed with methanol, and dried overnight at room temperature over silica gel. In addition, the crystalline precipitates were collected from the bottom of the autoclaves, washed, and dried for further analysis.

The secondary growth experiments at 1 h, 2 h, and 4 h were repeated to investigate the reproducibility of the growth process (see Table S1 of the Supporting Information).

To prove that the seed crystals actually initiate the layer growth, a reference membrane synthesis experiment was performed. In this case, the alumina support was dip-coated in an aqueous solution containing only 5.0% but no seed crystals.

X-ray Diffraction (XRD). XRD analysis of the membranes and powder samples was carried out on a Bruker D8 Advance diffractometer in reflection mode using $\text{Cu K}\alpha$ radiation. The 2θ range from 5° to 50° was scanned with a step size of 0.02°.

Scanning Electron Microscopy (SEM) and Energy-Dispersive X-ray Spectroscopy (EDXS). SEM and EDXS were performed on a JEOL JSM-6700F instrument with a field emitter as the electron source. For SEM, the films and membranes were simply broken and coated with Au to improve conductivity. Usually a low accelerating voltage (1–2 kV), a low current (3–5 μA), and a lens distance of 15 mm were used. For EDXS, the voltage and current were increased to 5 kV and 10 μA , respectively.

Transmission Electron Microscopy (TEM). For the preparation of a TEM specimen, a membrane was epoxy-glued against a silicon wafer. After curing, the sandwich was wire-sawed into about 1 mm thick slabs, which contained the glue line. The specimen bar was grinded and polished down to approximately 30 μm using polymer-embedded polishing films with propylene glycol as lubricant on an Allied High Tech Multiprep/Techprep device. The thin bar was epoxy-glued onto a supporting copper slot-grid and, after curing, locally thinned to electron transparency by 3 kV Ar^+ ion sputtering in a Gatan precision ion polishing system (PIPS). Observation of a membrane microstructure in cross-section was made at an electron energy of 200 kV in scanning transmission electron microscope (STEM) bright-field mode using a JEOL JEM-2100F field-emission instrument.

Permeation Experiments. Although a total of 10 ZIF-8 membranes have been prepared, only one of these membranes, showing a distinctive crystal orientation obtained after 2 h of secondary growth, was studied in permeation experiments. The measurements were carried out following a modified Wicke–Kallenbach technique³⁹ (Figure S1 of the Supporting Information). A sweep gas at 1 bar pressure (N_2 at 100 mL/min, purity 5.0) was used to continuously remove the permeate. The sweep gas composition was analyzed by using a gas chromatograph (HP Agilent 6890N, thermal conductivity detector) equipped with a Carboxen 1000 packed column (15 ft., 1/8 in., Supelco Sigma-Aldrich). The supported ZIF-8 membrane was tightly sealed in the permeation cell by using silicone and Viton O-rings (Eriks). The effective remaining membrane area was 1.09×10^{-4} m². Different hydrocarbons ($\text{C}_1 = \text{CH}_4$, $\text{C}_2 = \text{C}_2\text{H}_6$, $\text{C}_3 = n\text{-C}_3\text{H}_8$, purity ≥ 2.5) and CO_2 (food grade purity) were measured in equimolar gas mixture with hydrogen (purity 5.0) with a constant, total pressure of 200 kPa on the feed side or 100 kPa partial pressure for each gas, respectively. The feed flow was kept constant at total flow rates between 80 and 100 mL/min. Permeances in $\text{mol m}^{-2} \text{s}^{-1} \text{Pa}^{-1}$ were calculated on the basis of the measured flow rates (in mL min^{-1}) at room temperature (298.15 K) and ambient pressure (101.3 kPa) and from the applied partial pressure at the feed side of the membrane (100 kPa).

RESULTS AND DISCUSSION

After the dip-coating process described in the Experimental Section, the presence of the crystalline and phase-pure ZIF-8 seed layer was verified by XRD, as shown in Figure 1. The relative reflection intensities on the XRD pattern of the seed layer

approximately match those on the XRD pattern of the corresponding nanocrystals powder and a simulated pattern. Because it is assumed that in the powder sample the nanocrystals are randomly oriented, the same has to hold true for the seed layer.

Figure 2 shows SEM images of the well-intergrown polycrystalline ZIF-8 layer on top of the alumina support obtained after secondary growth for 2 h in top view as well as in cross-sectional view. In contrast, the reference membrane synthesis experiment performed using a PEI-coated alumina support without seeds resulted in poorly intergrown film with obvious gaps between clearly distinguishable ZIF-8 crystals of rhombic dodecahedral shape, as shown by the SEM image in Figure 3. This demonstrates that seeding is in fact necessary to grow a continuous, gap-free layer on top of the alumina support. The well-intergrown ZIF-8 layer shown in panel (b) of Figure 2 is around 12 μm thick and, therefore, much thinner than the well-intergrown ZIF-8 layer we prepared recently by in situ crystallization ($\sim 30 \mu\text{m}$).³¹ Elemental mapping by EDXS of the cross-section (Figure S2 of the Supporting Information) reveals a clear boundary between the ZIF-layer and the support. Hence, the crystal growth in the pores of the support seems to be disfavored. This is understandable because in the sub- μm top-layer pores of the asymmetric support, crystal growth is limited by size. As soon as the growing ZIF layer is sufficiently dense, the support pores are cut

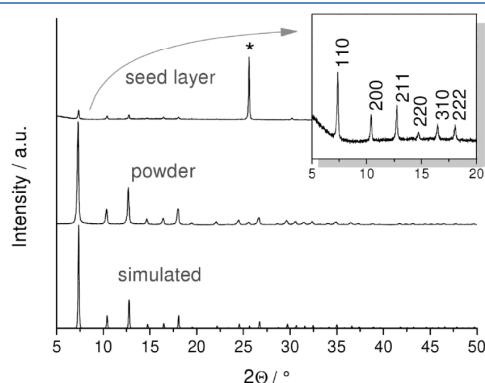


Figure 1. XRD pattern of the seed layer on top of the alumina support, XRD pattern of the corresponding nanocrystalline powder pattern, and XRD pattern simulated from crystal structure data²⁸ excluding guest species. Reflections of the alumina support are marked by an asterisk. Inset: magnification of the pattern of the seed layer including reflection indices.

from the nutrient solution and further intrapore growth is prevented. A TEM image of a very thin and polished sample from the cross-section of the membrane (Figure 4a) reveals the grain boundaries in the ZIF-8 layer. For clarity, the boundaries have been traced in panel (b) of Figure 4. Columnar crystals aligned roughly perpendicular to the support can be seen in the upper 2/3 of the layer, while in the lower 1/3 of the layer, the crystal grains are smaller and the grain boundaries are harder to trace.

The XRD patterns of the membrane and the ZIF-8 precipitate collected from the bottom of the autoclave are shown in panel (a) of Figure 5, while the XRD pattern of the reference membrane synthesis experiment is available in Figure S3 of the Supporting Information. The XRD pattern of the precipitate, which is assumed to have a random crystal orientation, and the XRD pattern of the reference experiment coincide in the reflection position and relative intensities. In contrast, the XRD pattern of the membrane exhibits a strongly increased relative intensity of the 200 reflection in relation to other reflections, which indicates a preferred crystal orientation of the $\{100\}$ planes parallel to the support. A quantitative measurement of the degree of crystal orientation in the ZIF-8 layer can be obtained from the crystallographic preferred orientation (CPO) index,^{40,41} which compares the ratio of integrated intensities I_{hkl} from a pair of characteristic reflections $hkl/h'k'l'$ of the layer in relation to the integrated intensities I_{hkl} of the same pair $hkl/h'k'l'$ of the precipitate (see Equation S1 of the Supporting Information).

The CPO indices of the dominant 200 reflection in relation to the 110 ($\text{CPO}_{200/110}$) and the 211 reflections ($\text{CPO}_{200/211}$) are calculated to be 83 and 81, respectively. Both values clearly demonstrate the pronounced $\{100\}$ orientation with only a low fraction of crystals taking different orientations.

At this point, it might be assumed that the slightly imperfect orientation is induced mainly from surface texture effects of the support. However, relating the columnar layer structure as observed by TEM (Figure 4) with the finding of oriented growth, it is indicated that only the upper 2/3 of the layer might be oriented, while the lower 1/3 is not or only partly oriented. Additional crystallizations with seeded supports were performed for 0.5, 1, and 4 h to study the secondary growth of the layer by XRD as function of time. Panel (b) of Figure 5 shows the XRD pattern of the obtained membranes. The corresponding $\text{CPO}_{200/110}$ and $\text{CPO}_{200/211}$ indices are available in Table 1. After 0.5 h, a very thin but continuous ZIF-8 layer had already formed as detected by SEM (Figure 6). The related XRD pattern of the

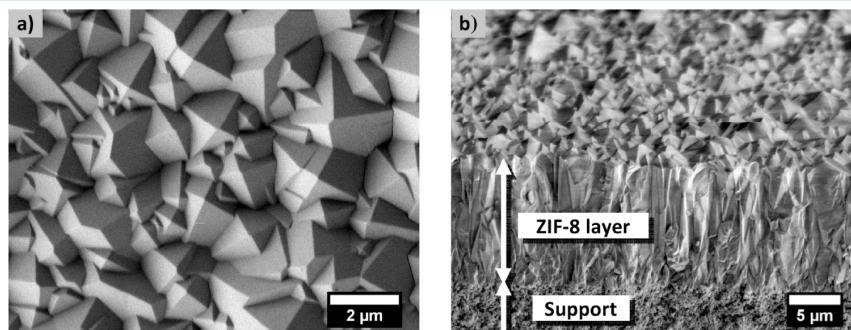


Figure 2. (a) SEM top view of the well-intergrown ZIF-8 layer after 2 h of secondary growth. (b) SEM top down view on the corresponding cross-section of the broken membrane.

membrane grown for 0.5 h matches that of the precipitate (Figure 5b), indicating random orientation of the crystals, which is quantitatively reflected by the low values of the CPO indices

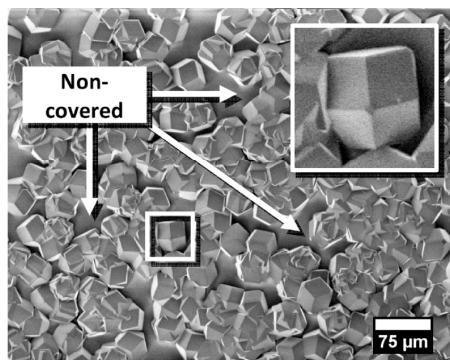


Figure 3. Supported ZIF-8 film grown from the reference membrane synthesis experiment (without seeds, only PEI-coated support) using the same solvothermal synthesis as for the seeded ZIF-8 membrane. Inset: magnification of a clearly distinguishable crystal with rhombic dodecahedral shape.

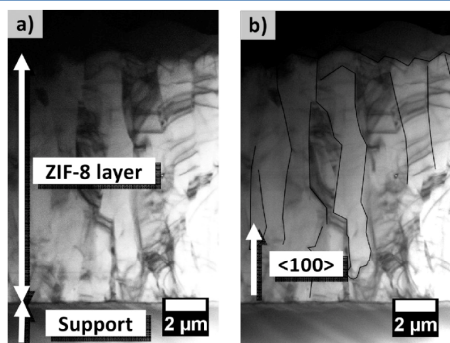


Figure 4. (a) TEM of the cross-section of the supported ZIF-8 membrane after 2 h of secondary growth as shown in panel (a) of Figure 2 and (b) with traced grain boundaries for improved visibility of the columnar growth and denoted $\langle 100 \rangle$ direction.

(Table 1). After 1 h, the 200 reflection already has increased remarkably in its relative intensity and is already stronger than the 110 reflection, which is dominating in the case of the randomly orientated powder. The CPO indices, however, are still very low, indicating that a large amount of crystals is still randomly oriented (Table 1). After 2 and 4 h of secondary growth, the intensities of all reflections apart from the 200 reflection are very low and can, according to the above measurements, be traced back mainly to the lower, less-oriented region of the ZIF-8 layer near to the support. The growth process was investigated to be generally reproducible (see Table S1 of the Supporting Information).

The preferred crystal orientation may be explained with the evolutionary selection model by van der Drift,⁴² which is commonly used to explain oriented growth of zeolite layers by secondary growth.⁴³ Starting from a randomly oriented seed layer on a planar surface, at first all seed crystals will start to grow at the same time and with the same face-dependent growth rates. After a certain time, which critically depends on the seed concentration on top of the surface, the crystals will meet their lateral neighbors. Crystals that have the fastest growth direction perpendicular or nearly perpendicular to the support surface will eventually overgrow their neighbors and thus form the top layer. The microstructure of the polycrystalline layer usually found after the evolutionary process is columnar-like in cross-sectional view. This is in fact observed for the ZIF-8 membranes (Figures 2a and 4). Ideal evolutionary selection, however, only takes place if (i) the crystals exhibit significant anisotropic growth, (ii) all crystals start to grow at the same time, and (iii) there are competing crystals in close neighborhood. A comparatively low heterogeneous nucleation rate, resulting in a lower concentration of nuclei on the support surface, might explain why in situ crystallizations under similar synthesis conditions

Table 1. Development of CPO Indices with Increasing Time of Secondary Growth

time (h)	CPO _{200/110}	CPO _{200/211}
0.5	-0.1	0.5
1	8.8	4.0
2	83.0	81.1
4	134.6	79.9

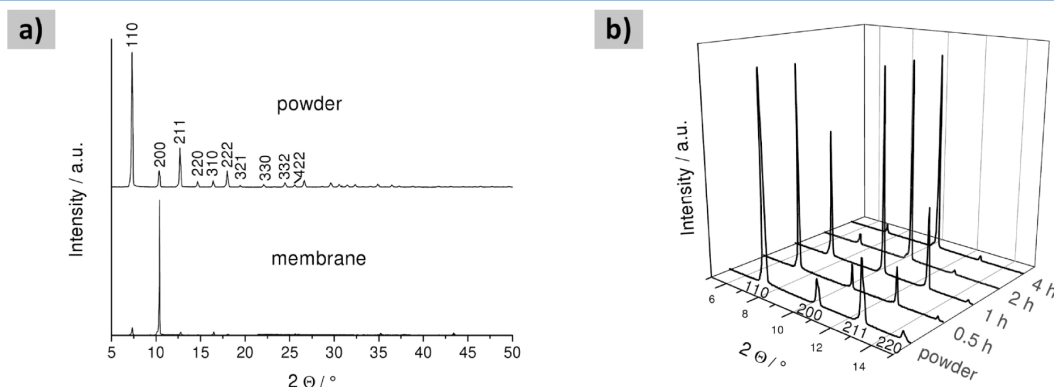


Figure 5. (a) XRD pattern of the oriented ZIF-8 layer after 2 h of secondary growth on top of the alumina support (lower pattern) and the corresponding precipitate (top pattern). The first 10 hkl -indices are denoted. (b) XRD patterns between 5° and 15° 2θ of ZIF-8 layers after secondary growth for 0.5 h, 1 h, 2 h, and 4 h in comparison with the powder pattern.

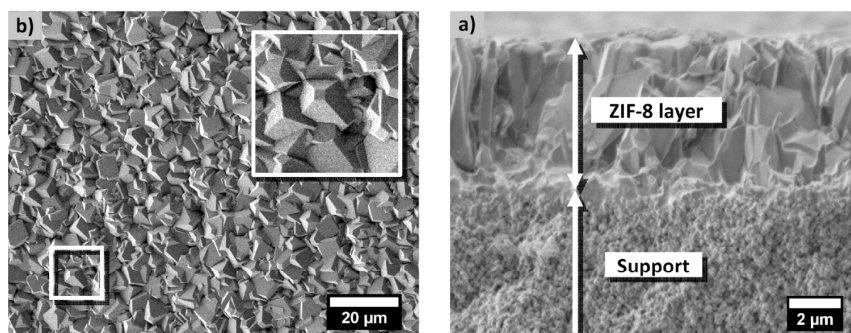


Figure 6. (a) SEM top view of the supported ZIF-8 layer which is, after secondary growth for 0.5 h, still randomly oriented. Inset: magnification showing a rhombic dodecahedral crystal with orientation near to $\langle 100 \rangle$, which might become a part of the final, oriented layer when increasing the synthesis time. (b) Corresponding cross-section of the about $5 \mu\text{m}$ thick layer formed at 0.5 h of secondary growth.

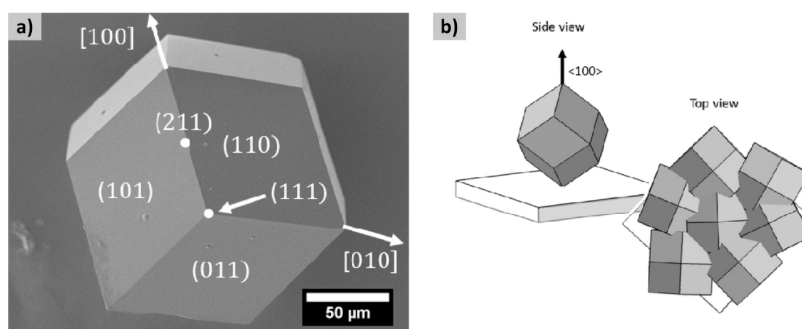


Figure 7. (a) SEM image of a ZIF-8 crystal with rhombic dodecahedral shape. The polyhedron exhibits 12 faces perpendicular to $\langle 110 \rangle$ and 24 edges perpendicular to $\langle 211 \rangle$. Six corners point along $\langle 100 \rangle$ (4-fold rotation axis), and eight corners point along $\langle 111 \rangle$ (3-fold rotation axis). (b) Schematic of an individual rhombic dodecahedral crystal as viewed perpendicular to $\langle 100 \rangle$ and microstructure of an intergrown layer of $\{100\}$ oriented rhombic dodecahedral crystals (top view).

only result in a randomly oriented layer on titania supports, as previously reported.³¹

According to the above model, our findings of strongly preferred $\{100\}$ crystal orientation is the result of fastest growth along the $\langle 100 \rangle$ direction. This is also in agreement with the crystal morphology. The equilibrium shape of ZIF-8 is apparently rhombic dodecahedral for both nanocrystals³⁸ (as those used for seeding) and large macrocrystals that are synthesized under similar conditions as the membranes (Figure 7a). Parallel work of Cravillon et al. have observed that in room-temperature syntheses cube-shaped crystals ($\{100\}$ crystal form) first develop in early stages and eventually transform into rhombic dodecahedra ($\{110\}$ crystal form).⁴⁴ The polyhedron (crystallographic point group symmetry $\bar{4}3m$) consists of 12 rhombic faces perpendicular to $\langle 110 \rangle$. When viewed along the $\langle 100 \rangle$ direction, one out of six corners is seen that lay on a 4-fold rotation axis (Figure 7b, upper left). Such corners are expected to be clearly visible in top view of a layer of intergrown micrometer-sized crystals with preferred $\{100\}$ orientation (Figure 7b, lower right), as is indeed revealed on SEM images of the ZIF-8 membranes (Figure 2a).

As proposed by Bons and Bons,⁴⁵ the final distribution of orientations, which survive the evolutionary selection, depends not only on the vertical but also on the lateral growth vector. They performed 2-D computer simulations of zeolite MFI crystals growing simultaneously in close neighborhood to each

other. Orthorhombic MFI usually grows in a coffin-like crystal shape, with the vector of fastest growth in the $[100]$ direction (c -axis). The simulation showed that with increasing lateral growth rate of MFI crystals, the fractions of crystals with orientations other than c decreases. Bons and Bons explain their results by the higher chance of c -oriented crystals to overgrow crystals with different orientations and, hence, completely stop their growth.

For the ZIF-7 membrane recently reported,³⁶ evolutionary growth of needle-like crystals was found, resulting in a c -oriented, polycrystalline layer. However, according to SEM studies, a large part of the crystals exhibited a tilted rather than a perfect c -orientation with respect to the support. These findings are in complete agreement with the model by Bons and Bons. The distinct needle-like morphology of ZIF-7 suggests that the growth rate along the c -axis is significantly larger than that along perpendicular directions, thus explaining the nonperfect c -orientation. On the other hand, for the present case of ZIF-8, a highly oriented layer is obtained, which might be unexpected at first glance because of the cubic crystal structure and, hence, “isotropic” crystal growth. However, for the observed preferred $\{100\}$ orientation, fastest growth occurs not only perpendicular but simultaneously parallel to the support surface (because, e.g., $[100]$ and $[010]$ are perpendicular to each other). Hence, the highly oriented growth is, again, in complete agreement with the model by Bons and Bons.

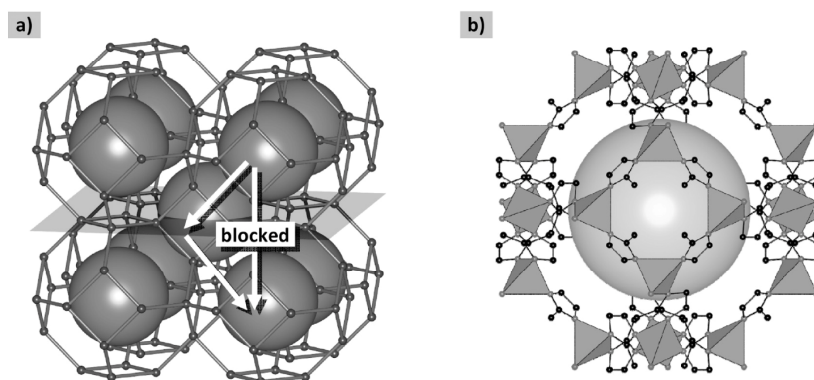


Figure 8. (a) Perspective drawing of the ZIF-8 SOD topology with a $\{100\}$ plane propagating through the structure. The arrows indicate possible pathways of a molecule through the pore system (large cages connected by six-membered ring windows). The straight passage from one cage to the one below is blocked because of the very small size of the four-membered ring windows. (b) View along $\langle 100 \rangle$ on a $[4^6 6^8]$ truncated octahedral cage of the ZIF-8 structure.

The propagation of a $\{100\}$ plane through the ZIF-8 structure with SOD topology is shown in panel (a) of Figure 8. The plane runs parallel to the very narrow four-membered ring windows, while the larger six-membered ring windows are aligned parallel to $\{111\}$ planes (Figure 8b). This means that for our $\{100\}$ oriented ZIF-8 layer the four-membered ring windows are aligned parallel to the support. However, the contribution of the four-membered ring windows to mass transport through the pore network is assumed to be negligible. As implied by the arrows in panel (a) of Figure 8, a molecule, driven by a vertical concentration gradient, cannot pass straight from one cage to the one below. Instead it has to follow a zigzag path through an adjacent cage, connected by the six-membered ring windows. The size of these windows can be estimated to be 3.4 Å from rigid framework models. Hence, in terms of diffusion through a membrane, parallel orientation of the $\{100\}$ planes (and the four-membered ring windows) to the support is rather a disadvantage, while a parallel alignment of the $\{111\}$ planes (and the six-membered ring-windows) would be the most desired orientation. However, because of the cubic symmetry of the 3-D pore network of ZIF-8, the crystal orientation is expected to be only of minor influence on the macroscopic level on membrane permeation and the separation performance.

As shown in various studies, the pore size in ZIFs seems to be larger than the value estimated from the crystallographic structures, assuming rigid framework structures. Kinetic uptake experiments and chromatographic studies showed that ethane (~ 3.8 Å),⁴⁶ propane (~ 4.0 Å),⁴⁶ and even *i*-butane can be adsorbed in ZIF-8, despite that their molecular diameters are significantly larger than the estimated six-membered pore window size of 3.4 Å.^{47–49} Recent investigations using IR microscopy for the *in situ* detection of molecular uptake came to the same conclusions.^{32,50} The obvious discrepancies between the predictions and the experimental findings might be explained by a dynamic flipping or rotation of the imidazolate linker. Gücüyener et al. postulated gate-opening effects in ZIF-7.⁵¹ In fact, dynamic benzene-ring flipping of the terephthalate linker in MIL type MOFs was recently found by Kolokolov et al. using ²H NMR spectroscopy.⁵² Molecular Dynamics (MD) simulations revealed huge differences in diffusion coefficients of guest molecules in rigid and flexible ZIF structures.⁵³

In Figure 9, the results of H_2/C_nX_m ($X = H, O$) and H_2/CH_4 gas mixture permeation measurements on the ZIF-8 membrane obtained after 2 h of secondary growth are reported. The permeances of H_2 and C_nX_m from the mixtures were calculated from the applied partial pressure (see Experimental Section). The corresponding mixture separation factor α was calculated following IUPAC definition.¹⁷ As already explained above, the ZIF-8 pore windows are permeable for gases with kinetic diameters larger than 3.4 Å, which is the pore size estimated from the rigid structure model. Hence, a sharp molecular sieve effect, which completely separates H_2 from CH_4 (kinetic diameter: 3.8 Å) is not observed. However, for the ZIF-8 membrane reported here, a sharp cutoff in α for H_2/C_nX_m separation is observed when increasing the hydrocarbon chain length from C_2 to C_3 (Figure 9). According to Combariza et al.,⁴⁶ the smallest pore diameters through which a molecule would fit are 3.8 Å for CH_4 and C_2H_6 and 4.0 Å for C_3H_8 . Hence, a very small difference in diameter of only 0.2 Å between C_2H_6 and C_3H_8 seems to have large effect on the molecular mobility. Of course, C_3H_8 exhibits much larger spatial dimensions than C_2H_6 , so the lower mobility might at first be not surprising. However, CH_4 and C_2H_6 exhibit a similar difference in molecular dimensions, but no such difference in mobility is found for C_2H_6 compared to that of CH_4 . This might either indicate that there is a sharp loss in gate opening flexibility at a size of ~ 4.0 Å or that there is a more complex interaction of the pore gates with penetrating molecules.

Panel (b) of Figure 9 compares the H_2 and CH_4 permeances and separation factors measured in this work with the corresponding values of the non-oriented ZIF-8 membranes on which we³¹ and McCarthy et al.²⁵ reported recently. All experiments were performed at $T = 25$ °C and at similar concentration gradients across the membrane (1 bar partial pressure at the feed side and near zero at the permeate side) and, hence, should be comparable. With respect to the H_2/CH_4 separation factor of $\alpha \approx 15$, the oriented membrane shows a slightly higher selectivity in comparison to our non-oriented ZIF-8 ($\alpha \approx 11$) membrane and the membrane prepared by McCarthy et al. (pure gas or ideal separation factor: ≈ 13). We explain this result by an improved microstructure quality of the oriented ZIF-8 membrane, i.e., a better intergrowth of the grains and consequently lower leak transport, rather than by the crystal orientation. However, in industrial applications, the

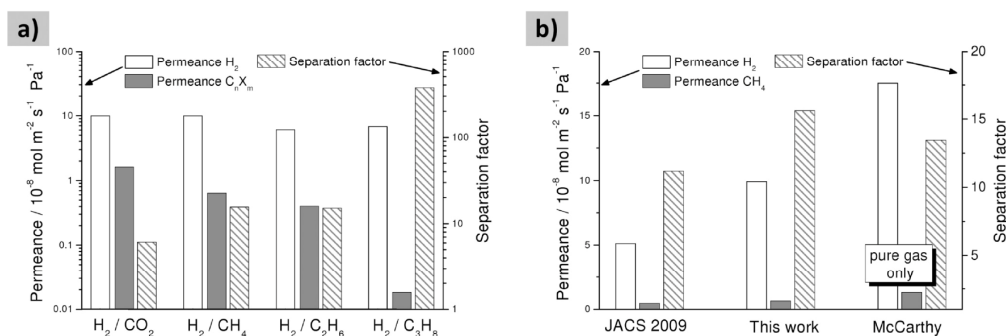


Figure 9. (a) Permeances and separation factors (in logarithmic scale) of equimolar H₂/C_nX_m gas mixtures at room temperature measured on the ZIF-8 membrane prepared by 2 h of secondary growth. (b) Comparison of the H₂/CH₄ permeances and separation factor with our previously reported ZIF-8 membrane (JACS 2009)³¹ as well as with data from the work of McCarthy et al.³⁵

permeance (which is the pressure-normalized flux in mol m⁻² s⁻¹ Pa⁻¹) of a membrane is at least as important as its separation factor. In comparison to our non-oriented ZIF-8 membrane, the decrease in layer thickness from 30 to 12 μm resulted in an almost doubled H₂ permeance. However, following Fick's first law from which the permeance through the membrane is reciprocally correlated with the membrane thickness, we would expect an increase in the permeance by the factor 2.5. The difference between the actual and expected increase in permeance can be explained by the improved quality of the novel, oriented ZIF-8 membrane, as indicated by the higher H₂/CH₄ separation factor (Figure 9b). The permeances of the 30 μm thick membrane likely include a higher contribution of undefined mass transport through defects or leaks, which results in a lower selectivity.

The ZIF-8 membrane reported by McCarthy et al. exhibits a layer thickness of around 20 μm, while the permeances were found to be even higher than those reported here. Though McCarthy et al. performed pure gas measurements only (and we have previously shown that there is a slight but noticeable reduction of the permeances in H₂/CH₄ mixed gas separation compared to the pure gases),³¹ the deviation might be explained primarily by the different experimental measurement methods. For the permeation measurements, McCarthy et al. used an instantaneous time lag method,⁵⁴ where a constant gas pressure is applied to the feed side of the membrane, while the time-dependent pressure increase at the evacuated permeate side of the membrane is monitored. Permeances can be calculated from the recorded pressure-time curves, and it is ideally assumed that the permeate side pressure is near zero. In our experiments, we used a modified, stationary Wicke–Kallenbach technique (see Experimental Section), where the permeate partial pressure is kept near zero by sweeping with an inert gas. Hence, in idealized theory, the boundary conditions of permeation are the same for both experiments. However, because the porous alumina support might act as dead volume, the idealized assumption of a zero partial pressure at the permeate side might be problematic. To minimize this concentration polarization, the alumina supports have an asymmetric structure and consist of only a thin layer with a small pore size (~70 nm) supporting the ZIF-8 layer and a thick coarse layer as mechanical support with a large pore size (~10 μm). This asymmetric structure reduces the pressure loss across the membrane. Even a small increase in the residual partial pressure at the permeate side can, however, highly influence the concentration gradient (see Figure S4 of the Supporting Information) and reduce our measured permeances. Further influences of different experimental configurations

in the Wicke–Kallenbach technique are very well investigated on zeolite membranes by van de Graaf et al.⁵⁵

Recently Aguado et al. showed permeation measurements for tubular composite membranes of SIM-1 (Zn(4m5cim)₂, 4m5cim = 4-methyl-5-imidazolecarboxaldehyde) with a layer thickness of 25 μm.⁵⁶ SIM-1 is iso-structural to ZIF-8, and the membrane shows permeances of light gases in a similar order of magnitude as for the here shown ZIF-8 membranes.

CONCLUSIONS

We prepared for the first time a continuous ZIF-8 layer on top of a porous alumina support by secondary seeded growth. This method allows us to obtain much thinner ZIF-8 membranes than in previous in situ crystallizations. Columnar crystal grains aligned perpendicular to the support surface were observed by SEM and TEM. XRD and SEM demonstrated that the well-intergrown crystals exhibit a high degree of {100} orientation. The highly oriented growth can be well explained by the evolutionary selection model by van der Drift,⁴² which predicts that the crystals with the highest vector of vertical growth survive the selection process, and the model by Bons and Bons,⁴⁵ which correlates the degree of preferred orientation with the lateral growth vectors. Permeation measurements on the ZIF-8 membrane obtained after 2 h of secondary growth showed a slightly higher H₂/CH₄ separation factor in comparison with that of the membrane prepared by in situ crystallization.³¹ We explain this finding with the improved quality of the microstructure of the new membrane. Until now, ZIF-membranes showed only a smooth molecular sieve effect in the separation of lighter gases (e.g., H₂, CO₂, and CH₄), rather than a sharp cutoff at the crystallographic pore size of 3.4 Å as estimated from rigid framework structure models.⁵⁷ Here, we demonstrate that the new ZIF-8 membrane shows a sharp H₂/C₃H₈ molecular sieve separation. This indicates that the large derivations of the experimentally measured separation factors for light gases from the ones predicted recently from rigid framework structure models cannot be entirely attributed to mass transfer through, e.g., grain boundaries, cracks, or leaking gaskets.

ASSOCIATED CONTENT

S Supporting Information. Explanatory schematics (Wicke–Kallenbach technique, diffusion through membranes), additional CPO data, EDXS element mapping, and additional XRD patterns. This material is available free of charge via the Internet at <http://pubs.acs.org>.

AUTHOR INFORMATION

Corresponding Author

*armin.feldhoff@pci.uni-hannover.de (A.F.), helge.bux@pci.uni-hannover.de (H.B.).

ACKNOWLEDGMENT

This work is part of the German Research Foundation priority program SPP 1362 "Porous Metal-Organic Frameworks", organized by S. Kaskel. We gratefully acknowledge financial support.

REFERENCES

- Yaghi, O. M.; O'Keeffe, M.; Ockwig, N. W.; Chae, H. K.; Eddaoudi, M.; Kim, J. *Nature* **2003**, *423* (6941), 705–714.
- Ferey, G. *Chem. Soc. Rev.* **2008**, *37* (1), 191–214.
- Kitagawa, S.; Kitaura, R.; Noro, S. *Angew. Chem., Int. Ed.* **2004**, *43* (18), 2334–2375.
- Murray, L. J.; Dinca, M.; Long, J. R. *Chem. Soc. Rev.* **2009**, *38* (5), 1294–1314.
- Ma, S. Q.; Zhou, H. C. *Chem. Commun.* **2010**, *46* (1), 44–53.
- Horcajada, P.; Serre, C.; Maurin, G.; Ramsahye, N. A.; Balas, F.; Vallet-Regi, M.; Sebba, M.; Taulelle, F.; Ferey, G. *J. Am. Chem. Soc.* **2008**, *130* (21), 6774–6780.
- Horcajada, P.; Chalati, T.; Serre, C.; Gillet, B.; Sebrie, C.; Baati, T.; Eubank, J. F.; Heurtaux, D.; Clayette, P.; Kreuz, C.; Chang, J. S.; Hwang, Y. K.; Marsaud, V.; Bories, P. N.; Cynober, L.; Gil, S.; Ferey, G.; Couvreur, P.; Gref, R. *Nat. Mater.* **2010**, *9* (2), 172–178.
- McKinlay, A. C.; Morris, R. E.; Horcajada, P.; Ferey, G.; Gref, R.; Couvreur, P.; Serre, C. *Angew. Chem., Int. Ed.* **2010**, *49* (36), 6260–6266.
- Lee, J.; Farha, O. K.; Roberts, J.; Scheidt, K. A.; Nguyen, S. T.; Hupp, J. T. *Chem. Soc. Rev.* **2009**, *38* (5), 1450–1459.
- Harbuzaru, B. V.; Corma, A.; Rey, F.; Jorda, J. L.; Ananias, D.; Carlos, L. D.; Rocha, J. *Angew. Chem., Int. Ed.* **2009**, *48* (35), 6476–6479.
- Lu, G.; Hupp, J. T. *J. Am. Chem. Soc.* **2010**, *132* (23), 7832–7833.
- Li, J. R.; Kuppler, R. J.; Zhou, H. C. *Chem. Soc. Rev.* **2009**, *38* (5), 1477–1504.
- Gascon, J.; Kapteijn, F. *Angew. Chem., Int. Ed.* **2010**, *49* (9), 1530–1532.
- Keskin, S.; van Heest, T. M.; Sholl, D. S. *ChemSusChem* **2010**, *3* (8), 879–891.
- Eddaoudi, M.; Kim, J.; Rosi, N.; Vodak, D.; Wachter, J.; O'Keeffe, M.; Yaghi, O. M. *Science* **2002**, *295* (5554), 469–472.
- Tanabe, K. K.; Wang, Z. Q.; Cohen, S. M. *J. Am. Chem. Soc.* **2008**, *130* (26), 8508–8517.
- Koros, W. J.; Ma, Y. H.; Shimidzu, T. *J. Membr. Sci.* **1996**, *120* (2), 149–159.
- Liu, Y. Y.; Ng, Z. F.; Khan, E. A.; Jeong, H. K.; Ching, C. B.; Lai, Z. P. *Microporous Mesoporous Mater.* **2009**, *118* (1–3), 296–301.
- Yoo, Y.; Lai, Z. P.; Jeong, H. K. *Microporous Mesoporous Mater.* **2009**, *123* (1–3), 100–106.
- Guo, H. L.; Zhu, G. S.; Hewitt, I. J.; Qiu, S. L. *J. Am. Chem. Soc.* **2009**, *131* (5), 1646–1647.
- Ranjan, R.; Tsapatsis, M. *Chem. Mater.* **2009**, *21* (20), 4920–4924.
- Guerrero, V. V.; Yoo, Y.; McCarthy, M. C.; Jeong, H. K. *J. Mater. Chem.* **2010**, *20* (19), 3938–3943.
- Huang, A.; Dou, W.; Caro, J. *J. Am. Chem. Soc.* **2010**, *132* (44), 15562–15564.
- Liu, Y. Y.; Hu, E. P.; Khan, E. A.; Lai, Z. P. *J. Membr. Sci.* **2010**, *353* (1–2), 36–40.
- McCarthy, M. C.; Varela-Guerrero, V.; Barnett, G. V.; Jeong, H. K. *Langmuir* **2010**, *26* (18), 14636–14641.
- Venna, S. R.; Carreon, M. A. *J. Am. Chem. Soc.* **2010**, *132* (1), 76–78.
- Yoo, Y.; Jeong, H. K. *Cryst. Growth Des.* **2010**, *10* (3), 1283–1288.
- Park, K. S.; Ni, Z.; Cote, A. P.; Choi, J. Y.; Huang, R. D.; Uribe-Romo, F. J.; Chae, H. K.; O'Keeffe, M.; Yaghi, O. M. *Proc. Natl. Acad. Sci. U.S.A.* **2006**, *103* (27), 10186–10191.
- Hayashi, H.; Cote, A. P.; Furukawa, H.; O'Keeffe, M.; Yaghi, O. M. *Nat. Mater.* **2007**, *6* (7), 501–506.
- Phan, A.; Doonan, C. J.; Uribe-Romo, F. J.; Knobler, C. B.; O'Keeffe, M.; Yaghi, O. M. *Acc. Chem. Res.* **2010**, *43* (1), 58–67.
- Bux, H.; Liang, F. Y.; Li, Y. S.; Cravillon, J.; Wiebcke, M.; Caro, J. *J. Am. Chem. Soc.* **2009**, *131* (44), 16000–16001.
- Bux, H.; Chmelik, C.; van Baten, J. M.; Krishna, R.; Caro, J. *Adv. Mater.* **2010**, *22* (42), 4741–4743.
- Huang, A. S.; Bux, H.; Steinbach, F.; Caro, J. *Angew. Chem., Int. Ed.* **2010**, *49* (29), 4958–4961.
- Li, Y. S.; Liang, F. Y.; Bux, H.; Feldhoff, A.; Yang, W. S.; Caro, J. *Angew. Chem., Int. Ed.* **2010**, *49* (3), 548–551.
- Li, Y. S.; Liang, F. Y.; Bux, H. G.; Yang, W. S.; Caro, J. *J. Membr. Sci.* **2010**, *354* (1–2), 48–54.
- Li, Y. S.; Bux, H.; Feldhoff, A.; Li, G. L.; Yang, W. S.; Caro, J. *Adv. Mater.* **2010**, *22* (30), 3322–3326.
- Breck, D. W. *Zeolite Molecular Sieves: Structure, Chemistry, and Use*; Wiley: New York, 1974.
- Cravillon, J.; Munzer, S.; Lohmeier, S. J.; Feldhoff, A.; Huber, K.; Wiebcke, M. *Chem. Mater.* **2009**, *21* (8), 1410–1412.
- Wicke, E.; Kallenbach, R. *Colloid Polym. Sci.* **1941**, *97* (2), 135–151.
- Verduijn, J. P.; Bons, A. J.; Anthonis, M. H.; Czarnetzki, L. H. WO Patent 96/01683, 1996.
- Jeong, H. K.; Krohn, J.; Sujaoti, K.; Tsapatsis, M. *J. Am. Chem. Soc.* **2002**, *124* (44), 12966–12968.
- van der Drift, A. *Philips Res. Rep.* **1967**, *22*, 267–288.
- Caro, J.; Noack, M.; Kolsch, P. *Adsorption* **2005**, *11* (3–4), 215–227.
- Cravillon, J.; Nayuk, R.; Springer, S.; Feldhoff, A.; Huber, K.; Wiebcke, M. *Chem. Mater.*, accepted for publication, DOI: 10.1021/cm103571y.
- Bons, A. J.; Bons, P. D. *Microporous Mesoporous Mater.* **2003**, *62* (1–2), 9–16.
- Combariza, A. F.; Sastre, G.; Corma, A. *J. Phys. Chem. C* **2010**, *115* (4), 875–884.
- Luebbers, M. T.; Wu, T. J.; Shen, L. J.; Masel, R. I. *Langmuir* **2010**, *26* (19), 15625–15633.
- Li, K. H.; Olson, D. H.; Seidel, J.; Emge, T. J.; Gong, H. W.; Zeng, H. P.; Li, J. *J. Am. Chem. Soc.* **2009**, *131* (30), 10368–10369.
- Ferey, G.; Demessence, A.; Boissiere, C.; Grosso, D.; Horcajada, P.; Serre, C.; Ferey, G.; Soler-Illia, G.; Sanchez, C. *J. Mater. Chem.* **2010**, *20* (36), 7676–7681.
- Chmelik, C.; Bux, H.; Caro, J.; Heinke, L.; Hibbe, F.; Titze, T.; Kaerger, J. *Phys. Rev. Lett.* **2010**, *104* (8), 085902.
- Güçüyener, C.; van den Bergh, J.; Gascon, J.; Kapteijn, F. *J. Am. Chem. Soc.* **2010**, *132* (50), 17704–17706.
- Kolokolov, D. I.; Jobic, H.; Stepanov, A. G.; Guillerme, V.; Devic, T.; Serre, C.; Férey, G. *Angew. Chem., Int. Ed.* **2010**, *49* (28), 4791–4794.
- Hertäg, L.; Bux, H.; Caro, J.; Chmelik, C.; Remsungen, T.; Knauth, M.; Fritzsche, S. *J. Membr. Sci.*, **2011**, DOI:10.1016/j.memsci.2011.01.019.
- Rutherford, S. W.; Do, D. D. *Adsorption* **1997**, *3* (4), 283–312.
- van de Graaf, J. M.; Kapteijn, F.; Moulijn, J. A. *J. Membr. Sci.* **1998**, *144* (1–2), 87–104.
- Aguado, S.; Nicolas, C.-H.; Moizan-Basle, V.; Nieto, C.; Amrouche, H.; Bats, N.; Audebrand, N.; Farrusseng, D. *New J. Chem.* **2011**, *35* (1), 41–44.
- Haldoupis, E.; Nair, S.; Sholl, D. S. *J. Am. Chem. Soc.* **2010**, *132* (21), 7528–7539.

6. Syntheses of ZIF-8 Composite Nanofibers Using Electrospinning

6.1 Summary

In cooperation with Dr. Rainer Ostermann and Prof. Dr. Bernd Smarsly (Justus Liebig University Gießen) the synthesis of polymer-ZIF-8 composite nanofibers by electrospinning was developed. This is the first report of such nanofibers containing metal-organic framework crystals. Different polymers such as PVP (polyvinylpyrrolidone), PS (polystyrene) and PEO (polyethylene oxide) were applied for nanofiber fabrication. The preformed ZIF-8 nanocrystals were homogeneously dispersed within the polymers and the capability of gas species to enter the ZIF-8 particles through the polymer matrix was demonstrated using physisorption measurements. Composite nanofibers consisting of ZIF-8@PVP and ZIF-8@PS exhibited a large inner surface area, which correlated with the inner surface of the used ZIF-8 nanocrystals. The particles' pore system was almost 100% accessible. The gas adsorption kinetics of nanofibers was compared to those of pure microcrystalline and nanocrystalline ZIF-8 samples. These experiments showed that the pure nanoparticles exhibited the fastest adsorption kinetics while the adsorption speed of ZIF-8@PVP and microcrystalline ZIF-8 was similar. This could be explained with the larger surface-to-volume ratio of the nanocrystals and the encapsulating effect of the polymer in the case of nanofibers.

6.2 Metal-Organic Framework Nanofibers *via* Electrospinning

Rainer Ostermann, Janosch Cravillon, Cristoph Weidmann, Michael Wiebcke and Bernd M. Smarsly.

Chem. Commun. **2011**, 47, 442-444.

DOI: 10.1039/C0CC02271C

Web: <http://pubs.rsc.org/en/Content/ArticleLanding/2011/CC/c0cc02271c>

Supporting information: <http://www.rsc.org/suppdata/cc/c0/c0cc02271c>

Reproduced by permission of The Royal Society of Chemistry.

Copyright 2011.

Metal–organic framework nanofibers *via* electrospinning†‡

Rainer Ostermann,^a Janosch Cravillon,^b Christoph Weidmann,^a Michael Wiebcke^b and Bernd M. Smarsly*^a

Received 30th June 2010, Accepted 1st September 2010

DOI: 10.1039/c0cc02271c

A hierarchical system of highly porous nanofibers has been prepared by electrospinning MOF (metal–organic framework) nanoparticles with suitable carrier polymers. Nitrogen adsorption proved the MOF nanoparticles to be fully accessible inside the polymeric fibers.

The design of hierarchical nanostructures is a long-sought goal of materials science and there has been extensive research into various “top-down” and “bottom-up” methods to create these nanostructures. Electrospinning is one of the simplest top-down methods that allows for an easy generation of nanofibers from a wide variety of materials, especially polymers which were proven to be useful for many applications like filtration or controlled drug-release.^{1,2}

However, in spite of various attempts, the preparation of porous polymeric nanofibers with high surface areas could not be realized so far.

Isotactic polymers like PLLA (poly-L-lactide) and blends thereof^{3,4} have been electrospun from solvent mixtures to produce porous fibers.⁵ Another approach applicable to various polymers is to use a cryogenic liquid to trap some of the solvent inside the fibers, followed by an extraction of the solvent under reduced pressure to yield some porosity.⁶ However, the specific surface area of such “porous” polymeric fibers is always quite low, usually in the range of 10–15 m² g⁻¹, corresponding only to an increase by a factor of 2–3 compared to the corresponding “non-porous” fibers. Only in inorganic or carbonized PAN (polyacrylonitrile) fibers sufficient micro-porosity can be found allowing for surface areas of up to 300 or 600 m² g⁻¹ respectively.^{7,8} Highly porous polymers remain special cases with a high degree of (hyper)cross-linking like PIMs (polymers of intrinsic porosity)^{9–11} and have not been prepared in the form of nanofibers so far.

In contrast, metal–organic frameworks (MOF) are crystalline coordination polymers that are well known for their extremely high porosity and surface areas.¹² Zeolitic imidazolate framework (ZIF) materials constitute a new subclass of MOFs that combine the properties of porous MOFs with high chemical and thermal stability.¹³ Various MOFs, including

ZIFs, have been very recently used as fillers for the fabrication of mixed matrix membranes.^{14,15}

In order to achieve a homogeneous distribution of filler particles within an organic polymer matrix it should be beneficial to use monodisperse nanoparticles. Recently, Cravillon *et al.* succeeded in preparing nanocrystals of a prototypical ZIF material, ZIF-8, that are 50 nm in size and have a rather narrow size distribution.¹⁶

Similar nanocrystals have recently been shown to exhibit distinct advantages like faster adsorption kinetics for porous coordination polymers.¹⁷

In this work we present for the first time the synthesis and characterization of composite MOF–polymer nanofibers combining the advantages of both types of materials to achieve a novel class of hierarchical nanostructure.

The colloidal suspensions of ZIF-8 nanoparticles in methanol were prepared as described before.¹⁶ Briefly, a solution of appropriate amounts of Zn(NO₃)₂·6H₂O and 2-methylimidazole in methanol was stirred at room temperature for 1 h, before separating the resulting nanocrystals by centrifugation. The ZIF-8 nanoparticles were redispersed in fresh methanol by vortex mixing and ultrasonic agitation and a part of the solution was dried at 80 °C under reduced pressure to determine the concentration to be 3.5–4.5 wt% of ZIF-8. In a typical electrospinning experiment, 500 mg of a solution of 12 wt% PVP (polyvinylpyrrolidone, molecular weight (MW) = 1 300 000) in methanol was added to 400–2000 mg of the ZIF-8 dispersion and mixed thoroughly. The solution was diluted or concentrated under reduced pressure to yield a final concentration of 3.5 wt% of PVP. This solution was fed through a metallic needle by a syringe pump (KDS scientific) at the rate of 0.35 ml h⁻¹. The needle is placed at a distance of 6–8 cm from the aluminium foil that serves as collector and a voltage of 5 kV (Spellman CZE1000R high-voltage power supply) was applied to produce a non-woven mat (see Fig. 1–3). The composite PVP–ZIF-8 nanofibers and the dried ZIF nanoparticles were characterized by SEM (LEO Gemini 982), TEM (Philips CM30-ST), XRD (Panalytical X'Pert PRO diffractometer) and N₂ adsorption (Quantachrome Autosorb 1 and 6).

The diameter of the nanofibers could be adjusted by the polymer concentration and was found to be roughly 150–300 nm. The nanoparticle loading could be as high as 1 : 1 by weight ratio of ZIF-8 to PVP. SEM and TEM revealed a homogeneous distribution of the nanoparticles inside the fibers with a smooth polymeric surface.

As can be seen from Fig. 3, macroscopic non-wovens can be obtained on the centimetre scale. Thus, the composite fibers can be regarded as a “MOF textile”, combining the properties of polymeric fibers and MOFs.

^a Institute of Physical Chemistry, Justus-Liebig-University Giessen, 35392 Giessen, Germany.

E-mail: bernd.smarsly@phys.chemie.uni-giessen.de;
Fax: +49 641 9934509; Tel: +49 641 9934590

^b Institute of Inorganic Chemistry, Leibniz University Hannover, Callinstrasse 9, D-30167 Hannover, Germany

† This article is part of the ‘Emerging Investigators’ themed issue for ChemComm.

‡ Electronic supplementary information (ESI) available: XRD data; SEM images; adsorption kinetics; description of fiber generation. See DOI: 10.1039/c0cc02271c

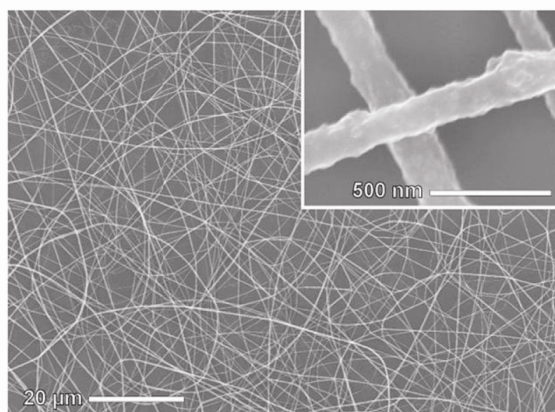


Fig. 1 SEM of ZIF-8 nanoparticles in PVP.

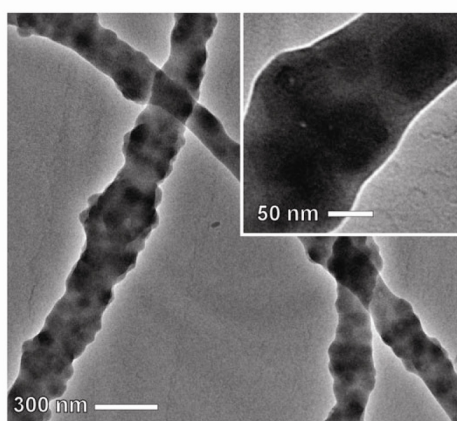


Fig. 2 TEM of ZIF-8 nanoparticles in PVP.

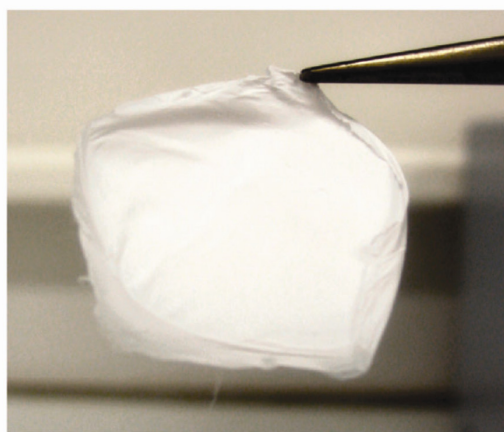


Fig. 3 Digital photograph of a non-woven ZIF-8-PVP fiber mat. The diameter is *ca.* 1.5 cm.

A comparison of XRD patterns of the ZIF-8 nanofibers and the pure nanoparticles showed the crystal structure to be preserved (see ESI†). From N_2 adsorption measurements (Fig. 4) including micropore analysis, the surface area according to the BET model was $960 \text{ m}^2 \text{ g}^{-1}$ for the pure ZIF-8, while the

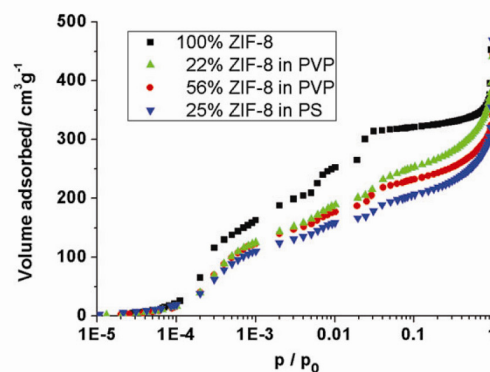


Fig. 4 Nitrogen adsorption isotherms of ZIF-8 nanoparticles in PS and PVP (with different loadings of ZIF-8). For clarity the desorption branch is omitted and the curves have been scaled to 100% ZIF-8 content.

Table 1 Nitrogen adsorption data

Sample	ZIF-8 concentration ^a (wt%)	Micropore volume/ $\text{cm}^3 \text{ g}^{-1}$	Surface area ^b / $\text{m}^2 \text{ g}^{-1}$	Accessible ZIF-8 fraction ^b (wt%)
ZIF-8	100	0.49	960	100
ZIF in PVP	56	0.18	530	55.1
ZIF in PVP	22	0.07	180	19.1
ZIF in PS	25	0.07	210	22.7
PVP only	0	<0.002	10	n/a

^a As weighed in. ^b According to the BET model.

fibers possessed surface areas of up to $530 \text{ m}^2 \text{ g}^{-1}$ for a weight ratio of approx. 1 : 1 ZIF-8 to PVP. As can be seen in Fig. 4, the adsorption branch for the fibers is shifted to higher pressure. The two steps on the adsorption isotherms that have been ascribed¹⁸ to pressure-induced adsorbate reorganization are less pronounced, but still visible for the composite fibers. For lower loadings of ZIF-8 (see Table 1) the surface area decreased accordingly, proving the ZIF-8 nanoparticles to be fully accessible inside the polymeric nanofibers.

The nanofibers are stable in the as-prepared form up to $150 \text{ }^\circ\text{C}$ and do not degrade in organic solvents such as hexane, but are sensitive to polar solvents of the polymer such as alcohol or water, causing the nanofibers to coalesce.

Using other polymers like polystyrene (PS) and polyethylene oxide (PEO) allows increasing the fibers' stability and widening the range of possible applications.

In particular, the PS-ZIF-8 nanofibers are stable in alcohols and water and the surface area was fully accessible (determined by nitrogen sorption), even if the ZIF-8 loading up to 25 wt% was slightly lower. Higher loadings should be possible by tuning the synthesis parameter and functionalizing the surface of the ZIF-8 nanoparticles with less polar molecules (see ESI† for details of preparation).

The adsorption measurements show that the ZIF-8 nanoparticles are fully accessible. We further compared the adsorption kinetics of the nanofibers to bare nano- and micrometer-size particles (prepared by classical solvothermal synthesis and

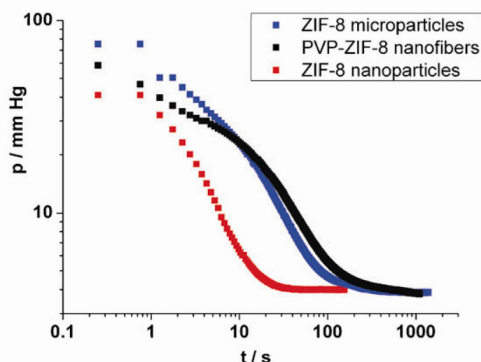


Fig. 5 N_2 adsorption kinetics studied as cell pressure over time.

referred to as “microparticles”) by determining the time to reach equilibrium pressure after dosing a defined amount of adsorbate into the evacuated sample cell.

Although we cannot propose a model yet, it is obvious that diffusion inside the ZIF-8 is much slower than in the gas phase and that external surface area and the presence of a polymer layer determine the kinetics of adsorption.

As can be seen in Fig. 5 the nanoparticles attain equilibrium after 30 s, while the microparticles and the nanofibers require 100–120 s.

Most of the faster kinetics of the nanoparticles can probably be accounted for by the larger external surface area being ten times larger compared to the microparticles, while diffusion inside ZIF-8 is fast. The polymer layer around the fibers constitutes an additional diffusion barrier, therefore the nitrogen uptake is also slower than for the pure nanoparticles, but still as fast as for the microparticles. In fact, a low thickness of the polymer layer is crucial, as for polymer films or coalesced fiber mats, the kinetics become too slow to observe significant adsorption and accessible surface areas drop below $20 \text{ m}^2 \text{ g}^{-1}$.

The results from N_2 adsorption were corroborated by CO_2 as adsorbate (see ESI† for isotherms and kinetics data).

Further results indicate that the different carrier polymers also affect the adsorption kinetics. It is found that the uptake is faster for PVP than for PS- and PEO-based nanofibers (see ESI† for SEM pictures, N_2 isotherms and kinetics data). In this regard, blends of polymers hold great promise as well.

As the carrier polymers and the degree of nanoparticle coverage by the polymer should also influence the absorption, this might allow tuning the selectivity of adsorption, especially with different gases. Therefore we are planning a systematic study for more relevant adsorbates like hydrogen, carbon

dioxide or monoxide. Due to their low resistance to fluid flow, the nanofiber mats could ultimately be useful to selectively adsorb specific gases, for example carbon monoxide in gas masks.

In conclusion, we could prepare nanofibers of a metal–organic framework for the first time by electrospinning preformed nanoparticles, thereby creating hierarchical nanofibers with high surface areas and good accessibility. With the anticipated availability of other MOF materials as nanoparticles, a broad variety of MOF nanofibers should be accessible with various applications, for example in gas adsorption and separation.

Dr A. Möller (Institut für Nichtklassische Chemie, Leipzig, Germany) is acknowledged for CO_2 sorption measurements.

Notes and references

- 1 D. Li and Y. Xia, *Adv. Mater.*, 2004, **16**, 1151–1170.
- 2 A. Greiner and J. Wendorff, *Angew. Chem., Int. Ed.*, 2007, **46**, 5670–5703.
- 3 M. Bognitzki, W. Czado, T. Frese, A. Schaper, M. Hellwig, M. Steinhart, A. Greiner and J. H. Wendorff, *Adv. Mater.*, 2001, **13**, 70–72.
- 4 M. Bognitzki, T. Frese, M. Steinhart, A. Greiner, J. H. Wendorff, A. Schaper and M. Hellwig, *Polym. Eng. Sci.*, 2001, **41**, 982–989.
- 5 Z. Qi, H. Yu, Y. Chen and M. Zhu, *Mater. Lett.*, 2009, **63**, 415–418.
- 6 J. T. McCann, M. Marquez and Y. Xia, *J. Am. Chem. Soc.*, 2006, **128**, 1436–1437.
- 7 M. Kanehata, B. Ding and S. Shiratori, *Nanotechnology*, 2007, **18**, 315602.
- 8 Z. Zhang, X. Li, C. Wang, S. Fu, Y. Liu and C. Shao, *Macromol. Mater. Eng.*, 2009, **294**, 673–678.
- 9 N. B. McKeown, S. Hanif, K. Msayib, C. E. Tattershall and P. M. Budd, *Chem. Commun.*, 2002, 2782–2783.
- 10 P. M. Budd, E. Elabas, B. Ghanem, S. Makhseed, N. McKeown, K. Msayib, C. Tattershall and D. Wang, *Adv. Mater.*, 2004, **16**, 456–459.
- 11 N. B. McKeown, B. Ghanem, K. J. Msayib, P. M. Budd, C. E. Tattershall, K. Mahmood, S. Tan, D. Book, H. W. Langmi and A. Walton, *Angew. Chem., Int. Ed.*, 2006, **45**, 1804–1807.
- 12 G. Ferey, *Chem. Soc. Rev.*, 2008, **37**, 191–214.
- 13 A. Phan, C. J. Doonan, F. J. Uribe-Romo, C. B. Knobler, M. O’Keeffe and O. M. Yaghi, *Acc. Chem. Res.*, 2010, **43**, 58–67.
- 14 K. Díaz, L. Garrido, M. López-González, L. F. del Castillo and E. Riande, *Macromolecules*, 2010, **43**, 316–325.
- 15 S. Basu, M. Maes, A. Cano-Odena, L. Alaerts, D. E. De Vos and I. F. Vankelecom, *J. Membr. Sci.*, 2009, **344**, 190–198.
- 16 J. Cravillon, S. Muenzer, S. Lohmeier, A. Feldhoff, K. Huber and M. Wiebcke, *Chem. Mater.*, 2009, **21**, 1410–1412.
- 17 D. Tanaka, A. Henke, K. Albrecht, M. Moeller, K. Nakagawa, S. Kitagawa and J. Groll, *Nat. Chem.*, 2010, **2**, 410–416.
- 18 K. S. Park, Z. Ni, A. P. Côté, J. Y. Choi, R. Huang, F. J. Uribe-Romo, H. K. Chae, M. O’Keeffe and O. M. Yaghi, *Proc. Natl. Acad. Sci. U. S. A.*, 2006, **103**, 10186–10191.

7. Curriculum Vitae

Janosch Cravillon

Date of birth	November the 07 th 1982
Place of birth	Hildesheim, Germany
Family status	single
Nationality	german
Focus	Porous inorganic-organic hybrid material, MOFs

Education

**September 2008 –
December 2011**

Dissertation at the
Institute of Inorganic Chemistry of the Leibniz
University of Hannover in the group of Prof. Dr.
Peter Behrens. Title: “*Microporous metal
imidazoles: Synthesis and characterization of
nano- and microcrystals as well as membranes
and investigation of the mechanisms of
crystallization*”

October 2003 - August 2008

Study of chemistry (Diplom)
Diplom in August 2008
Final grade: sehr gut (1.2)
Title of diploma thesis: “*Synthese und
Charakterisierung von Nanokristallen ionischer
Verbindungen*” at the Institute of Inorganic
Chemistry of the Leibniz University of Hannover
in the group of Prof. Dr. Peter Behrens

July 2002 – April 2003

Civil Service at
Short Step, drug rehabilitation, Wedemark,
Hannover

September 1989 – June 2002

School Education at the
IGS Roderbruch, Hannover
Abitur (A-levels)

Skills

Languages

German (mother language)
English (proficient)
Latin (qualification: Latinum)

Awards

September 2010

LNQE poster award by the *Freundeskreis der Leibniz Universität Hannover* for the poster „Control of ZIF-8 Formation in Room-Temperature Syntheses: Investigation by a Time-Resolved In-Situ Synchrotron SAXS/WAXS Study” at the *LNQE NanoDay 2010* Hannover, Germany. Authors: **J. Cravillon**, C.A. Schröder, R. Nayuk, K. Huber, J. Gummel, T. Narayana, M. Wiebcke

March 2009

George-Kokotailo poster award by the *DECHEMA Fachsektion Zeolithe* for the poster „First steps in preparation of ZIF-8 membranes by secondary growth crystallization at the 21. Deutsche Zeolith-Tagung Kiel, Germany. Authors: H. Bux, J. Caro, **J. Cravillon**, M. Wiebcke

8. List of Publications

8.1 Peer-Reviewed Paper

T. Hikov, C. A. Schröder, **J. Cravillon**, M. Wiebcke, K. Huber, *Phys. Chem. Chem. Phys.* **2012**, *14*, 511-521. Title: „*In-situ static and dynamic light scattering and scanning electron microscopy study on the crystallization of the dense zinc imidazolate framework ZIF-zn*”

J. Cravillon, C. A. Schröder, H. Bux, A. Rothkirch, J. Caro, M. Wiebcke, *CrystEngComm*. **2011**, DOI: 10.1039/C1CE06002C. Title: „*Formate modulated solvothermal synthesis of ZIF-8 investigated using time-resolved in situ X-ray diffraction and scanning electron microscopy*”

J. Cravillon, C. A. Schröder, R. Nayuk, J. Gummel, M. Wiebcke, *Angew. Chem. Int. Ed.* **2011**, *50*, 8067-8071. Title: „*Fast Nucleation and Growth of ZIF-8 Nanocrystals Monitored by Time-Resolved In Situ Small-Angle and Wide-Angle X-Ray Scattering*”

H. Bux, A. Feldhoff, **J. Cravillon**, M. Wiebcke, Y. Li, J. Caro, *Chem. Mater.* **2011**, *23*, 2130-2141. Title: „*Oriented Zeolitic Imidazolate Framework-8 Membrane with Sharp H₂ / C₃H₈ Molecular Sieve Separation*”

J. Cravillon, R. Nayuk, S. Springer, A. Feldhoff, K. Huber, M. Wiebcke, *Chem. Mater.* **2011**, *23*, 2262-2269. Title: „*Controlling Zeolitic Imidazolate Framework Nano- and Microcrystal Formation: Insight into Crystal Growth by Time-Resolved In-Situ Static Light Scattering*”

R. Ostermann, **J. Cravillon**, C. Weidmann, M. Wiebcke, B. M. Smarsly, *Chem. Commun.* **2011**, *47*, 442-444. Title: „*Metal-organic framework nanofibers via electrospinning*”

H. Bux, F. Liang, Y. Li, **J. Cravillon**, M. Wiebcke, J. Caro, *J. Am. Chem. Soc.* **2009**, *131*, 16000-16001. Title: „*Zeolitic Imidazolate Framework Membrane with Molecular Sieving Properties by Microwave-Assisted Solvothermal Synthesis*”

J. Cravillon, S. Münzer, S.-J. Lohmeier, A. Feldhoff, K. Huber, M. Wiebcke, *Chem. Mater.* **2009**, *21*, 1410-1412. Title: „*Rapid Room-Temperature Synthesis and Characterization of Nanocrystals of a Prototypical Zeolitic Imidazolate Framework*”

8.2 Conference Proceedings

C. Schröder, **J. Cravillon**, R. Nayuk, K. Huber, J. Gummel, T. Narayanan, M. Wiebcke, *Z. Anorg. Allg. Chem.* DOI: 10.1002/zaac.201009047. Title: „*ZIF-8 Nanocrystal Formation: An In-Situ Synchrotron SAXS/WAXS Study*“

J. Cravillon, M. Wiebcke, *Z. Anorg. Allg. Chem.* DOI: 10.1002/zaac.200870050. Title: „*Zeolitic imidazolate framework nanocrystals: Synthesis and characterization*”

8.3 Scientific Talks

LNQE NanoDay 2011 Hannover, Germany. Authors: **J. Cravillon**, C. A. Schröder, R. Nayuk, Jeremie Gummel K. Huber, M. Wiebcke. Title: „*Poröse metallorganische Gerüstverbindungen - Nanokristallbildung aus der Lösung*“

EUROMAT2011 Montpellier, France. Authors: H. Bux, A. Feldhoff, A. Huang, Y. A. Li, **J. Cravillon**, M. Wiebcke, C. Chmelik, J. Kärger, L. Hertäg, M. Knauth, S. Fritzsche, J. Caro. Title: „*Zeolitic Imidazolate Framework Molecular Sieve Membranes: Status and Progress*“

International Symposium on Metal-Organic Frameworks Dresden, Germany. Authors: **J. Cravillon**, C. A. Schröder, R. Nayuk, H. Bux, J. Caro, K. Huber, M. Wiebcke. Title: “*Size-Controlled Synthesis of ZIF-8 Crystals on Multiple Length Scales: Investigations into the Mechanisms of Nucleation and Crystal Growth*“

23. *Deutsche Zeolith-Tagung* Erlangen, Germany. Autoren: R. Ostermann, B.M. Smarsly, C. Weidmann, **J. Cravillon**, M. Wiebcke. Title: „*Sorption kinetics in Metal Organic Framework nanofibers prepared via electrospinning*”

MOF2010 - Metal Organic Frameworks Marseille, France. Authors: H. Bux, J. Caro, F.Y. Li, **J. Cravillon**, M. Wiebcke, C. Chmelik, J. Kärger, S. Fritzsche, L. Hertäg. Title: „*Zeolitic imidazolate framework-8 molecular sieve membrane: from molecular modeling to membrane permeation*”

IZMM 2010 – 5th International Zeolite Membrane Meeting Loutraki, Greece. Authors: H. Bux, F. Liang, **J. Cravillon**, M. Wiebcke, Y. Li, J. Caro. Title: „*Zeolitic imidazolate framework molecular sieving membrane*”

22. *Deutsche Zeolith-Tagung* München, Germany. Authors: H. Bux, F.-Y. Liang, Y.-S. Li, **J. Cravillon**, M. Wiebcke, C. Chmelik, J. Kärger, S. Fritzsche, J. Caro. Title: „*Transport through zeolitic imidazolate frameworks: from molecular diffusion to membrane permeation*”

21. *Deutsche Zeolith-Tagung* Kiel, Germany. Authors: **J. Cravillon**, S.-J. Lohmeier, A. Feldhoff, M. Wiebcke. Title: „*Rapid room-temperature synthesis of zeolite imidazolate framework nanocrystals*”

8.4 Poster

23. *Deutsche Zeolith-Tagung* Erlangen, Germany. Authors: **J. Cravillon**, S. Springer, R. Nayuk, K. Huber, M. Wiebcke. Title: „*Fine-tuning of ZIF-8 nanocrystal size*”

23. *Deutsche Zeolith-Tagung* Erlangen, Germany. Authors: **J. Cravillon**, C. A. Schröder, A. Rothkirch, H. Bux, J. Caro, M. Wiebcke. Title: „*Fast synthesis of big ZIF-8 crystals investigated using time-resolved in-situ synchrotron EDXRD in tandem with ex-situ SEM*”

23. *Deutsche Zeolith-Tagung* Erlangen, Germany. Authors: H. Bux, J. Caro, A. Feldhoff, Y.-S. Li, **J. Cravillon**, M. Wiebcke. Title: „*Zeolitic imidazolate frameworks as molecular sieve membranes*”

LNQE Nanoday 2010 Hannover, Germany. Authors: **J. Cravillon**, C. A. Schröder, R. Nayuk, K. Huber, J. Gummel, T. Narayana, M. Wiebcke. Title: „*Control of ZIF-8 Formation in Room-Temperature Syntheses: Investigation by a Time-Resolved In-Situ Synchrotron SAXS/WAXS Study*”

15. *Vortragstagung Festkörperchemie 2010* Berlin, Germany. Authors: C. A. Schröder, **J. Cravillon**, R. Nayuk, K. Huber, J. Gummel, T. Narayanan, **M. Wiebcke**. Title: „*ZIF-8 Nanocrystal Formation: An In-Situ Synchrotron SAXS/WAXS Study*”

MOF2010 - Metal Organic Frameworks Marseille, France. Authors: **J. Cravillon**, F. Brieler, A. Feldhoff, M. Wiebcke. Title: „*Zeolitic imidazolate framework nanocrystal aggregates with hierarchical porosity and high thermal stability*”

MOF2010 - Metal Organic Frameworks Marseille, France. Authors: **J. Cravillon**, C. A. Schröder, R. Nayuk, K. Huber, J. Gummel, T. Narayanan, M. Wiebcke. Title: „*ZIF-8 nanocrystal nucleation and growth: a time-resolved In-Situ synchrotron SAXS/WAXS study*”

MOF2010 - Metal Organic Frameworks Marseille, France. Authors: **J. Cravillon**, M. Wiebcke, D. Zacher, R. A. Fischer, R. Schweins, T. Narayanan, R. Nayuk, K. Huber. Title: „*Analysis of the formation of mof particles by time resolved scattering including sls, saxs and sans*”

IZMM 2010 – 5th International Zeolite Membrane Meeting Loutraki, Greece. Authors: **J. Cravillon**, F. Liang, H. Bux, J. Caro, M. Wiebcke. Title: „*Room-temperature synthesis of supported ZIF-8 membranes*”

22. *Deutsche Zeolith-Tagung* München, Germany. Authors: **J. Cravillon**, C. A. Schröder, R. Nayuk, K. Huber, J. Gummel, M. Wiebcke. Title: „*First understanding of ZIF-8 nanocrystal formation by time-resolved synchrotron SAXS/WAXS and SLS studies*”

22. *Deutsche Zeolith-Tagung* München, Germany. Authors: **J. Cravillon**, R. Nayuk, K. Huber, M. Wiebcke. Title: „*Control of nano- and microcrystal formation of ZIF-8 in room-temperature syntheses*”

22. *Deutsche Zeolith-Tagung* München, Germany. Authors: **R. Ostermann**, **J. Cravillon**, M. Wiebcke, B. M. Smarsly, C. Weidmann. Title: „*MOF nanofibers via electrospinning*”

LNQE Nanoday 2009 Hannover, Germany. Authors: **J. Cravillon**, F. Liang, H. Bux, J. Caro, M. Wiebcke. Title: „*Room-Temperature Synthesis of ZIF-8, a Microporous Coordination Polymer: From Nanocrystals to Supported Membrane*”

ECSSC XII 2009 – European Conference on Solid State Chemistry Münster, Germany. Authors: **M. Wiebcke**, **J. Cravillon**, H. Bux, A. Feldhoff, K. Huber. Title: „*Control of Crystal Growth of a Zeolitic Imidazolate Framework*”

MOFCAT Workshop 2009 – Metal Organic Frameworks on the Road to Applications Oslo, Norway. Authors: **J. Cravillon**, S.-J. Lohmeier, A. Feldhoff, K. Huber, M. Wiebcke. Title: „*Rapid Room-Temperature Synthesis and Characterization of Nanocrystals of a Prototypical Zeolitic Imidazolate Framework*”

21. *Deutsche Zeolith-Tagung* Kiel, Germany. Authors: **H. Bux**, J. Caro, **J. Cravillon**, M. Wiebcke. Title: „*First steps in preparation of ZIF-8 membranes by secondary growth crystallization*”

1st International Conference on Metal-Organic Frameworks and Open Framework Compounds Augsburg, Germany. Authors: **J. Cravillon**, S. Münzer, M. Wiebcke, A. Feldhoff. Title: „*Synthesis of zeolitic imidazolate framework nanocrystals*”

14. *Vortragstagung der Fachgruppe Festkörperchemie und Materialforschung der Gesellschaft Deutscher Chemiker*, Bayreuth, Germany. Authors: **J. Cravillon**, M. Wiebcke. Title: *„Zeolitic imidazolate framework nanocrystals: Synthesis and characterization*
